CURING CHARACTERISTICS OF PHOTOPOLYMER RESIN WITH DISPERSED GLASS MICROSPHERES IN VAT POLYMERIZATION 3D PRINTING

Jingyu Liang

Thesis submitted to the faculty of the

Virginia Polytechnic Institute and State University

in partial fulfillment of the requirements for the degree of

Master of Science

in

Mechanical Engineering

Bart Raeymaekers, Chair

Christopher Williams

Robert West

May 10th, 2023

Blacksburg, Virginia

Keywords: Vat polymerization, photopolymer, glass microspheres, filler material, degree of cure, curing depth, surface roughness

CURING CHARACTERISTICS OF PHOTOPOLYMER RESIN WITH DISPERSED GLASS MICROSPHERES IN VAT POLYMERIZATION 3D PRINTING

Jingyu Liang

Abstract

The curing characteristics of photopolymer resin determine the relationship between the vat polymerization (VP) process parameters and the layer thickness, geometric accuracy, and surface quality of the 3D printed specimen. Dispersing filler material into the photopolymer resin changes its curing characteristics because the filler scatters and absorbs light, which modifies the curing reaction. However, the ability to cure photopolymer resin with high filler volume fraction is important to 3D print material specimens for specific engineering applications, e.g. structural polymer composite materials, electrical and thermal conductive materials, and ceramic materials for biological and high-temperature environments. We methodically measure the curing characteristics of diacrylate/epoxy photopolymer resin with dispersed glass microspheres. The experiments show that the curing depth, degree-of-cure, and surface roughness depend on both the light exposure dose and the filler fraction. We determine that the degree-of-cure increases with increasing filler fraction for constant exposure dose, and approaches 90% with increasing exposure dose, independent of the filler fraction. The geometric accuracy of the 3D printed specimens decreases with increasing exposure dose and with increasing filler volume fraction due to so-called profile broadening. Finally, we show that the average surface roughness of the 3D printed specimens decreases with increasing exposure dose and filler fraction. This work has implications for VP of photopolymer resins with high filler fraction.

CURING CHARACTERISTICS OF PHOTOPOLYMER RESIN WITH DISPERSED GLASS MICROSPHERES IN VAT POLYMERIZATION 3D PRINTING

Jingyu Liang

General Audience Abstract

Photopolymer resin is a gel-like liquid material that hardens (cures) into solid after absorbing light energy, and such a material is often used in the field of additive manufacturing (3D printing) to create complex geometry. Certain types of filler materials, such as metal powder or carbon fiber, can be added into the photopolymer resin to tailor the material properties, and thus, affects the curing behavior of photopolymer resin mixed with these filler materials. We conducted an experiment to understand how adding glass microspheres to a consumer grade photopolymer resin affects the process of creating 3D objects. This is important in the context of 3D printing engineered composite materials that derive their function from the organization and orientation of filler material in a matrix. To do this, we created many samples in the shape of a "VT" logo using the composite resin we made and measured their thickness (curing depth), degree-of-cure, surface roughness, and geometric accuracy, as a function of the amount of light energy being exposed to the resin (exposure dose) and the amount of the glass filler being added into the resin (filler fraction). We observed that when we increased the amount of light exposure, it resulted specimens that are thicker and more in degree of cure. Adding the glass filler to the liquid had mixed effects on the hardening process, because glass can scatter light and change how light travels within the resin. As a result, the printed objects became less accurate in shape and have smoother surface with increasing exposure dose and filler fraction, because more light is scattered off the designed curing profile and unintentionally cured the surrounding resin.

Dedication

Grateful for those who challenged me to rise,

Guided me to my path, and stood by my side,

Thanks to all for resilience, wisdom, and love,

My gratitude to you, like shining stars above.

Acknowledgement

I want to express my deepest gratitude to my parents and sister, who gave me unconditional support, even in the darkest moment in my life. The building block of my faith and confidence cannot be established without them.

I want to express my sincere appreciation to my academic advisor, my professor, Dr. Bart Raeymaekers, and my team of committee, Dr. Robert West, and Dr. Christopher Williams, as well as Dr. Alan Asbeck as my previous committee. This thesis cannot be completed without their invaluable guidance and support throughout my academic journey.

Finally, the author acknowledges support from the National Science Foundation under award no. 2130083. Additionally, this work was made possible by the use of Virginia Tech's Materials Characterization Facility, which is supported by the Institute for Critical Technology and Applied Science, the Macromolecules Innovation Institute, and the Office of the Vice President for Research and Innovation.

Table of Contents

List of Figures

List of Tables

List of Abbreviations

AM: Additive manufacturing, a.k.a. 3D printing, is a manufacturing method by stacking materials to build a part instead of cutting materials.

VP: Vat-polymerization, a 3D printing method with light-sensitive photopolymer materials.

SLA: Stereolithography, a VP technology that uses laser to selectively cure photopolymer materials.

TPP: Two-Photon Polymerization, a VP variation based on SLA.

DLP: Digital Light Processing, a VP technology that uses image projector to cure photopolymer materials.

CLIP: Continuous Liquid Interface Polymerization, a VP variation based on DLP.

LCD: Liquid Crystal Display, a VP technology that uses LCD screen to mask printing area.

UV-DIW: UV-assist Direct Ink Writing, a VP technology by extruding photopolymer resin onto build plate with an extruder nozzle and cure to build a 3D model.

CAL: Computed Axial Lithography, a VP technology that uses computed tomography images to cure photopolymer materials.

CT: Computed Tomography, an imaging technology.

FTIR: Fourier Transform Infrared, a spectroscopy technology that measures the absorbance of material in IR wavelength.

UV-Vis-IR: Ultraviolet-Visible-Infrared, a spectroscopy technology that measures the absorbance of materials in the three wavelength ranges.

DSC: Differential Scanning Calorimetry, a calorimetry technology that measures the heat released from a material as a function of temperature or time.

TGA: Thermogravimetric Analysis, a thermal analysis technology that analyze weight changes with temperature.

TMA: Thermomechanical Analysis, a thermal analysis technology that analyze mechanical property changes with temperature.

NMR: Nuclear Magnetic Resonance, a spectroscopy technology.

SEM: Scanning Electron Microscopy, a microscopy technology that uses a high energy beam of electron to generate surface images of a sample.

$\boldsymbol{D_p}$**:** Curing depth [mm], the measurement of cured layer thickness of photopolymer material by a single light exposure.

***DoC*:** Degree of Cure [%], refers to the degree of transformation of a photopolymer resin from liquid to solid state.

***I*:** Light intensity [mW/cm^2], is the power of light energy emitted from a light source.

***t*:** Curing time [sec.], is the time in which light being absorbed by the photopolymer resin that causes resin to cure.

***E_0*:** Exposure dose [mJ/cm^2], is the amount of light energy being exposed to the building surface of the photopolymer resin. $E_0 = I * t$.

Φ: Volume fraction [vol.%], in this paper, refers to the measurement of filler material concentration by volume in a composite photopolymer resin.

***E_c*:** Critical exposure dose [mJ/cm^2], the minimal amount of light energy required for the photopolymer resin to initiate curing.

1. Introduction

1.1. Problem description, significance, and research objective

Vat polymerization (VP) is a class of additive manufacturing (AM) processes that relies on selectively curing photosensitive polymer (photopolymer) resin using visible or ultraviolet (UV) light, in a layer-by-layer fashion, to create a specimen with three dimensional (3D) free-form geometry [1]. Figure 1 shows examples of several parts manufactured with different VP techniques. We describe the different VP techniques in detail in Section 1.3.

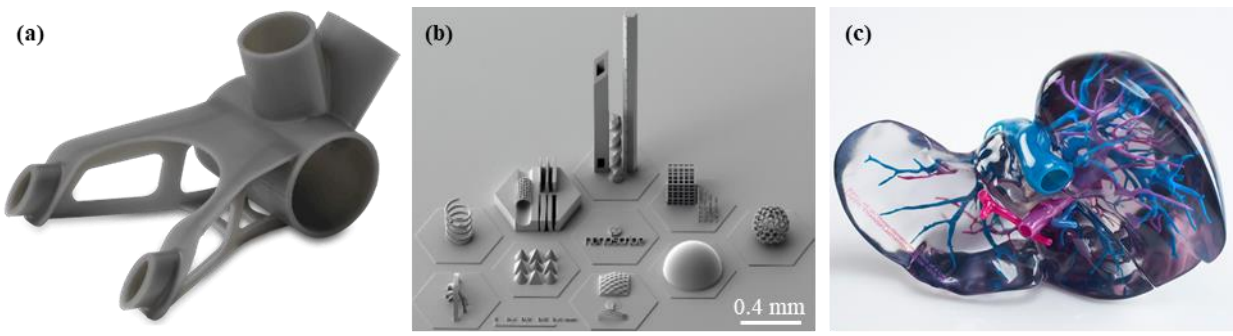

Figure 1: (a) A bike yoke prototype printed using stereolithography (SLA) [2]; (b) Nanoscale microstructures manufactured using two-photon polymerization (TPP) [3]; (c) A 3D liver medical model fabricated using PolyJet (PJ) multi-material printing [4]. These images are reprinted from their respective source of references. Source: (a) https://formlabs.com/3d-printers/form-3/ (b) https://3dprintingindustry.com/news/nanoscribe-introduces-quantum-x-a-two-photon-3d-printer-for-microoptics-157656/ (c) https://www.stratasys.com/en/guide-to-3d-printing/technologies-and-materials/polyjet-technology.

Photopolymer resin typically comprises a mixture of monomers, oligomers, and photo-initiators, and exposure to light initiates cross-linking of polymer chains, which modifies its properties and cures the liquid photopolymer resin into a solid material [5]. We describe the photopolymerization process in detail in Section 1.2.3. The curing characteristics of photopolymer resin determine the relationship between the VP process parameters and the layer thickness, lateral resolution, geometric accuracy, and surface quality of the 3D printed specimen.

Polymer matrix composite materials comprise a polymer matrix and filler material. The polymer matrix defines the free-form geometry of the part, whereas the properties of the matrix and filler materials, the interaction between them, and the spatial organization and orientation of the filler in the matrix determine its properties (e.g., structural, electrical, optical, multi-functional). Hence, to 3D print polymer matrix composites, filler materials are dispersed into the photopolymer resin, to modify the properties of the 3D printed composite material. Figure 2 shows examples of polymer matrix composite material specimens manufactured with VP, including parts with glass fiber filler (Fig. 2 (a)), and ceramic filler (Fig. 2 (b)).

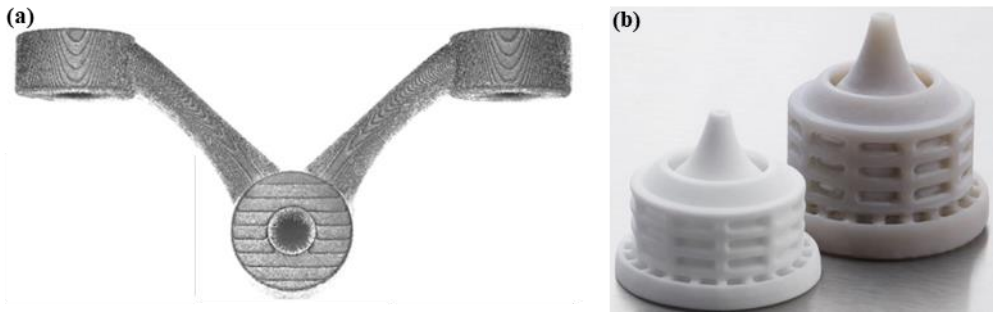

Figure 2: (a) A drone engine mount fabricated using glass fiber filled photopolymer resin [6]. Figure reprinted with permission. (b) Fire nozzles manufactured using ceramic photopolymer resin that can withstand high temperature [7]. Source: https://formlabs.com/materials/ceramics/. Images reprinted with permission.

The effects of the filler material on the properties of the 3D printed parts depends on its material properties, shape, size, volume or weight fraction, and spatial distribution (organization and orientation) [8]. Furthermore, dispersing filler material into the photopolymer resin changes its curing characteristics because the filler scatters and blocks light, which prevents it from penetrating into the photopolymer resin [9]. Additionally, it increases the viscosity of the photopolymer resin, which restricts the rate of polymerization [10]. Thus, this phenomenon becomes increasingly important with increasing filler fraction in the photopolymer resin. However, the ability to increase the filler fraction dispersed in the photopolymer resin is important for 3D

printing material specimens for specific engineering applications. Figure 3 illustrates applications of VP with high filler fraction, such as structural polymer matrix composite materials where the filler provides strength, stiffness, and wear resistance (Figure 3 (a)) [11–13], conductive polymer matrix composite material where the filler creates a percolated network (Figure 3 (b)) [14,15], or polymer matrix composite materials with ceramic filler for use in biological and high-temperature environments (Figure 3 (c)) [16–18]. Consequently, it is crucial to understand the curing characteristics of photopolymer resin as a function of filler fraction to enable VP of photopolymer resin with high filler fraction.

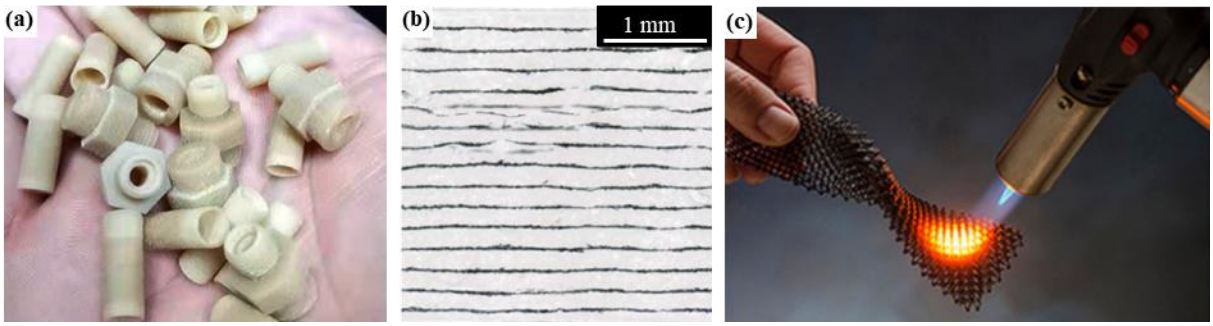

Figure 3: (a) Wear resistant bearings and nuts manufactured with 5% Kevlar filled photopolymer resin [13]; (b) Aligning carbon fiber in photopolymer resin using an acoustic focusing device [15]; (c) High temperature resistance SiC ceramic mesh [17]. Figures reprinted with permission.

The literature documents that dispersing filler in photopolymer resin can both enhance and inhibit photopolymer resin curing, depending on the properties of both the photopolymer resin and the filler [6,13,19,20]. For instance, studies show that dispersing translucent filler in photopolymer resin, such as nanosilica particles or glass fiber, increases the curing depth compared to virgin photopolymer [6,20]. In contrast, dispersing opaque filler in the photopolymer resin, such as metallic and ceramic particles, increases light absorption, which decreases the curing depth of the cured specimens compared to virgin photopolymer [19,21]. The filler fraction is another important parameter that affects the curing characteristics of photopolymer resin. Increasing the filler fraction

increases light intensity attenuation during curing, which prevent light from penetrating into the photopolymer resin, thus inhibiting curing [9]. Alternatively, the filler also scatters and redirects light back into the photopolymer resin, which enhances curing. Thus, these two competing phenomena determine the relationship between filler fraction and curing characteristics of the photopolymer resin.

The curing characteristics of photopolymer are often quantified using the curing depth, which is the thickness of the cured photopolymer specimen resulting from a specific light exposure dose [22], and the degree-of-cure, which quantifies the ratio of the fully cured versus total photopolymer resin content of the specimen [23]. Several research groups have employed different methods to study the curing characteristics of photopolymer resin with dispersed filler; (i) using mechanical testing, in which photopolymer curing relates to the mechanical properties of the specimen [13,19,20,24,25]; (ii) using spectroscopy techniques such as FTIR (Fourier-Transform InfraRed) [21,26–28] and Raman spectroscopy [29,30], which quantify the chemical composition and chemical bonds before and after curing; (iii) performing calorimetry measurements that relate the curing characteristics to heat generation during the exothermal curing reaction [31–33]; and (iv) implementing microscopy techniques that enable observing the material changes during the curing process [21,26,34,35]. Mechanical testing and thermal measurements average the curing measurement over the entire specimen, whereas Raman spectroscopy and microscopy average the curing measurement over a specific measurement location, which is typically substantially smaller than the specimen.

However, no studies methodically document the relationship between filler fraction, filler size, exposure dose, curing depth, degree-of-cure, and the surface topography of the 3D printed

specimens. Yet, this knowledge is important in the context of VP of photopolymer resin with dispersed filler, and especially with high filler fraction.

Thus, the research objective of this research is to experimentally determine the curing characteristics of diacrylate/epoxy photopolymer resin with dispersed glass microspheres. Specifically, we quantify the effect of exposure dose, filler fraction, and filler size, on the curing depth and the degree-of-cure in an open-source VP setup. We also evaluate the geometric accuracy and surface topography of the 3D printed specimens.

1.2. Photopolymer

Photopolymer takes the form of a liquid or paste, and comprises a mixture of monomers, oligomers, and photo-initiators. Exposure to light initiates cross-linking of polymer chains. Most photopolymers react with light in the ultraviolet (UV) wavelength range, but some can also react with light in the visible or even near-infrared (IR) range [36]. Figure 4 shows the wavelength spectrum of light, covering the UV to near-IR range.

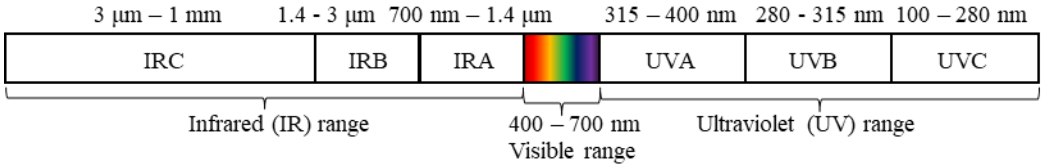

Figure 4: Wavelength spectrum of light, showing the IR, visible, and UV ranges [37,38].

1.2.1. Chemical composition of photopolymer

Monomers / oligomers: A monomer is a molecule that forms the basic building block of a polymer chain and determines the mechanical and chemical properties of the polymer [39]. An oligomer forms from a group of monomers, such as polyester acrylate (PEA), epoxy acrylates (EA), and urethane acrylates (UA) [1]. Monomers and oligomers chemically react to connect in the polymerization process and to form a polymer chain or network thereof. Examples of monomers include acrylate, ethylene, epoxy, and vinylether. Figure 5 shows an example of a diacrylate monomer (note that in Fig. 5 the C and H atoms are not explicitly indicated using letters).

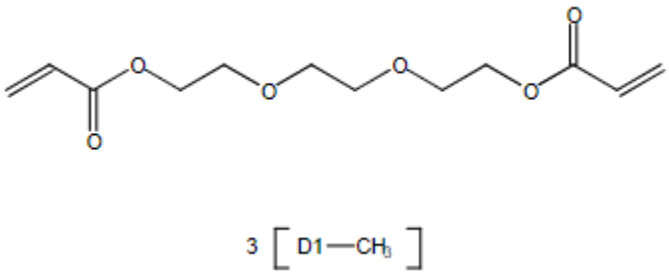

Figure 5: Example of a monomer: tripropylene glycol diacrylate ($C_{15}H_{24}O_6$) [40]. Source: CAS common chemistry database.

Photoinitiator: A photoinitiator is a chemical compound that decomposes into free radicals or cations after absorbing light energy. These species are highly reactive and can initiate the polymerization process by reacting with the monomers and oligomers [41]. Hence, a photoinitiator triggers the polymerization process when the photopolymer resin is exposed to light. Different photoinitiators are used for various types of photopolymer resin, depending on the specific light wavelength required to initiate photopolymerization, and on the chemical properties of the monomer [42]. Figure 6 shows an example of a photoinitiator.

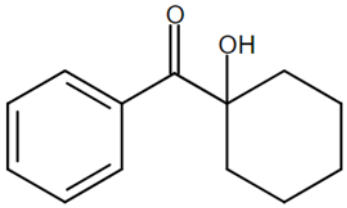

Figure 6: Example of a photoinitiator: hydroxycyclohexyl phenyl ketone, $C_{13}H_{16}O_2$ [43]. Source: CAS common chemistry database.

Other (optional) components: Other components, such as photoinhibitors and photostabilizers, which are not required in the polymerization process, can be part of the photopolymer resin to control the curing rate, prevent premature gelation, and improve the properties of the cured photopolymer [44]. Based on the specific reaction process, most of the commercially available photopolymers can be categorized as (i) free radical, (ii) cationic, and (iii) hybrid.

1.2.2. Types of photopolymers

Free radical: A free radical is a molecule that contains a single unpaired electron and, thus, is highly reactive with its environment [45]. In a free radical polymerization process, a monomer turns into a free radical after reacting with the photoinitiator, and it continues to react with other monomers to form a polymer chain. The free radical polymerization process usually shows a high curing rate compared to the cationic polymerization process and, therefore, it is commonly used. However, 3D printed parts made from pure free radical photopolymer usually experience significant volumetric shrinkage and geometric distortion, which is its major disadvantage [25,46,47]. Ethylene and acrylate are two examples of monomers that use free radical photopolymerization as its curing mechanism [48].

Cationic: A cationic photopolymer works based on the principle that the photoinitiator turns into a strong acid and releases cations such as hydrogen ions, after absorbing light energy [1]. These cations then react with the monomers and initiate the polymerization process. Compared to free radical photopolymerization, parts that are 3D printed using cationic photopolymers show less volumetric shrinkage, warpage, and geometric distortion than those printed with free radical photopolymers. Conversely, the curing rate of cationic photopolymer is slower, and it requires more light energy to initiate the curing process [25,49] than the free radical photopolymer. Epoxy and vinyl ether are two examples of monomers that use cationic photopolymerization [50].

Hybrid: A hybrid photopolymer comprises both free radical and cationic photopolymers. Such a hybrid photopolymer combines the advantages of both photopolymers, therefore showing high curing speed, low volumetric shrinkage and warpage [49,51]. The photopolymer resin that we have used in this work is a hybrid photopolymer that contains diacrylate and epoxy resin as its main components (see Section 2.2.1). Most photopolymer resins for hobbyist-type VP printers are of the hybrid type.

Figure 7 shows schematic examples of a free radical (Figure 7 (a)) and cationic (Figure 7 (b)) monomer, and Table 1 summarizes their properties.

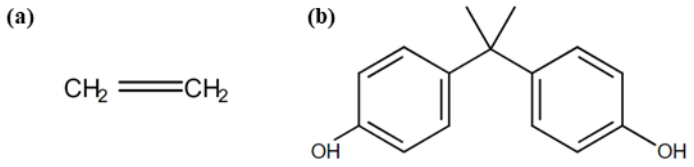

Figure 7: Examples of (a) a free radical monomer (ethylene, C_2H_4) [52], and (b) a cationic monomer (bisphenol A, an important component in the epoxy resin, $C_{15}H_{16}O_2$) [53]. Source: CAS common chemistry database.

Table 1: Properties of different types of photopolymers.

Type	Polymerization mechanism	Curing speed	Shrinkage control
Free radical	Combination of monomers and free radicals released from photoinitiator.	Fast	Inferior
Cationic	Combination of monomers and hydrogen cation released from photoinitiator.	Slow	Excellent
Hybrid	Blend of free radical and cationic polymerization.	Medium	Good

1.2.3. Photopolymerization process

Photopolymerization is the chemical reaction that involves cross-linking small size molecules (monomers and oligomers) into a large molecular chain or network (polymer chain) after exposure to light of a specific wavelength [54]. The size of a polymer chain contains only a few, or as many as thousands of monomers. The polymerization process is important in the context of VP because it determines the properties of the resulting material. In addition, tailoring the degree of polymerization allows controlling the volumetric shrinkage of the part, and ensures geometric accuracy. We describe the photopolymerization process in three stages: initiation, propagation, and termination [39].

Initiation: During the initiation stage, a photoinitiator molecule is excited by the absorption of light of a specific wavelength, which transforms it into a reactive species by undergoing a series of complex chemical reactions. The molecule either turns into a free radical that is highly reactive in the free radical polymerization process, or it turns into a strong acid that releases a highly reactive hydrogen cation in the cationic polymerization process. These species are capable of initiating the polymerization reaction by attracting hydrogen or carbon atoms from the double C=C bond of the monomer or oligomer, which combine to become the “head” of the polymer chain [23].

Propagation: During the propagation, the large radical (the "head") that forms during the initiation stage reacts with other monomers and oligomers, which results in a propagation of the polymerization reaction [39].

Termination: The polymerization reaction terminates with either of the following three situations: end-by-end connection between two polymer chains (recombination), donation and acceptance of ions between two chains to reach a neutral state (disproportionation), or when all reactive species are trapped within a solidified region in which they can no longer propagate (occlusion) [39]. The process also terminates when all reactive species or monomers have been consumed, so that the reactions cannot continue.

Figure 8 schematically illustrates the initiation and propagation stages for a free radical (with 2-hydroxyethyl acrylate) [23] (Figure 8 (a)) and cationic [55] (Figure 8 (b)) photopolymerization process.

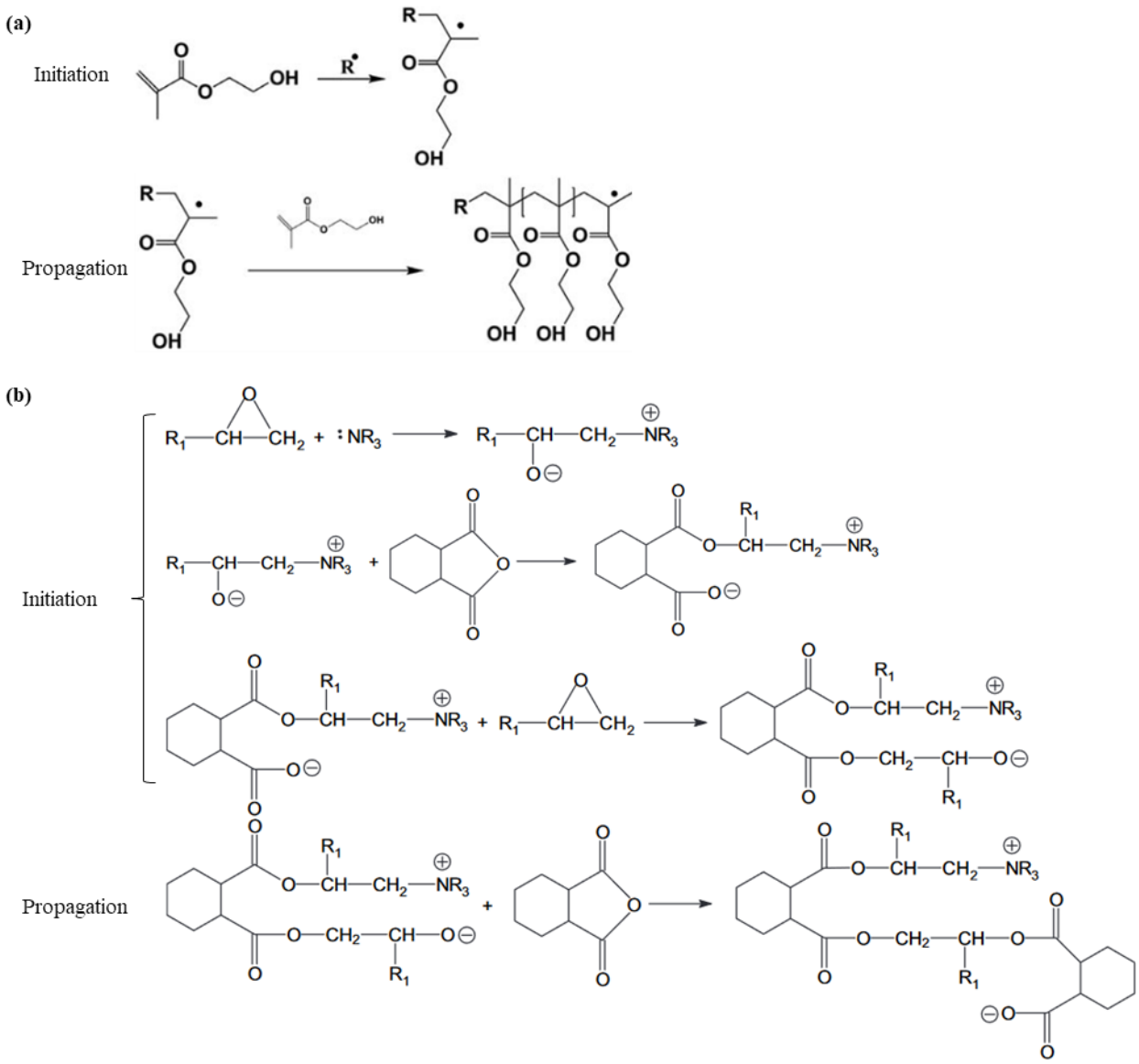

Figure 8: Schematic of the initiation and propagation stage for a (a) free radical [23], and (b) cationic photopolymerization process [55]. Figures reprinted with permission.

1.2.4. Loss of light intensity: Beer-Lambert law

The Beer-Lambert law describes the exponential loss of light intensity as a function of the penetration distance z into a medium [56,57], which is relevant to photopolymer curing in a VP setup, i.e.,

$$P_z = P_0 e^{-\frac{z}{D_p}}, \tag{1}$$

where P_z and P_0 represent the power of the light illumination at penetration depth z and at the surface of medium (where the light is incident), respectively. D_p is the depth at which the light intensity decreases to below P_0/e [22].

One of the most common applications of the Beer-Lambert law in terms of photopolymer resin curing in a VP setup, is the characterization of a working curve, which shows the relationship between the light exposure dose incident to the photopolymer resin E_0 and the curing depth C_d of the cured photopolymer specimen [58]. The working curve is expressed as

$$C_d = D_p \ln\left[\frac{E_0}{E_c}\right]. \tag{2}$$

Here, E_c is the so-called "gel point", which is the critical light exposure dose to initiate the phase transition of photopolymer resin from liquid to solid [57]. Figure 9 (a) schematically illustrates the Beer-Lambert law, demonstrating that the light intensity I decreases exponentially from the incident light intensity I_0, with increasing penetration depth z into the medium, resulting in a cured photopolymer with curing depth $z = C_d$. Figure 9 (b) shows an example of the working curve that characterizes the relationship between the curing depth C_d and light exposure dose E_0, typically presented as a semi-logarithmic plot. The working curve is important in the context of VP because it describes the photopolymer curing characteristics.

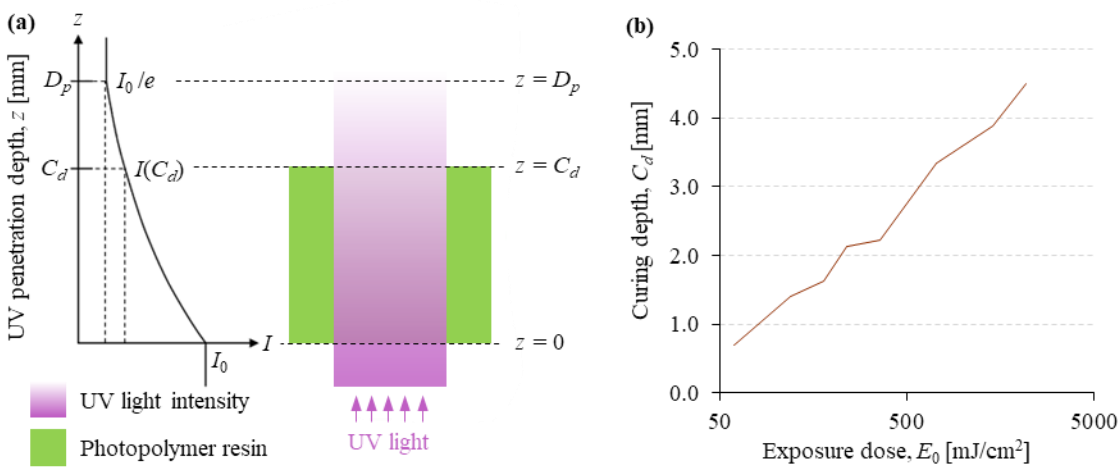

Figure 9: (a) Schematic illustrating the Beer-Lambert law, showing exponential light intensity attenuation with increasing penetration distance into the medium [57]. Figure reprinted with permission. (b) an example of the working curve (*x*-axis showing in log-scale) that defines the curing characteristics of the photopolymer resin.

1.3. VP 3D printing technologies

Many researchers have studied different aspects of VP 3D printing technology [11,13,59,60]. Several different VP techniques exist, with research and improvements geared towards enhancing printing performance and quality, lowering cost, or introducing novel features such as multi-material printing. In this section, we describe common types of VP technologies, and we discuss their advantages and limitations.

Stereolithography (SLA): SLA is the first AM technology that was patented in 1986 by Charles Hull [49]. Figure 10 (a) schematically illustrates the working principle of an SLA printer. It uses a laser beam, directed by a rotating mirror, to trace and selectively cure the geometry of a part within a container (vat) filled with photopolymer resin. A build plate sinks into the photopolymer resin vat and leaves a layer thickness of photopolymer resin between the window of the vat and the build plate, for the laser to selectively cure. After the laser traces the contours and features of a layer, i.e., a “slice” of the 3D part, the build plate rises (or lowers, depending on the

actual configuration of the 3D printer), which allows liquid resin to flow into the gap between the window and the previously cured layer. Subsequently, the laser beam traces the part geometry to cure the next layer, and the process repeats itself in a layer-by-layer fashion, until the entire 3D part is finished. The use of a short wavelength laser in an SLA printer affords the ability to use many photopolymer resin types, including free radical, cationic, and hybrid resin. Conversely, it shows slower printing speed and spatial resolution than other VP techniques (see further in this section) due to limited laser tracing speed and the laser spot size. Figure 10 (b) shows a commercially available SLA printer (Form 3+, FormLabs Inc., MA, U.S.A.) [2] that uses the SLA technology to 3D print parts.

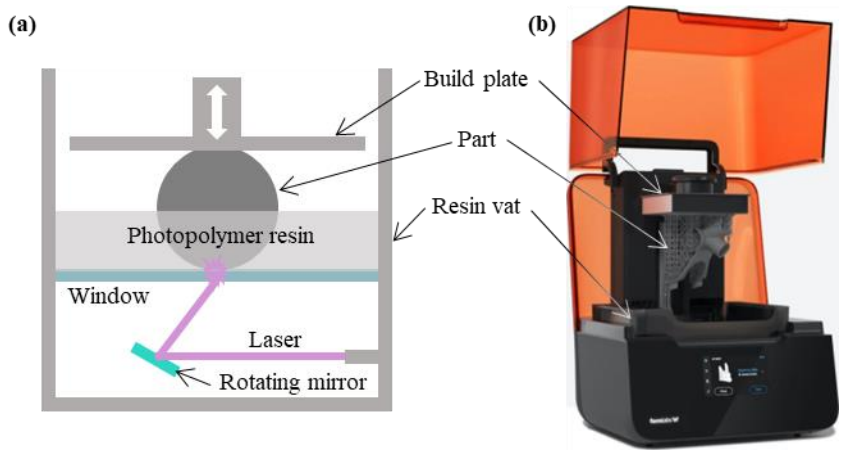

Figure 10: (a) Schematic illustration of an SLA printer, showing a laser beam directed by a rotating mirror and, (b) an example of a commercially available SLA 3D printer (Form 3+, FormLabs Inc., MA, U.S.A.) [2]. Image source: (b) https://formlabs.com/3d-printers/form-3/.

Two-Photon Polymerization (TPP): TPP is a VP technology that instead of using one high energy laser, like in SLA, uses two low energy laser beams (typically in the near-infrared region). Combined, they provide the same amount of energy as one high energy laser in SLA to cure the photopolymer resin. Hence, the curing only occurs at the focal point where the two laser beams intersect. As a result, the laser beams can penetrate deep into the photopolymer resin

without unintentionally curing photopolymer resin other than the intended curing spot. Consequently, there is no need for a moving build plate and, instead, 3D printing occurs inside the resin vat by scanning the focal point where two laser beams intersect along the 3D geometry of the part [58]. Figure 11 shows a schematic of a TPP printer. TPP achieves a higher printing resolution than SLA, extending down to the sub-micron level [61] and, thus, it is typically of interest to applications that involve microfabrication [62]. However, we note that the tool path generation (3D rasterization) can be time-consuming, which is a disadvantage of TPP compared to other VP technologies [58].

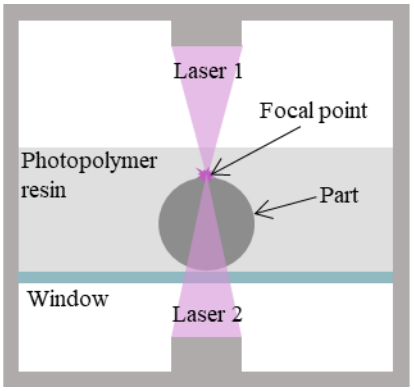

Figure 11: Schematic of a TPP 3D printer. Curing only occurs at the focal point where two lasers intersect.

Digital Light Processing (DLP): The DLP VP technique was enabled by the development of the Digital Micromirror Device (DMD) by Dr. Larry Hornback in 1987, and later commercialized by Texas instruments in 1996 [63]. Figure 12 shows a schematic of a DLP printer (Figure 12 (a)), and an example of a commercial DLP 3D printer (mUVe 3D, Grand Rapids, MI, USA) (Figure 12 (b)) [64]. DLP uses a digital light projector as the light source to project a virtual mask onto the build plate to cure the photopolymer resin in a layer-by-layer fashion. Since the light source projects an entire plane, which represents a layer or "slice" of the 3D part, on the window of the resin vat, DLP cures an entire layer at once. Hence, the printing speed of DLP

exceeds that of SLA and TPP. Additionally, it retains the high resolution afforded by the SLA technology. However, the printing area is limited by the focus area and field-of-view of the DLP projector [49].

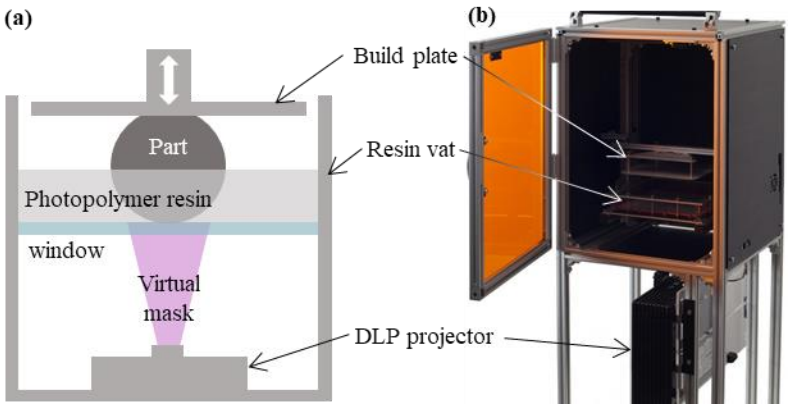

Figure 12: (a) Schematic illustration of DLP printer, showing the virtual mask projected onto the window using a DLP projector and, (b) an example of DLP 3D printer (mUVe 3D, Grand Rapids, MI, USA) [64]. Image source: (b) https://www.muve3d.net/press/product/muve-3d-dlp/.

Continuous Liquid Interface Production (CLIP): The CLIP technique originated in 2015 from Carbon 3D Corp. [65]. The photopolymer resin curing methodology of CLIP is the same as that of a DLP printer, but the window of the resin vat is replaced by a window that is permeable to oxygen. This oxygen permeable window allows both light and oxygen to pass though, which maintains a liquid layer of photopolymer resin between the build plate and the window, often referred to as the "dead zone", while the photopolymer cures against the build plate. Hence, the main advantage of this technology is that it enables continuous 3D printing, without discrete layers. As a result, CLIP provides a faster printing speed and better adhesion between layers than parts 3D printed with DLP and SLA [66]. Figure 13 shows a schematic of a CLIP 3D printer (Figure 13 (a)) and a picture of a commercially available CLIP 3D printer (Carbon 3D Corp., CA, USA) (Figure 13 (b)) [67].

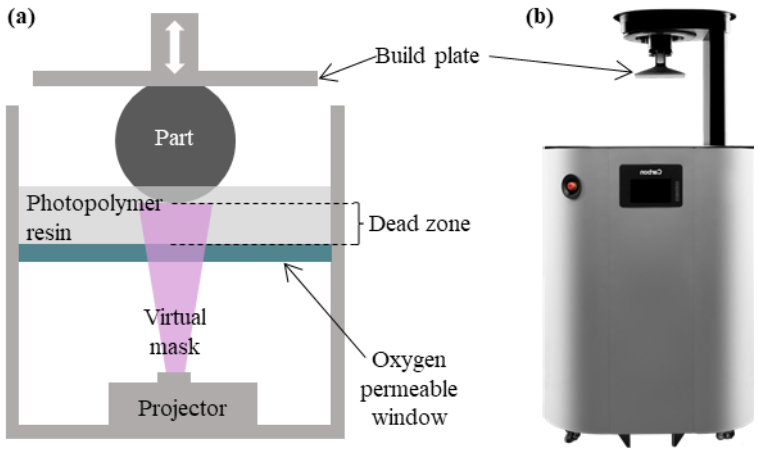

Figure 13: (a) Schematic illustration of CLIP technology, illustrating the dead zone between the oxygen permeable window and the build plate and, (b) an example of CLIP 3D printer (Carbon 3D Corp., CA, USA). Image source (b): https://www.carbon3d.com/products/m1-3d-printer.

Liquid Crystal Display (LCD): LCD is a newly adopted and affordable alternative VP technology to DLP. The principle of LCD is similar to DLP but uses a UV light as light source (usually in 405 nm wavelength) and an LCD screen as virtual mask instead of using a DLP projector. Liquid crystal molecules in the display panel rotate when applying an electric current through them, which allows light to either pass through or be blocked, thus creating a virtual mask for selective UV exposure of the photopolymer resin [68]. Consequently, the part is 3D printed in a layer-by-layer fashion, identical to the DLP technology. The resolution depends on the resolution of the LCD screen. Advancements in LCD screen technology have reduced the cost of equipment while maintaining high printing speed and resolution, rendering LCD VP more affordable and increasingly popular in the consumer market [69]. However, aging of liquid crystals in the display panel causes light leakage and, thus, it requires more frequent maintenance than a DLP printer [49]. Figure 14 shows a schematic of an LCD VP device (Figure 14 (a)) and a picture of a LCD 3D printer (Anycubic Photon Mono X, Anycubic 3D Inc., Shenzhen (China)) [70] (Figure 14 (b)).

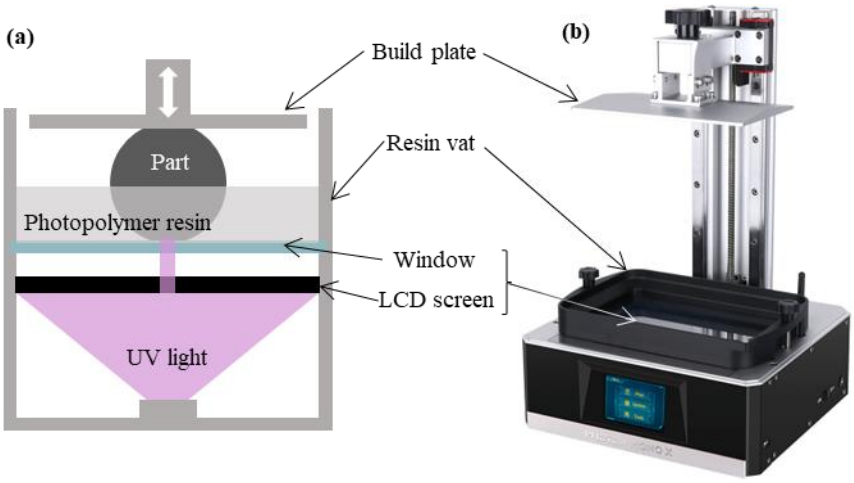

Figure 14: : (a) Schematic illustration of LCD printer, showing that the LCD screen masked out the printing geometry by UV light and, (b) an example of LCD 3D printer (Anycubic Photon Mono X, Anycubic 3D Inc., Shenzhen (China)) [70]. Image source (b): https://www.anycubic.com/products/photon-mono-x-resin-printer.

UV-assisted Direct Ink Writing (UV-DIW): A UV-DIW printer uses a print head that comprises an extruder nozzle to deposit photopolymer resin onto a build plate, prior to curing it using UV light. The print head includes a UV light source that moves along with the extruder nozzle to cure the extruded photopolymer resin, until the entire part is printed by stacking the photopolymer in a layer-by-layer fashion. One advantage of UV-DIW is its compatibility with a broad range of functional materials. However, one must control the viscosity of the photopolymer resin carefully to allow flow in the nozzle with rapid viscosity reconstruction after it exits the nozzle to maintain geometric accuracy [71]. Figure 15 shows the schematic of a UV-DIW printer.

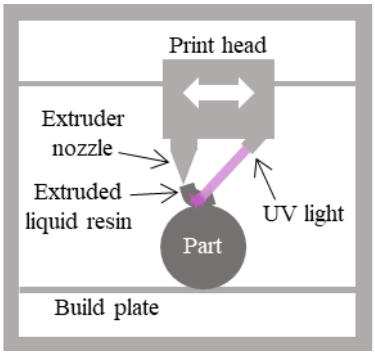

Figure 15: Schematic of a UV-DIW printer, showing that the UV light cures the liquid resin extruding from the extruder nozzle on the build plate while the printhead moves.

MultiJet / PolyJet (MJP / PJ): MultiJet and PolyJet technology, by 3D Systems Corp and Stratasys Ltd, respectively, are similar VP techniques. Figure 16 shows a schematic of the MJP/PJ technique (Figure 16 (a)) and an example of a PolyJet printer (J850 pro, Stratasys Ltd., Rehovot, Israel) [72] (Figure 16 (b)). Similar to an inkjet printer, both MJP and PJ printers comprise a printhead with multiple nozzles and an integrated UV light source. The nozzles disperse photopolymer resin onto a build plate, which the UV light source subsequently cures as the print head moves across. When a layer is completed, the build plate lowers and the process repeats until the entire 3D part has printed. The main distinctions between the MJP and PJ technologies are the types of support materials and post-processing methods they use. MJP printing employs paraffin wax as the support material, which can be removed by melting in an oven [73], whereas PJ printing uses a combination of support materials (Propylene, Acrylic monomer, Polyethylene, and Glycerin) that can be removed by high-pressure waterjet or a chemical bath [4,74]. MJP and PJ stand out among other VP technologies because of their ability to 3D print multiple materials simultaneously with high printing resolution (approximately 16 μm) [75]. However, the cost of the equipment in addition to the need to use low-viscosity photopolymer resins have limited their widespread use compared to other VP technologies we have previously described [49].

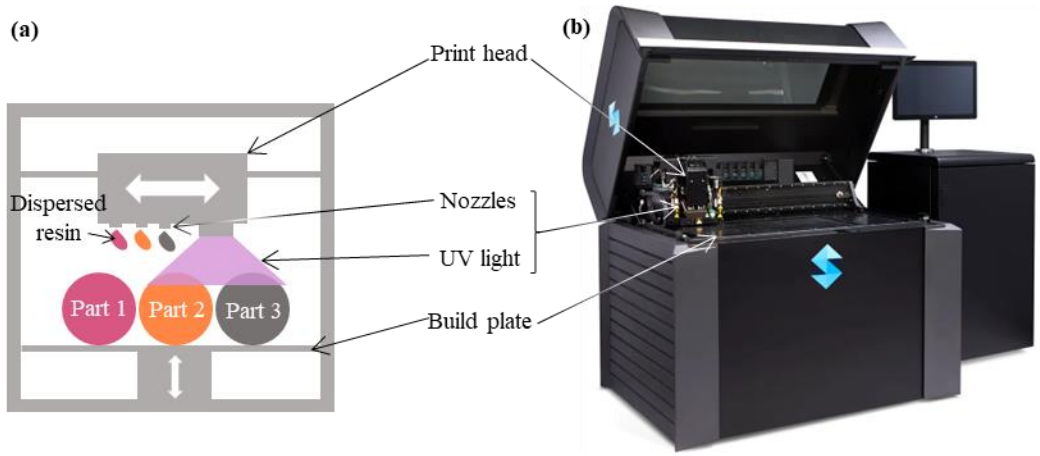

Figure 16: (a) Schematic of an MJP/PJ 3D printer, showing its capability to print multiple materials extruded from the nozzles and cured with UV light while the print head moving, and (b) a PolyJet 3D printer (J850 pro, Stratasys Ltd., Rehovot, Israel) [72]. Image source (b): https://www.goengineer.com/3d-printing/polyjet

Computed Axial Lithography (CAL): CAL was developed in 2017 jointly by the University of California, Berkeley and Lawrence Livermore National Laboratory [76]. CAL utilizes a digital light projector to project computed tomography (CT) images of a 3D part onto a rotating photopolymer resin vat, which enables 3D printing the entire part within seconds, with a resolution of approximately 80 μm [58]. CAL shows faster printing speeds and better bonding of the cured photopolymer material to itself, in comparison to other VP technologies, as a result of the elimination of discrete printed layers. However, this technique requires highly reactive, low absorption, and low viscosity photopolymer materials, which may not be suitable for high filler volume fraction composite photopolymer resins [58]. CAL is not yet commercially available. Figure 17 illustrates the CAL platform, showing its working principle (Figure 17 (a)), a schematic of the CAL printer (Figure 17 (b)), a time-laps of the photopolymer curing into a 3D part (Figure 17 (c)), and several examples of 3D printed parts (Figure 17 (d)-(g)) [77].

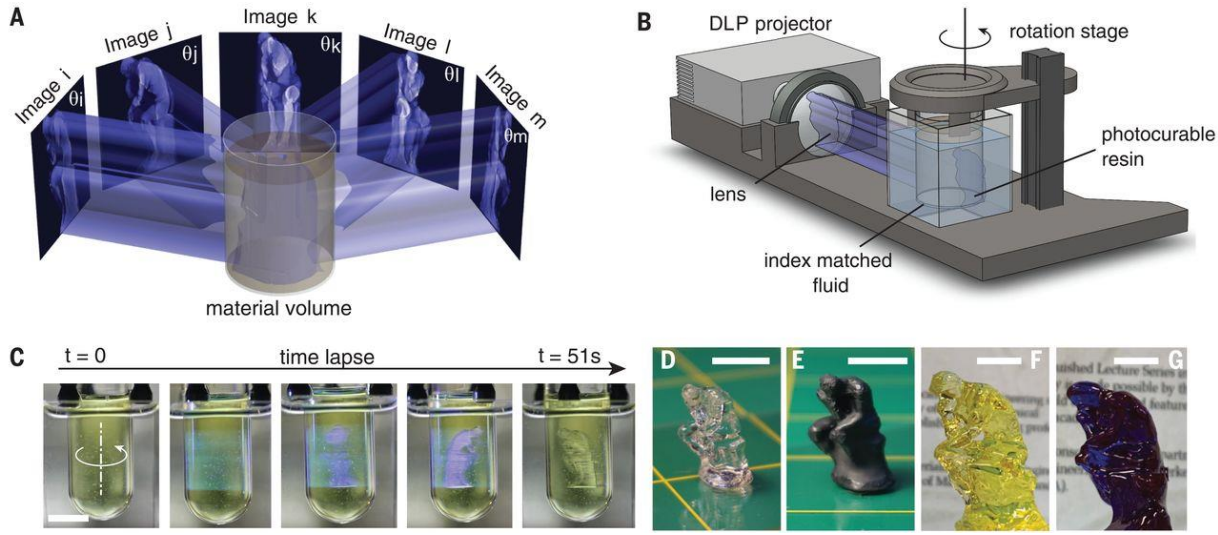

Figure 17: (a) The specimen is 3D printed by projecting computed tomographic images in a rotating photopolymer resin vat. (b) Schematic of a CAL printer. (c) Time-lapse of the process of the specimen curing. (d) The 3D printed specimen from (c). (e) 3D printed specimen with paint. (f) Specimen 3D printed at larger scale (40 mm tall). (g) Specimen 3D printed using an opaque resin. Scale bar: 10mm. From [77]. Reprinted with permission from AAAS.

In summary,

Table **2** provides an overview of the characteristics of the different VP technologies we describe in this chapter. We note that not all VP technologies are suitable for using a mixture of photopolymer resin and filler material, including MJP/PJ, UV-DIW, and CAL, which pose specific requirements on the properties of the photopolymer resin.

Table 2: Summary of the characteristics of different VP technologies.

Technique	Schematic	Printing speed	Printing resolution	Advantages	Disadvantages
SLA	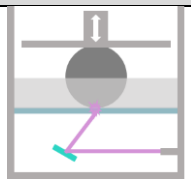	Fair	Fair	Wide range of material support.	Resolution and printing speed are limited by laser size and scanning speed.
TPP	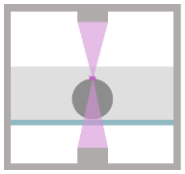	Fair	Excellent	Sub-micron resolution makes it suitable for microscale fabrications.	3D rasterization process can be very time consuming.
DLP	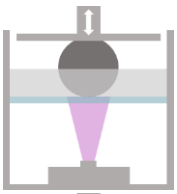	Good	Very good	Technique is the most mature among all.	- High equipment cost due to patent issue. - Limited printing size.
CLIP	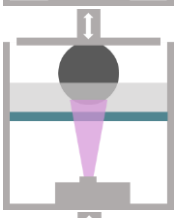	Excellent	Very good	Excellent printing speed and improved interlayer adhesion.	- High equipment cost. - Limited printing size.
LCD	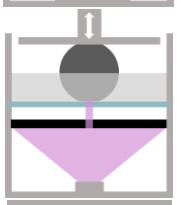	Good	Good	Most affordable technique among all.	Requires frequent equipment maintenance.
UV-DIW	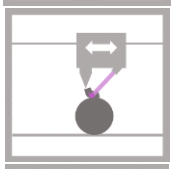	Fair	Good	Wide range of material support.	Imposes specific requirements for resin viscosity.
MJP / PJ		Good	Excellent	Capable of multi-material printing with excellent resolution.	Imposes specific requirements for resin viscosity.
CAL	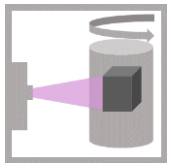	Excellent	Fair	- Fastest printing speed among all VP techniques. - Improved interlayer adhesion.	- Not yet commercialized. - Imposes specific requirements for resin viscosity, reactivity, and absorbance.

1.4. Curing characterization techniques

Different techniques exist to characterize curing of photopolymer resin.

1.4.1. Mechanical property measurements

Since the mechanical properties of cured photopolymer depend on the curing process, measuring the mechanical properties of cured specimens allows characterizing and quantifying the curing characteristics. Techniques to characterize mechanical properties include:

Strength and stiffness test: A Dynamic Mechanical Analysis (DMA) machine can be used to determine the stress-strain curve of a material, including the Young's modulus, ultimate tensile strength, yield stress, [24,31,78], and hardness [33,79,80].

Rheology: Rheology is the study of flow of viscous liquids, and allows determining viscosity, and viscoelastic properties of photopolymer [81–83].

Water contact angle (WCA): WCA or "wettability" reveals the hydrophobicity of the photopolymer, which relates to its curing characteristics [33,84].

Geometric dimensions: Curing depth [13,20,81], volume shrinkage [57,85,86], and geometric accuracy [6,85,87], which are the important properties that determines the printing quality of a printed part.

1.4.2. Thermal property measurements

Thermal experiments characterize photopolymer curing by means of measuring the change in material properties during the exothermal curing reaction. Such experiments shed light on

thermal stability, glass transition temperature, and coefficient of thermal expansion of the material. These experiments include:

Differential Scanning Photo-Calorimetry (Photo-DSC): Photo-DSC measures the heat flow during the exothermal curing reaction, and is commonly used to characterize photopolymer curing [88–90].

Thermogravimetric and thermomechanical analysis (TGA and TMA): TGA and TMA measures the change of the weight and mechanical properties with changing temperature of the photopolymer resin [24,32,33].

1.4.3. Spectroscopy

Spectroscopy is a non-destructive evaluation method to quantify the curing characteristics of photopolymer resins. It provides information about changes of the molecular structure and composition of the photopolymer. Spectroscopy techniques include:

Fourier Transform Infrared (FTIR) spectroscopy: FTIR spectroscopy measures the infrared absorbance spectrum of the photopolymer and quantifying the relative magnitude of different types of molecular bonds in the photopolymer [21,26,27,82].

Raman spectroscopy: Raman spectroscopy relies on inelastic scattering of photons, i.e., so-called “Raman scattering”, to detect the change in structure of molecules before and after curing. Raman spectroscopy also determine the composition of a photopolymer material, based on the difference in wavelength between incident and scattered light [29,30,55].

UV-Vis-IR Spectroscopy: This technique is similar to FTIR but measures absorbance in UV, visible, and infrared range [22,35,91], rather than infrared absorbance only.

Brillouin spectroscopy: This technique is Similar to Raman spectroscopy, but instead detects the inelastic scattering of photons at lower frequency shifts (Brillouin spectra) than Raman spectroscopy, which quantifies elastic properties of the material [92].

Nuclear Magnetic Resonance (NMR) spectroscopy: NMR detects the chemical structure of organic compounds by applying an external magnetic field to measure the nuclear spin energy states [24,93,94].

1.4.4. Microscopy and imaging

Microscopy and imaging techniques are used to visually examine the microstructure and surface topography of the cured photopolymer resin. Microscopy and imaging techniques include:

Scanning Electron Microscopy (SEM): SEM visualizes the specimens using a high energy electron beam [48,95–97].

Confocal Microscopy: Confocal microscopy is an optical microscopy technique that produces high quality images of a specimen by combining multiple images captured with different focal planes and filtering out the out-of-focus sections of each image [22,98].

X-ray Computed Tomography (X-ray CT): An X-ray CT detects the X-ray beam that transmits through the sample and reconstructs 3D images based on multiple, differently oriented images [9,99].

2. Materials and methods

2.1. Experimental setup

Figure 18 (a) shows the open-source DLP VP platform we use in this work (mUVe 3D, Grand Rapids, MI (USA)) [64]. The platform comprises a photopolymer resin vat with a 6 mm thick acrylic window that separates the photopolymer resin from the light source, and a digital light projector (ViewSonic PJD7820HD) equipped with a 210 W metal halide lamp that projects a combination of visible and UV light (300 – 730 nm wavelength) to selectively cure the photopolymer resin. Additionally, mini photopolymer resin vats located within the main resin vat afford the ability to simultaneously cure multiple specimens with different filler volume fraction. The mini resin vats have a 1.5 mm thick acrylic window covered with a thin fluorinated ethylene propylene (FEP) film that provides chemical stability, and oxygen permeability gives it non-stick properties to release the cured photopolymer resin from the window. We calibrate the projector to focus within the plane of the FEP film of the mini resin vats to ensure maximum accuracy of the 3D printed specimens. Figure 18 (b) illustrates the geometry of the material specimens we 3D print in this work, i.e., the Virginia Tech “VT” logo, which contains internal and external features, straight lines, and sharp corners and, thus, allows a qualitative and quantitative assessment of the geometry features after curing, as a function of the filler fraction and VP process parameters.

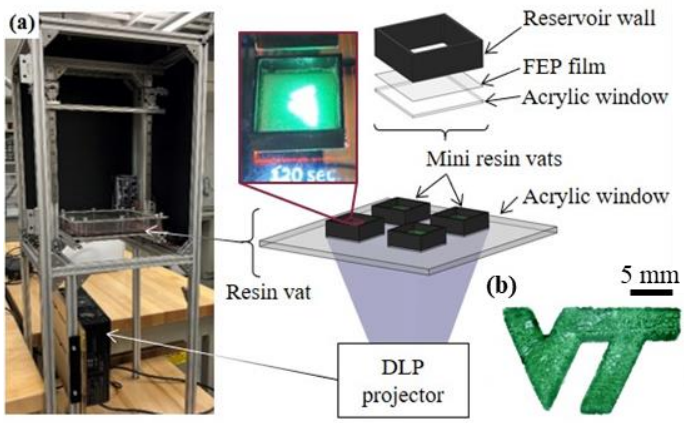

Figure 18: (a) Photo and schematic of the DLP VP platform, showing the setup with resin vat and acrylic window. Several mini resin vats with acrylic window and FEP film and (b) a typical material specimen we 3D print in this work (Virginia Tech "VT" logo).

2.2. Materials

2.2.1. Photopolymer resin

We use a consumer-grade photopolymer resin specifically formulated for DLP VP with a density of ρ_{resin} = 1.05-1.25 g/cm^3 (Anycubic standard UV resin translucent green, Anycubic 3D Inc., Shenzhen (China)), which consists of 60% epoxy resin, 35% tripropylene glycol diacrylate ($C_{15}H_{24}O_6$), and 5% hydroxycyclohexyl phenyl ketone ($C_{13}H_{16}O_2$) [100]. The epoxy resin is a cationic photopolymer, tripropylene glycol diacrylate is a free radical photopolymer, and hydroxycyclohexyl phenyl ketone is a photoinitiator that initializes curing after absorbing light. Table 3 summarizes the descriptions and diagrams of these chemicals.

Table 3: Name, descriptions, and diagrams of the chemical composition of the photopolymer we use in this study. Source: PubChem (National Library of Medicine) [101], and CAS Common Chemistry database (A division of the American Chemical Society) [40,43].

Name		Description	Diagram
Epoxy resin (cationic photopolymer)	**Bisphenol A ($C_{15}H_{16}O_2$ or $(CH_3)_2C(C_6H_4OH)_2$)**	Bisphenol A (BPA) is a colorless solid that is used in the synthesis of commercial plastics, including polycarbonates and epoxy resins, which are used for a wide variety of consumer goods.	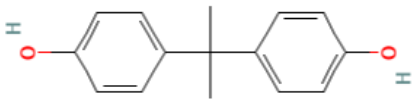
	Epichlorohydrin (C_3H_5ClO)	Epichlorohydrin is a volatile and flammable, clear, colorless, liquid… is used in the manufacture of epoxy resins, synthetic glycerin, and elastomers.	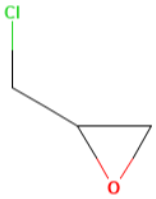
	Acrylic acid ($C_3H_4O_2$ or CH_2=CHCOOH)	Acrylic acid is a colorless liquid with a distinctive acrid odor. It is used in the manufacture of plastics, paint formulations, and other products.	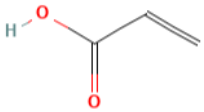
Tripropylene glycol diacrylate ($C_{15}H_{24}O_6$)		This is a type of free radical monomer which can be cross-linked by free radical polymerization process.	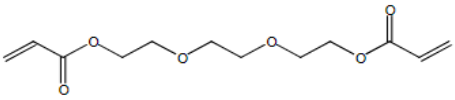
Hydroxycyclohexyl phenyl ketone ($C_{13}H_{16}O_2$)		This is a type of photoinitiator which reaches with the monomers and initiates polymerization process after absorbing photons.	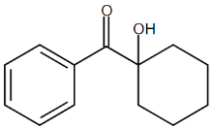

2.2.2. Filler material

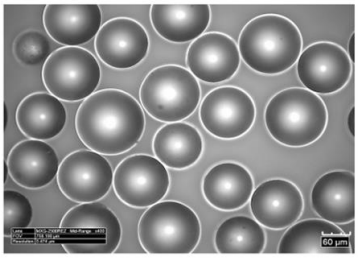

Typical Properties:

Appearance: Solid soda-lime glass microspheres with colorless in powder form.

Chemical Composition (Wt %):

SiO_2	Al_2O_3	CaO	MgO	Na_2O	Fe_2O_3
67-75	0-5	6-15	1-5	10-20	< 1

Physical Properties

Specific Gravity …. 2.4 - 2.6 (g/cm^3)
Bulk Density …. 1.5 - 1.6 (g/cm^3)
Softening Temperature …. 650 °C
Coefficient of Thermal Expansion …. 90 x 10^{-7} /°C (30-300 °C)
Compression Strength …. 40,000 (psi)
Index of Refraction …. 1.50 – 1.52 (n_D)

Figure 19: Data sheet showing the chemical composition and physical properties of the solid microsphere filler. Source: https://www.novumglass.com/.

We select translucent solid glass microspheres as filler material, with bulk density of ρ_{filler} = 1.5 - 1.6 g/cm^3 and refractive index of 1.50 - 1.52. Figure 19 shows the datasheet of the glass microspheres (Novum Glass LLC, Rolla, MO (USA)) [102]. We use two different size distributions with diameters 38 - 45 µm (small) and 212 - 250 µm (large), to study the effect of filler size on the curing characteristics of the photopolymer resin. The filler concentration is expressed as volume fraction Φ (vol.%), which relates to the weight fraction Φ_m (wt.%) as

$$\Phi = \frac{\Phi_m}{\Phi_m + (1-\Phi_m)\dfrac{\rho_{filler}}{\rho_{resin}}}, \qquad (3)$$

where ρ_{filler} = 1.55 g/cm^3 and ρ_{resin} = 1.15 g/cm^3 represent the average bulk density of filler and resin, respectively. We prepare mixtures of photopolymer resin and filler with Φ_m = 0, 15, 30, 45, and 60 wt.%, which corresponds to filler volume fractions Φ = 0, 12, 24, 38, and 53 vol.%, respectively. Additionally, we consider monodisperse mixtures that contain a single particle size distribution (small or large) and polydisperse mixtures with half of both small and large particle size distributions. Virgin photopolymer resin with $\Phi_m = \Phi = 0$ serves as benchmark throughout this work. Figure 20 shows the photopolymer resin and glass microspheres filler.

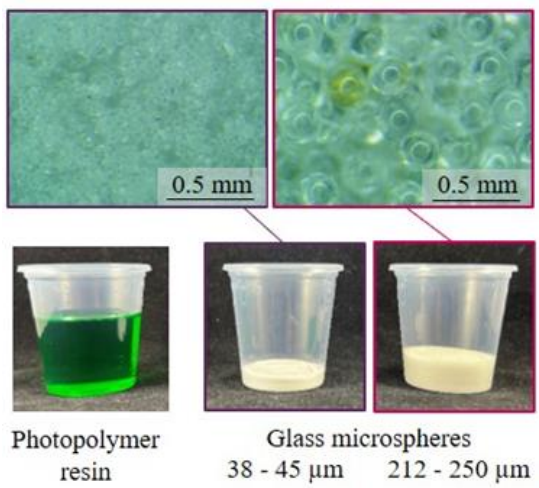

Figure 20: Translucent green photopolymer resin and solid glass microspheres (with optical microscopy images) that are used in this study.

2.2.3. Exposure dose E_0

The exposure dose E_0 in mJ/cm^2 is the amount of light energy incident to the photopolymer resin, measured at the curing surface of resin, during the photopolymerization process. The exposure dose

$$E_0 = I \times t \,, \tag{4}$$

where I is the light intensity in mW/cm^2 and t is the curing time in seconds [57]. We measure the light intensity I = 12 mW/cm^2 at the inside of the acrylic window of the mini resin vats using a UV light meter (Lingshang LLC LS126A, Shenzhen (China)), and it remains constant for all experiments in this work. Thus, we change the exposure dose using different curing times t = 5, 10, 15, 20, 30, 60, 120, and 180 seconds, which corresponds to E_0 = 60, 120, 180, 240, 360, 720, 1440, and 2160 mJ/cm^2. The choice of curing times t and corresponding exposure doses E_0 allow monitoring photopolymer resin curing within short (5 s) time intervals during the first 20 s when the resin cures fast, and within large (> 10 s) time intervals after the first 20 s, when curing slows down because solid, cured photopolymer with filler increasingly inhibits light from penetrating into the remaining liquid photopolymer resin. We note that we include exposure dose values in this work that are substantially larger than those typically used during VP, to obtain a complete picture of the curing characteristics of the photopolymer resin. Considering a full-factorial study of filler volume fraction Φ (five treatment levels), filler size distribution (three treatment levels: small, large, 50/50 mix), and exposure dose E_0 (eight treatment levels), with three replications of each experiment, we manufacture a total of 8 x 3 (Φ = 0%) + 4 x 3 x 8 x 3 (Φ > 0%) = 312 specimens.

2.3. Characterization methods

2.3.1. Curing depth, C_d

The curing depth C_d in mm is the thickness of a single cured layer of photopolymer resin, following a specific light exposure dose E_0. In this work, we measure the curing depth of each specimen at different four locations along the outer geometry of the “VT”-shaped specimen using

digital calipers, and we calculate the average thickness. Figure 21 (a) shows a photograph of the calipers we have used for this measurement, whereas Figure 21 (b) shows a typical "VT" specimen, indicating the four locations (1)-(4) where we measure its thickness. Calipers are inexpensive, fast, and reliable, even though more sophisticated methods have recently become available [83]. The curing depth C_d relates to the exposure dose E_0, and the critical energy to initiate the polymerization process E_c, often approximated using the Beer-Lambert Law. The curing depth data for all specimens is available in Appendix A.

Figure 21: (a) Digital calipers to measure the thickness of specimen; (b) thickness acquired at four locations (1) – (4).

2.3.2. Degree of Cure, DoC

The degree of cure DoC in % describes the state conversion from liquid resin to a cured solid. Ultimately, it describes the fraction of cross-linked polymer chains within the photopolymer resin between 0% (uncured) and 100% (fully cured). In this work, we use Raman spectroscopy (Horiba XploRA Plus, Horiba Instruments Inc, Irvine, CA (USA)) to determine the DoC of all specimens.

Figure 22 shows a picture of the Raman spectroscopy setup. The system comprises a camera and a motorized platform to visually locate the scan area on the samples. The camera then captures the reflected light through objective lenses and the computer processes the detected signal to convert into a Raman spectrum.

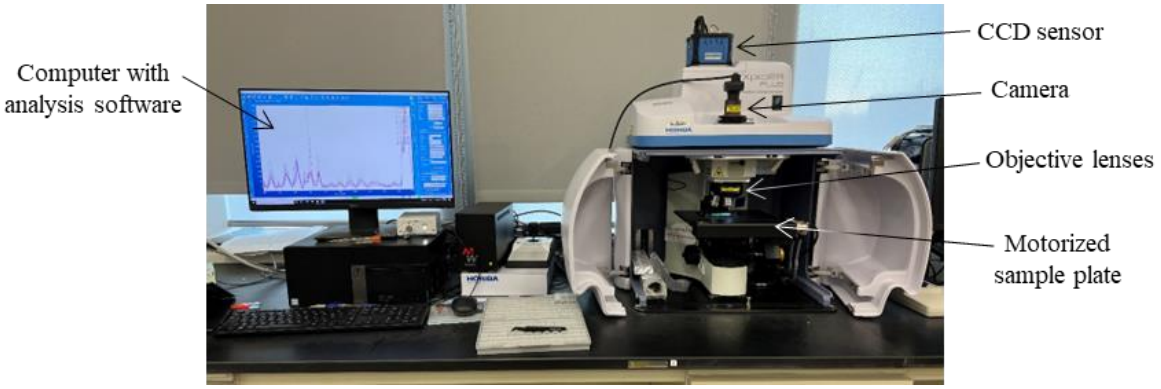

Figure 22: Horiba XploRA Plus Raman spectroscopy setup.

Table 4 lists several typical Raman peaks and their corresponding representation of different functional groups and intermolecular bonds [103]. Prior to analysis, we correct the baseline of all Raman spectra and normalize them with respect to an internal reference peak that corresponds to a Raman shift of 1455 cm^{-1}, which represents CH_2 bonds that do not participate in the photopolymerization reaction and, thus, remain invariant to the DoC [23]. During the polymerization reaction, the C=C bonds in the diacrylate monomers, which are characterized by a Raman shift of 1634cm^{-1}, break into single bonds and cross-link with other monomers [23]. Figure 23 (a) shows the Raman spectra of uncured liquid photopolymer resin (black dashed line) and of a solid photopolymer resin specimen cured with E_0 = 2160 mJ/cm^2 (orange solid line). We indicate the reference peak (1455 cm^{-1}) and, additionally, we observe that the 1634 cm^{-1} peak (C=C bonds) decreases with increasing DoC (black dashed line compared to orange solid line). Determining the magnitude of the 1634 cm^{-1} peak in the Raman spectrum is not straightforward because multiple peaks overlap and, thus, they must first be deconvoluted. Figure 23 (b) shows the Raman spectroscopy measurement data of a typical cured photopolymer resin specimen (orange dots) with a curve fit through the data points to obtain the Raman spectrum best fit (orange line). The deconvolution of the Raman spectrum is based on a Gaussian best fit to individual peaks (gray

lines) [104]. We indicate the area of the 1634 cm^{-1} peak (maroon), isolated from other, adjacent peaks that may be due to noise from, e.g., fluorescence, contamination, and other compounds in the photopolymer resin. Thus, comparing the area of the 1634 cm^{-1} peak (maroon) between different specimens allows quantifying the degree-of-cure (*DoC*) using the following equation [29]:

$$DoC = 1 - \frac{A_{1634}(t)}{A_{1634}(0)} \tag{5}$$

where $A_{1634}(t)$ and $A_{1634}(0)$ are the area of the 1634 cm^{-1} peak after curing time t and at time $t = 0$ (uncured), respectively. The DoC data and deconvoluted Raman spectra are included in Appendix B and C, respectively.

Table 4: Typical Raman bands and intensity representing different functional groups or intermolecular bonds [103]. Source: Horiba Jobin Yvon application note.

Raman peaks region (Raman shift, [cm^{-1}])	Group or bond representation	Peak intensity
1380	CH_3	Medium
1400 - 1470	CH_2 and CH_3 asymmetric stretching	Medium
1410 - 1440	N=N aromatic	Medium
1550 - 1580	N=N aliphatic	Medium
1610 - 1680	C=N	Strong
1500 – 1900	C=C	Strong
1680 – 1820	C=O	Medium

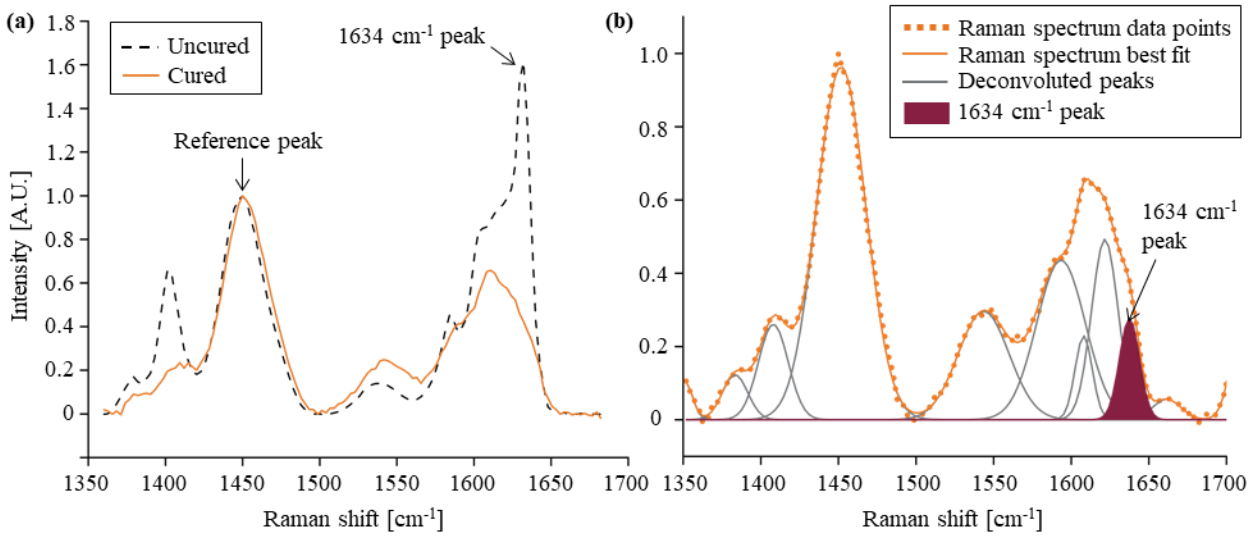

Figure 23: (a) Comparison between the Raman spectra of an uncured (black dashed line) and cured (orange solid line) photopolymer specimen (base-line corrected and normalized with the reference peak at 1455 cm^{-1} that is invariant to the *DoC*), showing the 1634 cm^{-1} peak that represents C=C bonds, which decrease with increasing *DoC*. (b) Typical Raman spectroscopy data (orange dots) with best fit (orange solid line) and deconvoluted peaks (gray solid lines) using a Gaussian best-fit. Comparing the area of the deconvoluted 1634 cm^{-1} peak between specimens allows quantifying the degree-of-cure.

2.3.3. Average surface roughness, *Sa*

The average surface roughness *Sa* in μm is a measurement of the average deviation of surface peaks and valleys with respect to the center line average of the surface topography, and is an important factor to consider in photopolymer curing as it is a measure of the overall printing quality of the material. In this work, we visually compare the shape of the 3D printed specimens to the CAD file used to define the specimen geometry using an optical microscope (AMSCOPE, Irvine, CA (USA)). We also quantify the surface topography of the top surface of the specimen, which represents a measure of the 3D printing quality, using a laser optical profilometer (Keyence VK-X3000, Raleigh, NC (USA)). Figure 24 (a) and (b) shows pictures of the optical microscope and laser profilometer we use in this study. The surface topography measurement relies on optical focus variation mode because the laser confocal mode produces invalid results due to laser scattering at the surface of specimen. We correct the surface topography measurements for

specimen tilt, and we shift the center plane of all surface heights to zero, prior to quantifying the mean surface height *Sa* [105]. Figure 24 (c) shows the 2D contour of the "VT" logo specimens, and a typical 3D printed specimen with E_0 = 240 mJ/cm^2 and Φ = 12%. A magnified inset image illustrates the surface topography of the top surface of the 3D printed specimen (*Sa* = 90.5 μm). The microscopy photos for all specimens and surface roughness data for selected specimens are included in Appendix D.

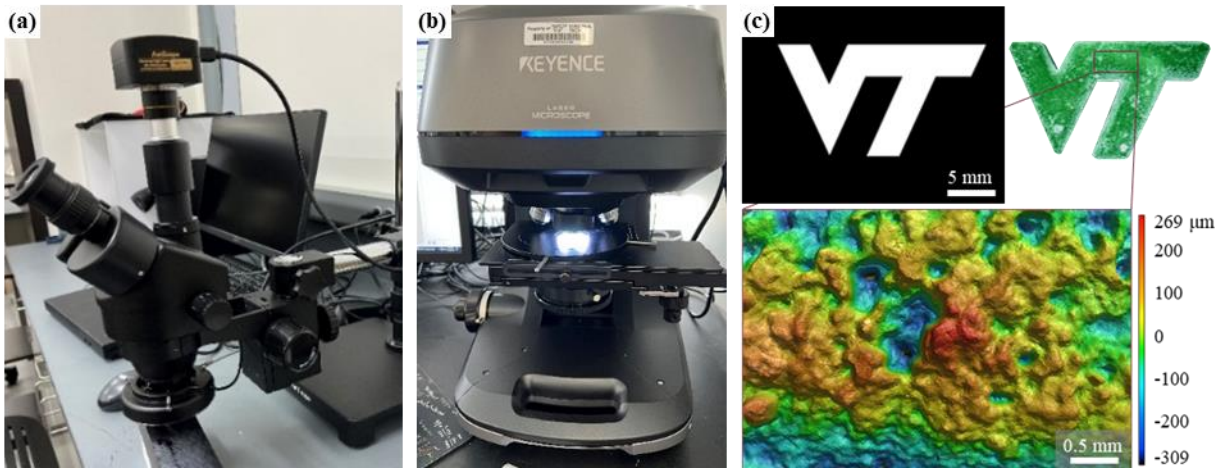

Figure 24: (a) AMSCOPE optical microscope for visual analysis of specimens; (b) Keyence VK-X3000 laser optical profilometer to measure surface topography; (c) 2D contour and corresponding 3D printed specimen with E_0 = 240 mJ/cm^2 and Φ = 12% ("VT" logo) and magnified inset image showing the surface topography of the top surface of the 3D printed specimen.

3. Results and discussion

3.1. Curing depth analysis

Figure 25 shows the curing depth C_d versus the exposure dose E_0 (semi-logarithmic plot), i.e., the "working curve", for different filler volume fractions Φ, and for different filler size distributions; (a) small, (b) 50/50 mix, and (c) large. The black line shows virgin photopolymer resin (Φ = 0 vol.%), with the light penetration depth D_p = 1.42 mm (slope of the working curve) and the critical exposure dose E_c = 61.7 mW/cm^2 (intercept with the light exposure axis). Each datapoint is the average of three measurements and the error bars show the minimum and maximum value. We add a logarithmic best fit of the experimental data for each filler volume fraction Φ to visualize the slope of the working curve, which represents the light penetration depth D_p. From Figure 25 we observe that the curing depth increases with increasing exposure dose, independent of the filler volume fraction, but the rate of curing depth decreases with increasing exposure dose, as expected from the Beer-Lambert law [58]. Additionally, we observe that the critical exposure dose E_c (intercept with the exposure dose axis) decreases with increasing filler size distribution and with increasing filler fraction.

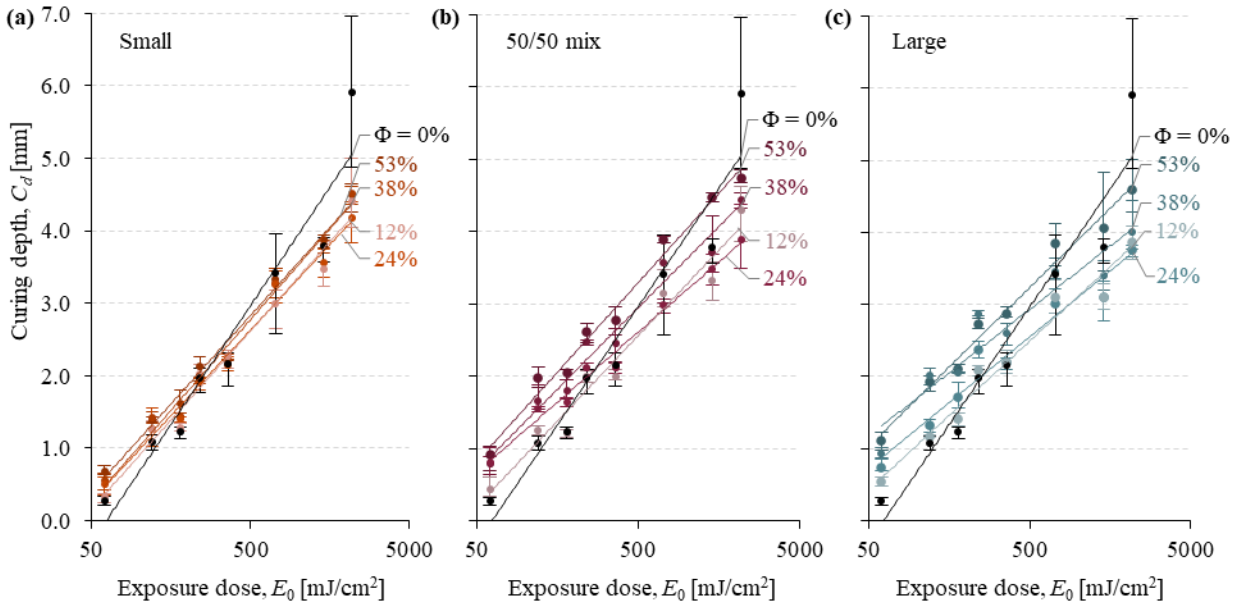

Figure 25: Curing depth C_d versus exposure dose E_0, for different filler volume fractions Φ and for different filler size distributions in best fit lines; (a) small, (b) 50/50 mix, and (c) large.

Figure 25 shows that the curing characteristics of photopolymer resin with dispersed translucent filler are driven by light scattering, which increases curing by re-directing light into the photopolymer resin, and light intensity attenuation, which decreases curing. Light scattering increases with increasing filler fraction and the intensity of the scattered light increases with increasing filler size distribution, thus lowering the threshold to initiate the curing reaction. Light intensity attenuation increases with increasing filler volume fraction, which we verified experimentally. Thus, it reduces the light penetration depth D_p, which is the slope of the working curve. Correspondingly, the working curve of the virgin photopolymer resin (Φ = 0 vol.%) shows a steeper slope than that of photopolymer with dispersed filler (Φ ≠ 0 vol.%) because the absence of filler reduces light intensity attenuation, which increases the light penetration depth, but also increases the critical exposure dose required to initiate the photopolymerization reaction. Thus, the slope of the working curve is almost independent of the filler volume fraction for constant filler

size distribution because increasing the filler volume fraction (within the range we evaluate) increases both light scattering and light intensity attenuation. In contrast, increasing the filler size distribution increases the intensity of the scattered light. It also decreases light intensity attenuation, which we confirmed experimentally, because the number of spherical filler particles and their surface to volume ratio decreases with increasing filler size. Thus, the slope of the working curve also decreases with increasing filler size distribution.

Figure 26 shows the curing depth C_d versus the filler volume fraction Φ for different values of the exposure dose E_0 and for different filler size distributions; (a) small, (b) 50/50 mix, and (c) large. Each datapoint is the average of three measurements and the error bars show the minimum and maximum value. The data of Figure 26 is identical to Figure 25, but instead reveals additional aspects of the curing characteristics of the photopolymer resin with dispersed filler compared to Figure 25. From Figure 26 we observe that the curing depth increases with increasing exposure dose, and with increasing filler size distribution. These results are in agreement with those documented by Choong et al. [20] and schlotthauer et al. [6]. However, they contrast results by, e.g. Xu et al. [19] and Xing et al. [21], who used opaque filler material, and documented decreasing curing depth with increasing filler fraction. We also observe that when $E_0 < 360$ mJ/cm^2, the curing depth increases with the increasing filler volume fraction, which agrees with results documented by Schlotthauer et al. [6]. However, when $E_0 > 720$ mJ/cm^2 the curing depth first decreases and then increases with increasing filler volume fraction.

Thus, when the filler volume fraction $\Phi < 30\%$ (and $E_0 > 720$ mJ/cm^2), we observe that light intensity attenuation dominates over light scattering for constant exposure dose, which results in decreasing curing depth with increasing filler volume fraction. However, for $\Phi > 30\%$ (and $E_0 >$ 720 mJ/cm^2) light scattering dominates over light intensity attenuation for constant exposure dose

E_0, which increases curing depth with increasing filler volume fraction. Note that the curing depth is maximum when Φ = 0 in combination with the maximum exposure dose, because the light penetration depth is maximum when Φ = 0, resulting from the steepest working curve (see Figure 25).

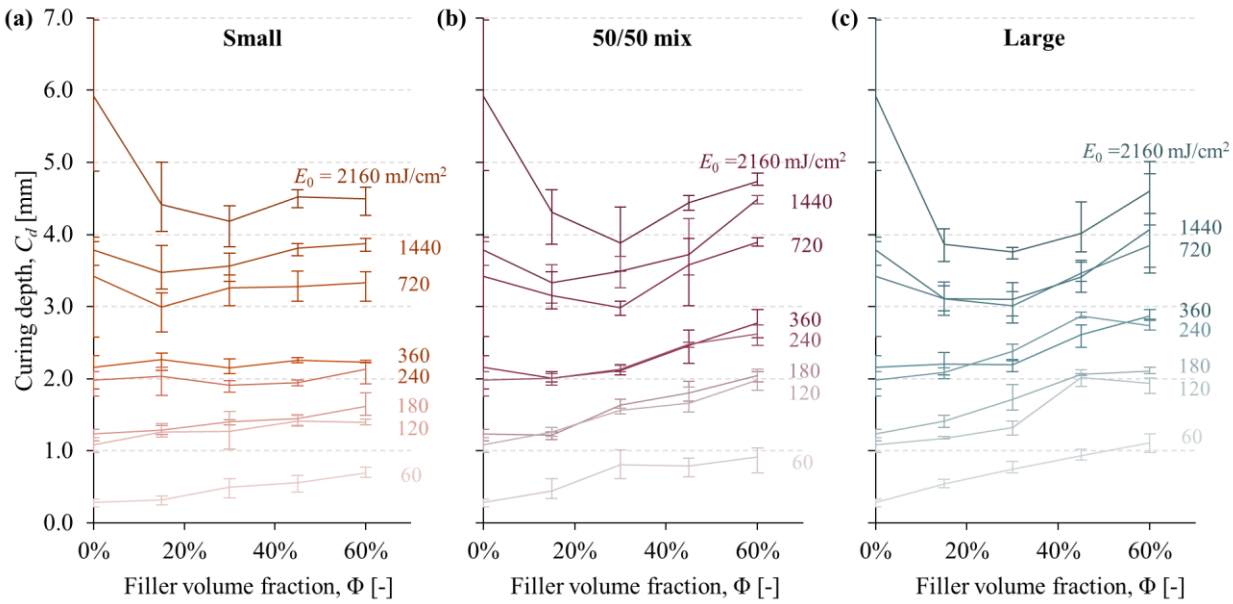

Figure 26: Curing depth C_d versus filler volume fraction Φ, for different values of the exposure dose E_0 and for different filler size distributions; (a) small, (b) 50/50 mix, and (c) large

Figure 27 schematically illustrates that light scattering and light intensity attenuation are the physical phenomena that drive the curing characteristics of photopolymer with dispersed filler particles, showing a small (E_0 = 60 mJ/cm^2) and large (E_0 = 2160 mJ/cm^2) exposure dose, for (a) virgin resin, (b) small size filler, and (c) large size filler. A low exposure dose results in a minimal curing depth for virgin resin, since it requires the highest critical exposure dose to initiate curing (black line in Fig. 25). However, the absence of filler also minimizes light intensity attenuation and, thus, we obtain the largest curing depth for a high exposure dose (Figure **27** (a)). Dispersing filler in the photopolymer resin increases scattering. In contrast to opaque filler material, which

absorbs light, the translucent glass microparticles reflect light back into the resin, thus increasing the curing depth for constant (low) exposure dose compared to virgin photopolymer (Figure 27 (b)). However, light intensity attenuation also increases with increasing exposure dose (and increasing depth-of-cure), which inhibits curing. Thus, two competing effects, light scattering and light intensity attenuation exist simultaneously and define the curing characteristics of the photopolymer resin. For instance, for high exposure doses, the curing depth first decreases and then increases with increasing filler fraction. For low filler fractions, light intensity attenuation dominates over light scattering, thus decreasing the curing depth with increasing filler fraction. In contrast, for high filler fractions, light scattering dominates over light intensity attenuation, thus increasing the curing depth with increasing filler fraction. Finally, comparing Figs. 27 (b) and (c), illustrates that the filler size also affects the curing characteristics of the photopolymer resin. The intensity of the scattered light increases with increasing filler size (increases curing), and the light intensity attenuation decreases with increasing filler fraction because the surface to volume ratio of the filler decreases with increasing size (increases curing). Hence, the curing depth increases for increasing filler size, and for constant filler fraction and exposure dose.

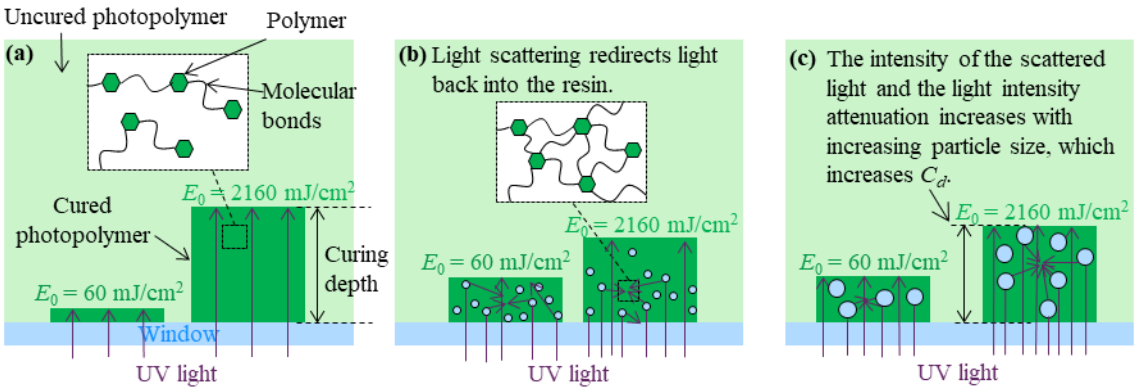

Figure 27: Light scattering and light intensity attenuation are the physical phenomena that drive the curing characteristics of photopolymer resin with dispersed filler particles. We schematically illustrate their interplay for examples with low (E_0 = 60 mJ/cm^2) and high (E_0 = 2160 mJ/cm^2) exposure dose, depicting (a) virgin resin, (b) small size filler, and (c) large size filler.

3.2. Degree of Cure analysis

Figure 28 shows the degree-of-cure versus the exposure dose E_0 for different values of filler volume fraction Φ, and for different filler size distributions; (a) small, (b) 50/50 mix, and (c) large. The dashed black line represents virgin photopolymer resin (Φ = 0 vol.%). We show magnified inset images for $E_0 < 250$ mJ/cm^2. Each datapoint is the average of three measurements and the error bars show the minimum and maximum value. From Figure 28 we observe that the degree-of-cure increases with increasing exposure dose, independent of the filler volume fraction and the filler size distribution. Furthermore, we observe that any combination of filler volume fraction and filler size distribution approaches a 90% degree-of-cure with increasing exposure dose, which is in agreement with results documented by Jiang and Drummer [89]. The glass microspheres scatter incident light and lower the critical exposure dose to initiate the photopolymer curing reaction, which explains that the degree-of-cure of photopolymer resin with filler (Φ ≠ 0 vol.%) exceeds that of virgin photopolymer resin (Φ = 0 vol.%), independent of exposure dose and filler size distribution. The degree-of-cure also appears to increase with increasing filler volume fraction, independent of the filler size distribution, which agrees with the results of Figure 26. However, the error bars overlap in Figure 28, which prevents a conclusive assessment.

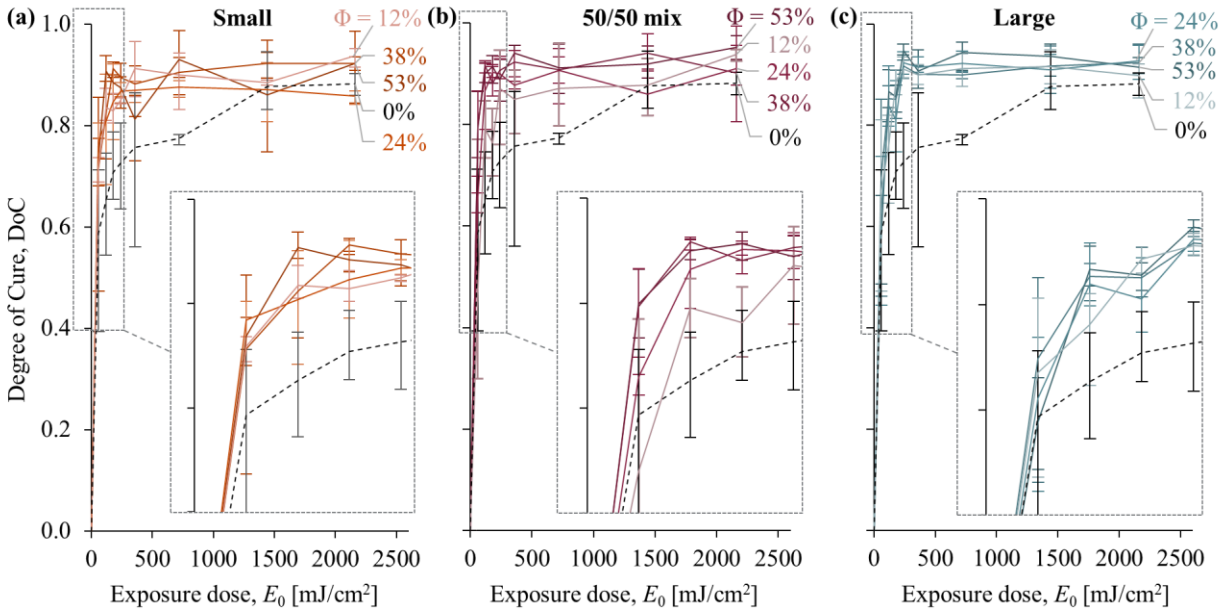

Figure 28: Degree-of-cure (DoC) versus exposure dose E_0, for different filler volume fractions Φ and for different filler size distributions; (a) small, (b) 50/50 mix, and (c) large.

3.3. Geometric accuracy

Figure 29 (a) shows a selection of optical images of "VT" logo 3D printed specimens, for different combinations of exposure dose E_0 (rows) and filler volume fraction Φ (columns) and for different filler size distributions; small (left) and large (right). From Figure 29 (a) we observe that the geometric accuracy of the 3D printed specimens decreases with increasing exposure dose, which is known as profile broadening, and is caused by light scattering from cured contours of the 3D printed specimen as well as the dispersed filler [6]. Consequently, the importance of profile broadening increases with increasing filler volume fraction and increasing exposure dose, which is apparent from Figure 29 (a). For instance, comparing a specimen with E_0 = 720 mJ/cm^2 and Φ = 38 vol.% to one with E_0 = 720 mJ/cm^2 and Φ = 53 vol.%, the latter displays more profile broadening than the former. In contrast, the equivalent specimens with E_0 = 240 mJ/cm^2 show almost no profile broadening. An exposure dose E_0 = 2160 mJ/cm^2 causes complete loss of shape

for all specimens, independent of the filler volume fraction. Profile broadening also increases with increasing filler size distribution because the effect of light scattering increases with increasing particle size, independent of the exposure dose and filler volume fraction [106].

Figure 29 (b) and (c) quantify profile broadening of the specimens of Figure 29 (a) for the x = 12.5 mm (solid line) and y = 10.5 mm (dashed line) measurement (inset image of Figure 29 (b)), as a function of exposure dose E_0, and for different values of the filler volume fraction Φ, for both the small (Figure 29 (b)) and large (Figure 29 (c)) filler size distribution. Each datapoint is the average of three measurements and the error bars show the minimum and maximum value. From Figure 29 (b) and (c) we observe that profile broadening increases with increasing exposure dose and increasing filler volume fraction for both the x- and y-measurement. We also observe a slight increase of profile broadening for the large versus the small filler size distribution. Side views of selected specimens (inset images in Figure 29 (b) and (c)) demonstrate that profile broadening decreases with increasing distance from the resin vat window (build direction), and is most significant closest to the window, where the light intensity is maximum. Note that the virgin photopolymer (Φ = 0%) displays minimal profile broadening because the absence of filler material reduces sources of light scattering to the cured contours of the specimen only.

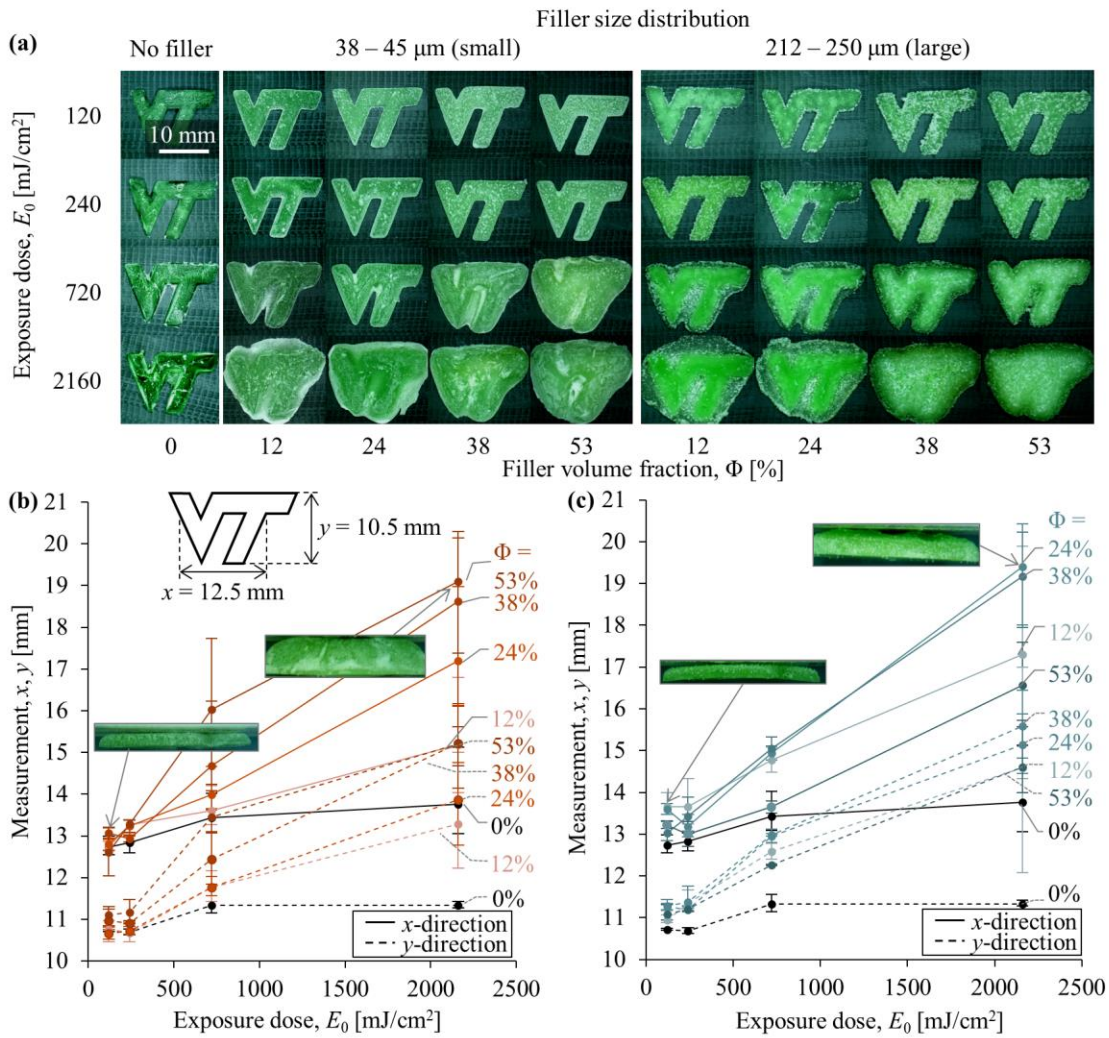

Figure 29: Profile broadening of the 3D printed "VT" logo specimens for different combinations of exposure dose E_0 and filler volume fraction Φ, and for two different filler size distributions; small (left) and large (right), showing (a) a selection of optical images of the specimens, qualitatively illustrating profile broadening, and *x*- (solid lines) and *y*- (dashed lines) measurement (indicated in the inset image) for filler size distribution (b) small and (c) large. Additional inset images show side (profile) views of the 3D printed specimens.

3.4. Surface roughness analysis

Figure 30 (a) shows the surface topography maps of the surface furthest away from the curing window (within the center portion between the letters V and T in the "VT" logo (see Figure 24 (c)), using a color scale to represent the surface height *z* at each *x* and *y* coordinate within the measurement area, i.e., $z = f(x,y)$. We observe that the surface topography of virgin photopolymer

specimens ($\Phi = 0$ vol.%) is spiky compared to that of specimens with dispersed filler ($\Phi \neq 0$ vol.%), because in the absence of filler, light scattering and absorption is minimum, and the incident UV light penetrates the virgin photopolymer resin (see also Figure 25 and Figure 26). Additionally, we observe that the surface topography features match the size of the filler size distribution, which is easiest to recognize for the surface topography maps of the specimens with large filler size distribution. When $0 < \Phi < 12\%$, the surface topography is mostly dominated by the cured photopolymer, when $12 < \Phi < 38\%$, a combination of resin and filler determines the surface topography, but when $\Phi > 38\%$, the surface topography almost entirely comprises filler material.

Figure 30 (b) and (c) show the average surface roughness *Sa* versus the exposure dose E_0 for different values of filler volume fraction Φ, and for different filler size distributions; (a) small, and (b) large. The dashed black line represents virgin photopolymer resin ($\Phi = 0$ vol.%). We observe the highest *Sa* values for the virgin photopolymer resin specimens ($\Phi = 0$ vol.%), which is caused by the spiky topography at the center of the surface and measurement domain. The center shows an increased curing depth compared to its surroundings, which we observe as "ridge"-type topography features in some of the sub-figures of Figure 30 (a), e.g. $E_0 = 2160$ mJ/cm^2 and $\Phi = 0\%$. These features are the result of self-focusing of the incident light due to partially cured photopolymer resin [6,54].

Furthermore, the average surface roughness decreases with increasing filler volume fraction, because the close-packing of filler material in combination with light scattering and absorption creates a smooth surface. We emphasize that profile broadening, which increases with increasing filler volume fraction, also smoothens the surface topography. Conversely, we observe from Figure 30 (b) and (c) that the average surface roughness first increases and then decreases

with increasing exposure dose, due to the interplay between light scattering, filler volume fraction, and light intensity. Finally, we observe that the average surface roughness *Sa* increases slightly with increasing filler size distribution, in particular for specimens cured with low exposure dose (E_0 < 240 mJ/cm^2), even though a clear pattern does not emerge from the results.

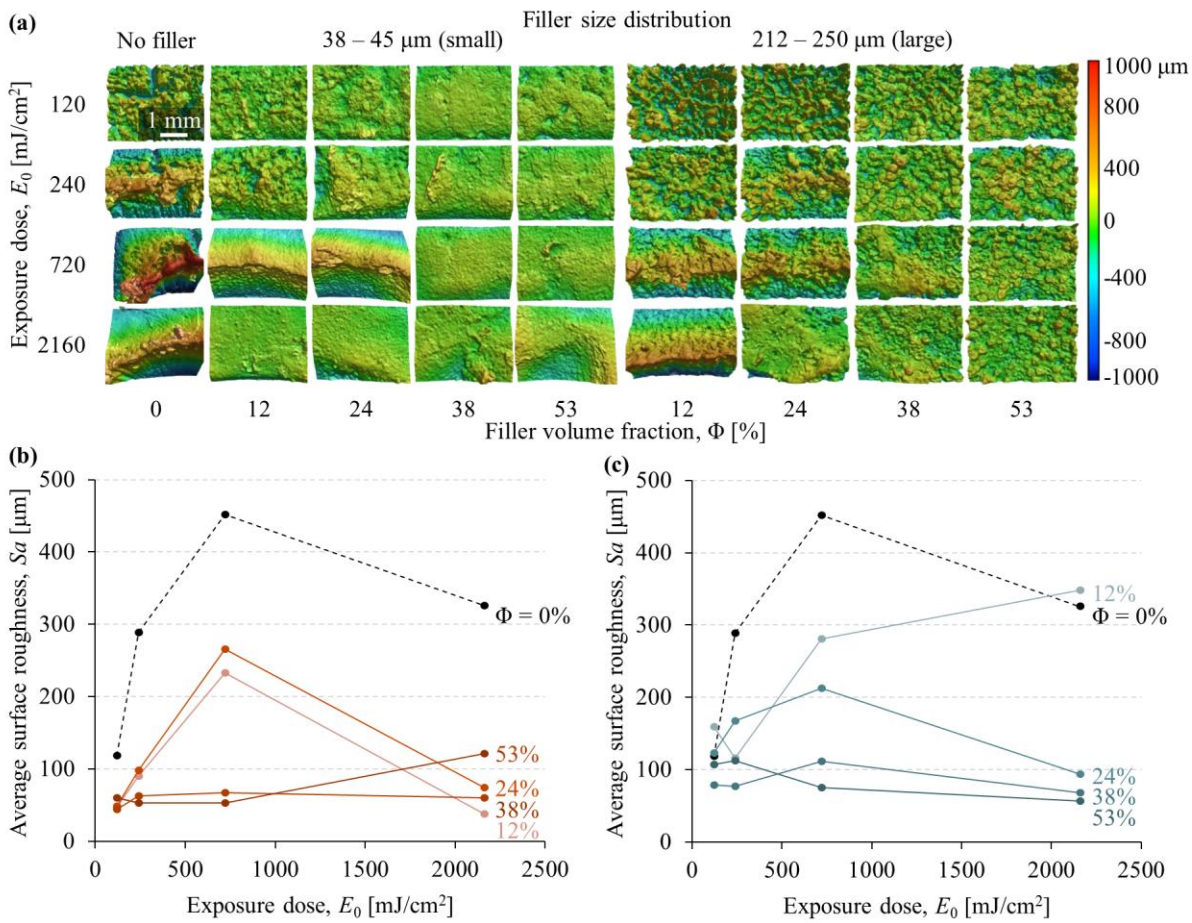

Figure 30: Surface topography of the surface of the 3D printed specimen furthest away from resin vat window for different combinations of exposure dose E_0 and filler volume fraction Φ, and for two different filler size distributions; small (left) and large (right), showing (a) surface topography maps, and the average surface roughness *Sa* for (b) small, and (c) large filler size distribution.

3.5. Limitations, alternative theory, and future work

This work provides physical insights into the curing characteristics of photopolymer resin with dispersed filler material in a VP setup, in the context of 3D printing photopolymer with high

volume fraction of filler material. We also acknowledge the limitations of this work. The “VT” specimen we use is a single-layer specimen. In contrast, 3D printing a multi-layer specimen might reveal additional useful information related to curing depth, degree of cure, surface topography, and geometric accuracy, as well as identifying problems that may arise during the VP 3D printing process. Furthermore, it would be beneficial to increase the sample size for exposure doses under 120 mJ/cm^2, where rapid curing occurs, to allow for a more detailed analysis of the early-stage curing process. Additionally, the variability of some of the measurement results, reflected by large error bars for some results, may have been caused by imperfect control of experimental conditions such as temperature, oxygen permeability, and operator variability. To enhance the repeatability and reproducibility of the study, future work could focus on minimizing the sources of variability and bias by further standardizing the experimental protocols and automating tasks using precision instruments. Additionally, comparing the results across different labs or instruments could help to assess the reproducibility of the findings and identify any systematic errors or biases.

4. Conclusion

We experimentally characterize the curing characteristics of diacrylate/epoxy photopolymer resin with dispersed glass microspheres. Specifically, we quantify the effect of exposure dose E_0, filler fraction Φ, and filler size distribution, on the degree-of-cure and the curing depth C_d during a VP process. We also evaluate the geometric accuracy of the resulting specimen and measure the surface roughness of the top surface of the printed specimens. We conclude the following.

(1) The curing characteristics of photopolymer resin with dispersed translucent filler (glass microparticles) depend on two competing phenomena; light scattering, which increases curing by redirecting light into the photopolymer resin, and light intensity attenuation, which decreases curing by reducing the penetration depth of light into the photopolymer resin. Light scattering increases with increasing filler volume fraction and the intensity of the scattered light increases with increasing filler size distribution, thus increasing the amount of light that redirects into the photopolymer resin and, consequently, lowering the threshold to initiate the curing reaction. Additionally, light intensity attenuation increases with increasing filler volume fraction (and constant filler size) and with decreasing filler size distribution (and constant filler volume fraction), which we verified experimentally with light intensity measurements.

(2) The curing depth C_d depends on both the exposure dose E_0 and the filler volume fraction Φ. Both light scattering and light intensity attenuation increase with increasing filler volume fraction. When the exposure dose $E_0 < 360$ mJ/cm^2 light scattering dominates over light intensity attenuation, and the curing depth increases with increasing exposure dose, filler volume fraction, and filler size distribution. In contrast, when the exposure dose $E_0 >$ 720 mJ/cm^2, light intensity attenuation dominates over light scattering for small filler

volume fraction (Φ < 30 vol.%), which decreases the curing depth with increasing filler volume fraction, and light scattering dominates over light intensity attenuation for large filler volume fraction (Φ > 30 vol.%), which increases the curing depth with increasing filler volume fraction.

(3) The degree-of-cure DoC increases with increasing exposure dose E_0 and increasing filler volume fraction Φ, but ultimately approaches 90% with increasing exposure dose. The addition of filler ($\Phi \neq 0$ vol.%) decreases the slope of the photopolymer working curve compared to virgin photopolymer resin (Φ = 0 vol.%) and, thus, decreases the critical exposure dose, i.e., the addition of filler lowers the threshold to initiate the curing reaction because light scattering redirects light back into the photopolymer.

(4) The geometric accuracy of the 3D printed specimens decreases with increasing exposure dose and with increasing filler volume fraction because light that scatters from filler and the contours of the 3D printed specimens induces undesirable curing, which is referred to as profile broadening. Furthermore, the average surface roughness *Sa* of the 3D printed specimens first increases and then decreases with increasing exposure dose E_0, and it decreases with increasing filler volume fraction Φ, due to interplay between filler volume fraction, light scattering, and light intensity.

Overall, despite providing physical insights into the curing of photopolymer resin with dispersed glass microparticles, this study has limitations that needs to be addressed in future studies. An actual 3D printing of multi-layer specimen could be performed in order to study printing properties such as curing depth, degree of cure, surface finish, and geometric accuracy, as well as identifying problems that may arise during the VP 3D printing process. In addition, the sample size was limited, and the results were inconsistent due to imperfect control of certain experimental

conditions. To improve the accuracy and repeatability of the study, future work could standardize experimental protocols, automate certain processes using precision instruments, and compare results across different labs or instruments.

References

[1] I. Gibson, D. Rosen, B. Stucker, Additive Manufacturing Technologies: 3D Printing, Rapid Prototyping, and Direct Digital Manufacturing, Springer, New York, NY, 2015. https://doi.org/10.1007/978-1-4939-2113-3.

[2] Form 3: Industrial-Quality Desktop SLA 3D Printer, Formlabs. (2023). https://formlabs.com/3d-printers/form-3/ (accessed February 24, 2023).

[3] U. Iftikhar, Nanoscribe introduces Quantum X, a two-photon 3D printer for microoptics, 3D Printing Industry. (2019). https://3dprintingindustry.com/news/nanoscribe-introduces-quantum-x-a-two-photon-3d-printer-for-microoptics-157656/ (accessed March 7, 2023).

[4] PolyJet Technology for 3D Printing | Stratasys, (2023). https://www.stratasys.com/en/guide-to-3d-printing/technologies-and-materials/polyjet-technology (accessed October 11, 2022).

[5] A. Bagheri, J. Jin, Photopolymerization in 3D Printing, ACS Applied Polymer Materials. 1 (2019) 593–611. https://doi.org/10.1021/acsapm.8b00165.

[6] T. Schlotthauer, D. Nolan, P. Middendorf, Influence of short carbon and glass fibers on the curing behavior and accuracy of photopolymers used in stereolithography, Additive Manufacturing. 42 (2021) 102005. https://doi.org/10.1016/j.addma.2021.102005.

[7] Ceramic Resin, Formlabs. (2023). https://formlabs.com/materials/ceramics/ (accessed March 7, 2023).

[8] J. Praveenkumara, P. Madhu, T.G. Yashas Gowda, M.R. Sanjay, S. Siengchin, A comprehensive review on the effect of synthetic filler materials on fiber-reinforced hybrid polymer composites, The Journal of The Textile Institute. 113 (2022) 1231–1239. https://doi.org/10.1080/00405000.2021.1920151.

[9] M.S. McClain, A. Afriat, J.F. Rhoads, I.E. Gunduz, S.F. Son, Development and Characterization of a Photopolymeric Binder for Additively Manufactured Composite Solid Propellant Using Vibration Assisted Printing, Propellants, Explosives, Pyrotechnics. 45 (2020) 853–863. https://doi.org/10.1002/prep.201900387.

[10] M. Atai, D.C. Watts, Z. Atai, Shrinkage strain-rates of dental resin-monomer and composite systems, Biomaterials. 26 (2005) 5015–5020. https://doi.org/10.1016/j.biomaterials.2005.01.022.

[11] M.D. Haslam, B. Raeymaekers, Aligning carbon nanotubes using bulk acoustic waves to reinforce polymer composites, Composites Part B: Engineering. 60 (2014) 91–97. https://doi.org/10.1016/j.compositesb.2013.12.027.

[12] M.-S. Scholz, B.W. Drinkwater, R.S. Trask, Ultrasonic assembly of anisotropic short fibre reinforced composites, Ultrasonics. 54 (2014) 1015–1019. https://doi.org/10.1016/j.ultras.2013.12.001.

[13] J. Zhao, Q. Li, F. Jin, N. He, Digital light processing 3D printing Kevlar composites based on dual curing resin, Additive Manufacturing. 41 (2021) 101962. https://doi.org/10.1016/j.addma.2021.101962.

[14] K. Niendorf, B. Raeymaekers, Combining ultrasound directed self-assembly and stereolithography to fabricate engineered polymer matrix composite materials with anisotropic electrical conductivity, Composites Part B: Engineering. 223 (2021) 109096. https://doi.org/10.1016/j.compositesb.2021.109096.

[15] D.S. Melchert, R.R. Collino, T.R. Ray, N.D. Dolinski, L. Friedrich, M.R. Begley, D.S. Gianola, Flexible Conductive Composites with Programmed Electrical Anisotropy Using

Acoustophoresis, Advanced Materials Technologies. 4 (2019) 1900586. https://doi.org/10.1002/admt.201900586.
[16] U. Kalsoom, A. Peristyy, P. N. Nesterenko, B. Paull, A 3D printable diamond polymer composite: a novel material for fabrication of low cost thermally conducting devices, RSC Advances. 6 (2016) 38140–38147. https://doi.org/10.1039/C6RA05261D.
[17] L. Ferrage, G. Bertrand, P. Lenormand, D. Grossin, B. Ben-Nissan, A review of the additive manufacturing (3DP) of bioceramics: alumina, zirconia (PSZ) and hydroxyapatite, J Aust Ceram Soc. 53 (2017) 11–20. https://doi.org/10.1007/s41779-016-0003-9.
[18] S. Zakeri, M. Vippola, E. Levänen, A comprehensive review of the photopolymerization of ceramic resins used in stereolithography, Additive Manufacturing. 35 (2020) 101177. https://doi.org/10.1016/j.addma.2020.101177.
[19] Y. Xu, Z. Ding, H. Zhu, Y. Zhang, S. Knopf, P. Xiao, J. Lalevée, Preparation of Iron Filler-Based Photocomposites and Application in 3D Printing, Macromolecular Materials and Engineering. 306 (2021) 2000720. https://doi.org/10.1002/mame.202000720.
[20] Y.Y.C. Choong, S. Maleksaeedi, H. Eng, S. Yu, J. Wei, P.-C. Su, High speed 4D printing of shape memory polymers with nanosilica, Applied Materials Today. 18 (2020) 100515. https://doi.org/10.1016/j.apmt.2019.100515.
[21] H. Xing, B. Zou, X. Liu, X. Wang, C. Huang, Y. Hu, Fabrication strategy of complicated Al2O3-Si3N4 functionally graded materials by stereolithography 3D printing, Journal of the European Ceramic Society. 40 (2020) 5797–5809. https://doi.org/10.1016/j.jeurceramsoc.2020.05.022.
[22] J. Bennett, Measuring UV curing parameters of commercial photopolymers used in additive manufacturing, Additive Manufacturing. 18 (2017) 203–212. https://doi.org/10.1016/j.addma.2017.10.009.
[23] B. Martin, J. Puentes, L. Wruck, T.A. Osswald, Degree of cure of epoxy/acrylic photopolymers: Characterization with raman spectroscopy and a modified phenomenological model, Polymer Engineering & Science. 58 (2018) 228–237. https://doi.org/10.1002/pen.24550.
[24] T. Zhao, R. Yu, X. Li, Y. Zhang, X. Yang, X. Zhao, W. Huang, A comparative study on 3D printed silicone-epoxy/acrylate hybrid polymers via pure photopolymerization and dual-curing mechanisms, J Mater Sci. 54 (2019) 5101–5111. https://doi.org/10.1007/s10853-018-3070-1.
[25] T. Jiao, Y. Lin, Y. Liu, J. Liu, G. Lu, Effect of modified calcium sulphate whiskers on free-radical/cationic hybrid photopolymers for 3D printing, Mater. Res. Express. 7 (2020) 015334. https://doi.org/10.1088/2053-1591/ab6898.
[26] Y. Xu, C. Jambou, K. Sun, J. Lalevée, A. Simon-Masseron, P. Xiao, Effect of Zeolite Fillers on the Photopolymerization Kinetics for Photocomposites and Lithography, ACS Appl. Polym. Mater. 1 (2019) 2854–2861. https://doi.org/10.1021/acsapm.9b00557.
[27] J. Wu, Z. Zhao, X. Kuang, C.M. Hamel, D. Fang, H.J. Qi, Reversible shape change structures by grayscale pattern 4D printing, Multifunct. Mater. 1 (2018) 015002. https://doi.org/10.1088/2399-7532/aac322.
[28] K.C. Wu, J.W. Halloran, Photopolymerization monitoring of ceramic stereolithography resins by FTIR methods, J Mater Sci. 40 (2005) 71–76. https://doi.org/10.1007/s10853-005-5689-y.

[29] Q. Mao, L. Bian, M. Huang, Study of the visible light curing of vinyl ester resins using in situ Raman spectroscopy, J Polym Res. 18 (2011) 1751–1756. https://doi.org/10.1007/s10965-011-9581-y.
[30] T. Jiang, Y. Wang, Y. Wang, N. Orlovskaya, L. An, Quantitative Raman Analysis of Free Carbon in Polymer-Derived Ceramics, Journal of the American Ceramic Society. 92 (2009) 2455–2458. https://doi.org/10.1111/j.1551-2916.2009.03233.x.
[31] J.-Y. Jeng, Y.S. Wong, C.T. Ho, Curing Characteristics of the Photopolymer Used in the Solid Laser-Diode Plotter RP System, Int J Adv Manuf Technol. 17 (2001) 535–542. https://doi.org/10.1007/s001700170155.
[32] F. Dawan, O.A. Ekuase, P.F. Mensah, Thermo-Mechanical Characterization of a Hybrid Reinforced Photopolymer Composite Via DLP 3D Printing, American Society for Composites 35th Annual Technical (Virtual) Conference. (2020). https://par.nsf.gov/biblio/10219201-thermo-mechanical-characterization-hybrid-reinforced-photopolymer-composite-via-dlp-printing (accessed October 4, 2022).
[33] M. Robakowska, Ł. Gierz, P. Mayer, K. Szcześniak, A. Marcinkowska, A. Lewandowska, P. Gajewski, Influence of the Addition of Sialon and Aluminum Nitride Fillers on the Photocuring Process of Polymer Coatings, Coatings. 12 (2022) 1389. https://doi.org/10.3390/coatings12101389.
[34] Y. Gao, W. Yang, R. Hu, J. Zhou, Y. Zhang, Validation of CL-20-based Propellant Formulations for Photopolymerization 3D Printing, Propellants, Explosives, Pyrotechnics. 46 (2021) 1844–1848. https://doi.org/10.1002/prep.202100196.
[35] S. Gaidukovs, A. Medvids, P. Onufrijevs, L. Grase, UV-light-induced curing of branched epoxy novolac resin for coatings, Express Polymer Letters. 12 (2018) 918–929. https://doi.org/10.3144/expresspolymlett.2018.78.
[36] X. Zou, Y. Zhao, Y. Zhu, R. Liu, Filling Aggregation-Induced Extinction Mechanism in Near-Infrared Photopolymerization for Gradient and Highly Filled Bulk Materials, Macromolecules. 55 (2022) 2075–2084. https://doi.org/10.1021/acs.macromol.1c02576.
[37] ICNIRP | Infrared (780 nm-1mm), (n.d.). https://www.icnirp.org/en/frequencies/infrared/index.html (accessed March 16, 2023).
[38] Radiation: Ultraviolet (UV) radiation, World Health Organization. (2016). https://www.who.int/news-room/questions-and-answers/item/radiation-ultraviolet-(uv) (accessed March 16, 2023).
[39] R.O. Ebewele, Polymer Science and Technology, CRC Press, 2000.
[40] Tripropylene glycol diacrylate, CAS Common Chemistry. (2023). https://commonchemistry.cas.org/detail?cas_rn=42978-66-5&search=42978-66-5 (accessed February 28, 2023).
[41] J.-P. Fouassier, J. Lalevée, Photoinitiators: Structures, Reactivity and Applications in Polymerization, John Wiley & Sons, 2021.
[42] L.D. Randolph, J. Steinhaus, B. Möginger, B. Gallez, J. Stansbury, W.M. Palin, G. Leloup, J.G. Leprince, Photopolymerization of highly filled dimethacrylate-based composites using Type I or Type II photoinitiators and varying co-monomer ratios, Dental Materials. 32 (2016) 136–148. https://doi.org/10.1016/j.dental.2015.11.032.
[43] 1-Hydroxycyclohexyl phenyl ketone, CAS Common Chemistry. (2023). https://commonchemistry.cas.org/detail?cas_rn=947-19-3&search=947-19-3 (accessed February 28, 2023).

[44] P. Xiao, J. Zhang, 3D Printing with Light, illustrated ed., Walter de Gruyter GmbH & Co KG, 2021.
[45] V. Lobo, A. Patil, A. Phatak, N. Chandra, Free radicals, antioxidants and functional foods: Impact on human health, Pharmacogn Rev. 4 (2010) 118–126. https://doi.org/10.4103/0973-7847.70902.
[46] Y. Qi, L. Li, Z. Fang, J. Zhong, Q. Dong, Effects of small molecular weight silicon-containing acrylate on kinetics, morphologies, and properties of free-radical/cationic hybrid UV-cured coatings, Journal of Applied Polymer Science. 131 (2014). https://doi.org/10.1002/app.40655.
[47] Y. Zhang, Y. Xu, A. Simon-Masseron, J. Lalevée, Radical photoinitiation with LEDs and applications in the 3D printing of composites, Chemical Society Reviews. 50 (2021) 3824–3841. https://doi.org/10.1039/D0CS01411G.
[48] P. Loginos, A. Patsidis, V. Georgakilas, UV-Cured Poly(Ethylene Glycol) Diacrylate/Carbon Nanostructure Thin Films. Preparation, Characterization, and Electrical Properties, Journal of Composites Science. 4 (2020) 4. https://doi.org/10.3390/jcs4010004.
[49] H. Quan, T. Zhang, H. Xu, S. Luo, J. Nie, X. Zhu, Photo-curing 3D printing technique and its challenges, Bioactive Materials. 5 (2020) 110–115. https://doi.org/10.1016/j.bioactmat.2019.12.003.
[50] R.K. Bregg, Frontiers in Polymer Research, illustrated ed., Nova Publishers, 2006.
[51] H. Okamura, Y. Ueda, M. Shirai, Hybrid UV Curing System Using Methacrylates Having a Chalcone Moiety, Journal of Photopolymer Science and Technology. 26 (2013) 245–248. https://doi.org/10.2494/photopolymer.26.245.
[52] Ethylene, CAS Common Chemistry. (2023). https://commonchemistry.cas.org/detail?cas_rn=74-85-1&search=ethylene (accessed March 7, 2023).
[53] 2,2-Bis(4-hydroxyphenyl)propane, CAS Common Chemistry. (2023). https://commonchemistry.cas.org/detail?cas_rn=80-05-7&search=bisphenol%20A (accessed March 7, 2023).
[54] P.F. Jacobs, Rapid Prototyping & Manufacturing: Fundamentals of Stereolithography, Society of Manufacturing Engineers, 1992.
[55] P. Musto, M. Abbate, G. Ragosta, G. Scarinzi, A study by Raman, near-infrared and dynamic-mechanical spectroscopies on the curing behaviour, molecular structure and viscoelastic properties of epoxy/anhydride networks, Polymer. 48 (2007) 3703–3716. https://doi.org/10.1016/j.polymer.2007.04.042.
[56] D.F. Swinehart, The Beer-Lambert Law, J. Chem. Educ. 39 (1962) 333. https://doi.org/10.1021/ed039p333.
[57] K. Sekmen, T. Rehbein, M. Johlitz, A. Lion, A. Constantinescu, Thermal analysis and shrinkage characterization of the photopolymers for DLP additive manufacturing processes, Continuum Mech. Thermodyn. (2022). https://doi.org/10.1007/s00161-022-01137-0.
[58] K.L. Sampson, B. Deore, A. Go, M.A. Nayak, A. Orth, M. Gallerneault, P.R.L. Malenfant, C. Paquet, Multimaterial Vat Polymerization Additive Manufacturing, ACS Appl. Polym. Mater. 3 (2021) 4304–4324. https://doi.org/10.1021/acsapm.1c00262.
[59] J. Greenhall, B. Raeymaekers, 3D Printing Macroscale Engineered Materials Using Ultrasound Directed Self-Assembly and Stereolithography, Advanced Materials Technologies. 2 (2017) 1700122. https://doi.org/10.1002/admt.201700122.

[60] Z. Yang, S. Peng, Z. Wang, J.-T. Miao, L. Zheng, L. Wu, Z. Weng, UV-Curable, Low-Viscosity Resin with a High Silica Filler Content for Preparing Ultrastiff, 3D-Printed Molds, ACS Appl. Polym. Mater. 4 (2022) 2636–2647. https://doi.org/10.1021/acsapm.1c01920.
[61] L.H. Nguyen, M. Straub, M. Gu, Acrylate-Based Photopolymer for Two-Photon Microfabrication and Photonic Applications, Advanced Functional Materials. 15 (2005) 209–216. https://doi.org/10.1002/adfm.200400212.
[62] Z. Faraji Rad, P.D. Prewett, G.J. Davies, High-resolution two-photon polymerization: the most versatile technique for the fabrication of microneedle arrays, Microsyst Nanoeng. 7 (2021) 1–17. https://doi.org/10.1038/s41378-021-00298-3.
[63] Y.-X. Ren, R.-D. Lu, L. Gong, Tailoring light with a digital micromirror device, Annalen Der Physik. 527 (2015) 447–470. https://doi.org/10.1002/andp.201500111.
[64] mUVe 3D DLP Maker and ULTIPro+ - mUVe 3D, (2016). https://www.muve3d.net/press/product/muve-3d-dlp/ (accessed March 1, 2023).
[65] J.R. Tumbleston, D. Shirvanyants, N. Ermoshkin, R. Janusziewicz, A.R. Johnson, D. Kelly, K. Chen, R. Pinschmidt, J.P. Rolland, A. Ermoshkin, E.T. Samulski, J.M. DeSimone, Continuous liquid interface production of 3D objects, Science. 347 (2015) 1349–1352. https://doi.org/10.1126/science.aaa2397.
[66] J. Balli, S. Kumpaty, V. Anewenter, Continuous Liquid Interface Production of 3D Objects: An Unconventional Technology and its Challenges and Opportunities, in: American Society of Mechanical Engineers Digital Collection, 2018. https://doi.org/10.1115/IMECE2017-71802.
[67] The Carbon M1 3D Printer - Start 3D Printing at Full Scale, Carbon. (2023). https://www.carbon3d.com/products/m1-3d-printer (accessed March 1, 2023).
[68] J. Xie, Y. He, W. Ma, T. Liu, J. Chen, Study on the liquid crystal display mask photo-curing of photosensitive resin reinforced with graphene oxide, Journal of Applied Polymer Science. 137 (2020) 49538. https://doi.org/10.1002/app.49538.
[69] Team Xometry, DLP vs. LCD: Differences and Comparison, Xometry. (2022). https://www.xometry.com/resources/3d-printing/dlp-vs-lcd-3d-printing/ (accessed February 24, 2023).
[70] Anycubic Photon Mono X, ANYCUBIC 3D Printing. (2023). https://www.anycubic.com/products/photon-mono-x-resin-printer (accessed March 1, 2023).
[71] F. Jiang, A. Wörz, M. Romeis, D. Drummer, Analysis of UV-Assisted direct ink writing rheological properties and curing degree, Polymer Testing. 105 (2022) 107428. https://doi.org/10.1016/j.polymertesting.2021.107428.
[72] Stratasys PolyJet 3D Printers | GoEngineer | Objet, J850, and More, (2023). https://www.goengineer.com/3d-printing/polyjet (accessed April 18, 2023).
[73] MultiJet Printing, 3D Systems. (2017). https://www.3dsystems.com/multi-jet-printing (accessed October 11, 2022).
[74] PolyJet vs MultiJet Printing(MJP), FacFox Docs. (2019). https://facfox.com/docs/kb/polyjet-mjp-comparison (accessed April 18, 2023).
[75] M. Šercer, T. Rezić, D. Godec, D. Oros, A. Pilipović, F. Ivušić, I. Rezić, M. Andlar, R. Ludwig, B. Šantek, Microreactor Production by PolyJet Matrix 3D-Printing Technology: Hydrodynamic Characterization, Food Technology and Biotechnology. 57 (2019) 272–281. https://doi.org/10.17113/ftb.57.02.19.5725.

[76] B. Kelly, I. Bhattacharya, M. Shusteff, R.M. Panas, H.K. Taylor, C.M. Spadaccini, Computed Axial Lithography (CAL): Toward Single Step 3D Printing of Arbitrary Geometries, (2017). https://doi.org/10.48550/arXiv.1705.05893.
[77] B.E. Kelly, I. Bhattacharya, H. Heidari, M. Shusteff, C.M. Spadaccini, H.K. Taylor, Volumetric additive manufacturing via tomographic reconstruction, Science. 363 (2019) 1075–1079. https://doi.org/10.1126/science.aau7114.
[78] J. Wu, Z. Zhao, C.M. Hamel, X. Mu, X. Kuang, Z. Guo, H.J. Qi, Evolution of material properties during free radical photopolymerization, Journal of the Mechanics and Physics of Solids. 112 (2018) 25–49. https://doi.org/10.1016/j.jmps.2017.11.018.
[79] M. Sadej, H. Gojzewski, E. Andrzejewska, Photocurable polymethacrylate-silica nanocomposites: correlation between dispersion stability, curing kinetics, morphology and properties, J Polym Res. 23 (2016) 116. https://doi.org/10.1007/s10965-016-1011-8.
[80] L. Fanfoni, M. De Biasi, G. Antollovich, R. Di Lenarda, D. Angerame, Evaluation of degree of conversion, rate of cure, microhardness, depth of cure, and contraction stress of new nanohybrid composites containing pre-polymerized spherical filler, J Mater Sci: Mater Med. 31 (2020) 127. https://doi.org/10.1007/s10856-020-06464-9.
[81] C. Hofstetter, S. Orman, S. Baudis, J. Stampfl, Combining cure depth and cure degree, a new way to fully characterize novel photopolymers, Additive Manufacturing. 24 (2018) 166–172. https://doi.org/10.1016/j.addma.2018.09.025.
[82] C. Gorsche, R. Harikrishna, S. Baudis, P. Knaack, B. Husar, J. Laeuger, H. Hoffmann, R. Liska, Real Time-NIR/MIR-Photorheology: A Versatile Tool for the in Situ Characterization of Photopolymerization Reactions, Anal. Chem. 89 (2017) 4958–4968. https://doi.org/10.1021/acs.analchem.7b00272.
[83] D.A. Rau, J.P. Reynolds, J.S. Bryant, M.J. Bortner, C.B. Williams, A Rheological Approach for Measuring Cure Depth of Filled and Unfilled Photopolymers at Additive Manufacturing Relevant Length Scales, Additive Manufacturing. (2022) 103207. https://doi.org/10.1016/j.addma.2022.103207.
[84] Y. Liu, Y. Lin, T. Jiao, G. Lu, J. Liu, Photocurable modification of inorganic fillers and their application in photopolymers for 3D printing, Polymer Chemistry. 10 (2019) 6350–6359. https://doi.org/10.1039/C9PY01445D.
[85] C. Villat, N. Pradelle-Plasse, B. Picard, P. Colon, Characterization method of photopolymerization kinetics of two dental composite resins using two types of light sources, Materials Science and Engineering: C. 28 (2008) 971–976. https://doi.org/10.1016/j.msec.2007.10.084.
[86] K. Kambly, Characterization of curing kinetics and polymerization shrinkage in ceramic-loaded photocurable resins for large area maskless photopolymerization (LAMP), Thesis, Georgia Institute of Technology, 2009. https://smartech.gatech.edu/handle/1853/31740 (accessed October 3, 2022).
[87] Y.Y.C. Choong, S. Maleksaeedi, H. Eng, J. Wei, P.-C. Su, 4D printing of high performance shape memory polymer using stereolithography, Materials & Design. 126 (2017) 219–225. https://doi.org/10.1016/j.matdes.2017.04.049.
[88] S. Sauerbrunn, D. Armbruster, Peter D. Shickel, DIFFERENTIAL PHOTOCALORIMETRY: ADVANCEMENTS FOR THE ANALYSIS AND CHARACTERIZATION OF FREE RADICAL, CATIONIC AND HYBRID PHOTOPOLYMERS, TA Instruments. (1997). https://www.semanticscholar.org/paper/Thermal-Analysis-%26-Rheology-

DIFFERENTIAL-FOR-THE-OF-Sauerbrunn-Armbruster/6b51c5bf52dafce4f5ca6edb8c2ee52a520b1546.
[89] F. Jiang, D. Drummer, Curing Kinetic Analysis of Acrylate Photopolymer for Additive Manufacturing by Photo-DSC., Polymers. 12 (2020) 1080. https://doi.org/10.3390/polym12051080.
[90] M. Sadej-Bajerlain, H. Gojzewski, E. Andrzejewska, Monomer/modified nanosilica systems: Photopolymerization kinetics and composite characterization, Polymer. 52 (2011) 1495–1503. https://doi.org/10.1016/j.polymer.2011.01.058.
[91] S. Fan, X. Sun, X. He, Y. Pang, Y. Xin, Y. Ding, Y. Zou, Coumarin Ketoxime Ester with Electron-Donating Substituents as Photoinitiators and Photosensitizers for Photopolymerization upon UV-Vis LED Irradiation, Polymers. 14 (2022) 4588. https://doi.org/10.3390/polym14214588.
[92] S.H. Oh, B.J. Cho, M.S. Jeong, J.-H. Ko, Evaluation of the isothermal curing process of UV-cured resin in terms of elasticity studied through micro-Brillouin light scattering, Journal of Information Display. 17 (2016) 87–91. https://doi.org/10.1080/15980316.2016.1178669.
[93] T.G. Nunes, S.G. Pereira, S. Kalachandra, Effect of treated filler loading on the photopolymerization inhibition and shrinkage of a dimethacrylate matrix, J Mater Sci: Mater Med. 19 (2008) 1881–1889. https://doi.org/10.1007/s10856-007-3247-7.
[94] W. Reusch, Nuclear Magnetic Resonance Spectroscopy, (2013). https://www2.chemistry.msu.edu/faculty/reusch/virttxtjml/spectrpy/nmr/nmr1.htm (accessed October 12, 2022).
[95] S. Swapp, Scanning Electron Microscopy (SEM), Techniques. (2017). https://serc.carleton.edu/research_education/geochemsheets/techniques/SEM.html (accessed October 11, 2022).
[96] R. Mitkus, M. Scharnofske, M. Sinapius, Characterization 0.1 wt.% Nanomaterial/Photopolymer Composites with Poor Nanomaterial Dispersion: Viscosity, Cure Depth and Dielectric Properties, Polymers. 13 (2021) 3948. https://doi.org/10.3390/polym13223948.
[97] M. Korčušková, V. Sevriugina, F. Ondreáš, J. Svatík, W. Tomal, V. Vishakha, J. Ortyl, P. Lepcio, Photoactivity, conversion kinetics, nanoreinforcement, post-curing, and electric/dielectric properties of functional 3D printable photopolymer resin filled with bare and alumina-doped ZnO nanoparticles, Polymer Testing. 116 (2022) 107798. https://doi.org/10.1016/j.polymertesting.2022.107798.
[98] Thomas J. Fellers, Michael W. Davidson, Confocal Microscopy - Introduction | Olympus LS, (n.d.). https://www.olympus-lifescience.com/en/microscope-resource/primer/techniques/confocal/confocalintro/ (accessed March 14, 2023).
[99] Computed Tomography (CT), National Institute of Biomedical Imaging and Bioengineering. (2022). https://www.nibib.nih.gov/science-education/science-topics/computed-tomography-ct (accessed October 12, 2022).
[100] Anycubic Resin User Manual & MSDS, ANYCUBIC 3D Printing. (2023). https://www.anycubic.com/pages/resin-user-manual (accessed January 27, 2023).
[101] PubChem, Epoxy resin, (2023). https://pubchem.ncbi.nlm.nih.gov/compound/169944 (accessed February 28, 2023).
[102] Spencer Tipping, Novum Glass, (2014). https://www.novumglass.com/ (accessed January 27, 2023).

[103] RAMAN DATA AND ANALYSIS , Raman Spectroscopy for Analysis and Monitoring, (n.d.). https://www.horiba.com/int/technology/molecular-spectroscopy/raman-spectroscopy/raman-academy/raman-tutorial/raman-scattering/ (accessed March 14, 2023).
[104] M. Bradley, Curve Fitting in Raman and IR Spectroscopy: Basic Theory of Line Shapes and Applications, Thermo Fisher Scientific Inc., 2007. https://www.semanticscholar.org/paper/Curve-Fitting-in-Raman-and-IR-Spectroscopy%3A-Basic-Bradley/b7af90bb8e17747eb33725b8ce9b584790fb67b8 (accessed December 28, 2022).
[105] ISO 25178-2:2021(en), Geometrical product specifications (GPS) — Surface texture: Areal — Part 2: Terms, definitions and surface texture parameters, Online Browsing Platform (OBP). (2021). https://www.iso.org/obp/ui/#iso:std:iso:25178:-2:ed-2:v1:en (accessed March 15, 2023).
[106] F. Caputo, J. Clogston, L. Calzolai, M. Rösslein, A. Prina-Mello, Measuring particle size distribution of nanoparticle enabled medicinal products, the joint view of EUNCL and NCI-NCL. A step by step approach combining orthogonal measurements with increasing complexity, Journal of Controlled Release. 299 (2019) 31–43. https://doi.org/10.1016/j.jconrel.2019.02.030.

Appendix A: Curing depth C_d data

No filler (pure resin)						
Filler vol.% -->	**0.00%**					
Filler wt.% -->	**0.00%**					
	↓Curing depth *Cd* (mm) ↓					
Exposure dose (mJ/cm^2)	**Trial 1**	**2**	**3**	**Avg.**	**Upper error**	**Lower error**
60	0.30	0.22	0.33	**0.28**	**0.05**	**0.06**
120	0.98	1.08	1.18	**1.08**	**0.10**	**0.10**
180	1.14	1.27	1.30	**1.24**	**0.06**	**0.10**
240	1.76	2.08	2.10	**1.98**	**0.12**	**0.22**
360	1.86	2.32	2.30	**2.16**	**0.16**	**0.30**
720	2.58	3.96	3.72	**3.42**	**0.54**	**0.84**
1440	3.57	3.90	3.89	**3.79**	**0.11**	**0.22**
2160	4.88	5.89	6.97	**5.91**	**1.06**	**1.03**

Filler size: small (38 - 45 microns)						
Filler vol.% -->	**11.58%**					
Filler wt.% -->	**15.00%**					
	↓Curing depth *Cd* (mm) ↓					
Exposure dose (mJ/cm^2)	**Trial 1**	**2**	**3**	**Avg.**	**Upper error**	**Lower error**
60	0.35	0.25	0.37	**0.32**	**0.05**	**0.07**
120	1.19	1.20	1.38	**1.26**	**0.12**	**0.07**
180	1.23	1.29	1.35	**1.29**	**0.06**	**0.06**
240	1.77	2.16	2.16	**2.03**	**0.13**	**0.26**
360	2.11	2.33	2.35	**2.26**	**0.09**	**0.15**
720	2.65	3.19	3.14	**2.99**	**0.20**	**0.34**
1440	3.32	3.24	3.85	**3.47**	**0.38**	**0.23**
2160	4.04	4.20	5.00	**4.41**	**0.59**	**0.37**
Filler vol.% -->	**24.13%**					
Filler wt.% -->	**30.00%**					
Exposure dose (mJ/cm^2)	**Trial 1**	**2**	**3**	**avg.**	**Upper error**	**Lower error**
60	0.35	0.54	0.61	**0.50**	**0.11**	**0.15**
120	1.02	1.25	1.55	**1.27**	**0.28**	**0.25**
180	1.36	1.43	1.43	**1.41**	**0.02**	**0.05**
240	1.81	1.95	1.97	**1.91**	**0.06**	**0.10**

360	2.27	2.11	2.07	**2.15**	**0.12**	**0.08**
720	3.01	3.44	3.32	**3.26**	**0.18**	**0.25**
1440	3.35	3.74	3.60	**3.56**	**0.18**	**0.21**
2160	3.83	4.33	4.40	**4.19**	**0.21**	**0.36**
Filler vol.% -->	**37.77%**					
Filler wt.% -->	**45.00%**					
Exposure dose (mJ/cm^2)	**Trial 1**	**2**	**3**	**avg.**	**Upper error**	**Lower error**
60	0.66	0.43	0.60	**0.56**	**0.10**	**0.13**
120	1.41	1.34	1.50	**1.42**	**0.08**	**0.08**
180	1.49	1.35	1.49	**1.44**	**0.05**	**0.09**
240	1.95	1.90	1.98	**1.94**	**0.04**	**0.04**
360	2.29	2.22	2.27	**2.26**	**0.03**	**0.04**
720	3.07	3.28	3.49	**3.28**	**0.21**	**0.21**
1440	3.70	3.87	3.85	**3.81**	**0.06**	**0.11**
2160	4.37	4.58	4.62	**4.52**	**0.10**	**0.15**
Filler vol.% -->	**52.67%**					
Filler wt.% -->	**60.00%**					
Exposure dose (mJ/cm^2)	**Trial 1**	**2**	**3**	**avg.**	**Upper error**	**Lower error**
60	0.63	0.67	0.77	**0.69**	**0.08**	**0.06**
120	1.36	1.44	1.39	**1.40**	**0.04**	**0.04**
180	1.80	1.49	1.57	**1.62**	**0.18**	**0.13**
240	2.26	1.93	2.20	**2.13**	**0.13**	**0.20**
360	2.23	2.22	2.23	**2.23**	**0.00**	**0.01**
720	3.07	3.45	3.48	**3.33**	**0.15**	**0.26**
1440	3.91	3.77	3.94	**3.87**	**0.07**	**0.10**
2160	4.26	4.65	4.58	**4.50**	**0.15**	**0.24**

Filler size: mixed (50/50 blend of small and large filler)						
Filler vol.% -->	**11.58%**					
Filler wt.% -->	**15.00%**					
	↓Curing depth *Cd* (mm) ↓					
Exposure dose (mJ/cm^2)	**Trial 1**	**2**	**3**	**Avg.**	**Upper error**	**Lower error**
60	0.61	0.34	0.38	**0.44**	**0.17**	**0.10**
120	1.20	1.32	1.26	**1.26**	**0.06**	**0.06**
180	1.15	1.24	1.26	**1.22**	**0.04**	**0.07**
240	1.91	2.03	2.07	**2.00**	**0.07**	**0.09**
360	1.95	1.96	2.10	**2.00**	**0.10**	**0.05**

720	2.97	3.01	3.48	**3.15**	**0.33**	**0.18**
1440	3.05	3.36	3.58	**3.33**	**0.25**	**0.28**
2160	3.86	4.43	4.62	**4.30**	**0.32**	**0.44**
Filler vol.% -->	**24.13%**					
Filler wt.% -->	**30.00%**					
Exposure dose (mJ/cm^2)	**Trial 1**	**2**	**3**	**avg.**	**Upper error**	**Lower error**
60	0.61	1.01	0.81	**0.81**	**0.20**	**0.20**
120	1.59	1.59	1.51	**1.56**	**0.03**	**0.05**
180	1.71	1.61	1.59	**1.64**	**0.07**	**0.05**
240	2.18	2.10	2.11	**2.13**	**0.05**	**0.03**
360	2.19	2.11	2.05	**2.12**	**0.07**	**0.07**
720	2.88	3.07	3.00	**2.98**	**0.09**	**0.10**
1440	3.26	3.69	3.52	**3.49**	**0.20**	**0.23**
2160	3.49	4.38	3.78	**3.88**	**0.50**	**0.39**
Filler vol.% -->	**37.77%**					
Filler wt.% -->	**45.00%**					
Exposure dose (mJ/cm^2)	**Trial 1**	**2**	**3**	**avg.**	**Upper error**	**Lower error**
60	0.64	0.90	0.84	**0.79**	**0.11**	**0.15**
120	1.88	1.54	1.56	**1.66**	**0.22**	**0.12**
180	1.96	1.75	1.69	**1.80**	**0.16**	**0.11**
240	2.49	2.50	2.43	**2.47**	**0.03**	**0.04**
360	2.21	2.51	2.67	**2.46**	**0.21**	**0.25**
720	3.01	3.78	3.94	**3.58**	**0.36**	**0.57**
1440	3.44	4.22	3.51	**3.72**	**0.50**	**0.28**
2160	4.45	4.54	4.33	**4.44**	**0.10**	**0.11**
Filler vol.% -->	**52.67%**					
Filler wt.% -->	**60.00%**					
Exposure dose (mJ/cm^2)	**Trial 1**	**2**	**3**	**avg.**	**Upper error**	**Lower error**
60	0.69	1.04	1.00	**0.91**	**0.13**	**0.22**
120	1.84	2.13	1.98	**1.98**	**0.15**	**0.14**
180	1.95	2.10	2.08	**2.04**	**0.06**	**0.09**
240	2.46	2.74	2.66	**2.62**	**0.12**	**0.16**
360	2.57	2.78	2.96	**2.77**	**0.19**	**0.20**
720	3.95	3.88	3.84	**3.89**	**0.06**	**0.05**
1440	4.54	4.42	4.49	**4.48**	**0.06**	**0.06**
2160	4.68	4.85	4.68	**4.74**	**0.11**	**0.06**

Filler size: large (212 – 250 microns)						
Filler vol.% -->	**11.58%**					
Filler wt.% -->	**15.00%**					
Exposure dose (mJ/cm^2)	**Trial 1**	**2**	**3**	**avg.**	**Upper error**	**Lower error**
60	0.52	0.49	0.60	**0.54**	**0.06**	**0.05**
120	1.20	1.16	1.16	**1.17**	**0.03**	**0.01**
180	1.32	1.49	1.42	**1.41**	**0.08**	**0.09**
240	2.00	2.15	2.12	**2.09**	**0.06**	**0.09**
360	2.05	2.20	2.36	**2.20**	**0.16**	**0.15**
720	2.88	3.34	3.10	**3.11**	**0.23**	**0.23**
1440	2.94	3.09	3.29	**3.11**	**0.18**	**0.17**
2160	3.90	3.62	4.08	**3.87**	**0.21**	**0.25**
Filler vol.% -->	**24.13%**					
Filler wt.% -->	**30.00%**					
Exposure dose (mJ/cm^2)	**Trial 1**	**2**	**3**	**avg.**	**Upper error**	**Lower error**
60	0.69	0.70	0.85	**0.75**	**0.10**	**0.06**
120	1.22	1.35	1.41	**1.33**	**0.08**	**0.11**
180	1.92	1.65	1.56	**1.71**	**0.21**	**0.15**
240	2.48	2.41	2.25	**2.38**	**0.10**	**0.13**
360	2.10	2.21	2.26	**2.19**	**0.07**	**0.09**
720	2.95	3.21	2.87	**3.01**	**0.20**	**0.14**
1440	2.77	3.21	3.33	**3.10**	**0.23**	**0.33**
2160	3.80	3.82	3.66	**3.76**	**0.06**	**0.10**
Filler vol.% -->	**37.77%**					
Filler wt.% -->	**45.00%**					
Exposure dose (mJ/cm^2)	**Trial 1**	**2**	**3**	**avg.**	**Upper error**	**Lower error**
60	0.87	0.91	1.02	**0.93**	**0.09**	**0.06**
120	2.12	1.89	2.04	**2.02**	**0.10**	**0.13**
180	2.07	2.04	2.06	**2.06**	**0.01**	**0.02**
240	2.85	2.84	2.92	**2.87**	**0.05**	**0.03**
360	2.74	2.66	2.43	**2.61**	**0.13**	**0.18**
720	3.35	3.64	3.40	**3.46**	**0.18**	**0.11**
1440	3.20	3.61	3.42	**3.41**	**0.20**	**0.21**
2160	4.45	3.76	3.82	**4.01**	**0.44**	**0.25**
Filler vol.% -->	**52.67%**					
Filler wt.% -->	**60.00%**					
Exposure dose (mJ/cm^2)	**Trial 1**	**2**	**3**	**avg.**	**Upper error**	**Lower error**

60	1.11	1.23	0.98	**1.11**	**0.12**	**0.13**
120	2.00	1.79	2.01	**1.93**	**0.08**	**0.14**
180	2.16	2.07	2.08	**2.10**	**0.06**	**0.03**
240	2.67	2.73	2.81	**2.74**	**0.07**	**0.07**
360	2.82	2.96	2.82	**2.87**	**0.09**	**0.05**
720	4.13	3.87	3.54	**3.85**	**0.28**	**0.31**
1440	4.84	3.90	3.46	**4.07**	**0.77**	**0.61**
2160	4.50	5.01	4.29	**4.60**	**0.41**	**0.31**

Appendix B: Degree of cure (DoC) data

Calculating degree of cure (DoC) from Raman spectra:

$$DoC = 1 - \frac{A_{1634}(t)}{A_{1634}(0)}$$

No filler (pure resin)									
Filler vol.%	**0.00%**								
Filler wt.%	**0%**								
	C=C peak (1634cm^-1) area			**DoC**					
Exposure dose (mJ/cm^2)	**Trial 1**	**2**	**3**	**1**	**2**	**3**	**Avg.**	**Upper error**	**Lower error**
0	38.39	38.39	38.39	0.00	0.00	0.00	0.00	0.00	0.00
60	11.07	13.23	23.29	0.71	0.66	0.39	0.59	0.12	0.19
120	9.77	12.72	17.49	0.75	0.67	0.54	0.65	0.09	0.11
180	8.20	12.19	13.29	0.79	0.68	0.65	0.71	0.08	0.05
240	14.00	9.97	7.52	0.64	0.74	0.80	0.73	0.08	0.09
360	5.21	16.90	5.92	0.86	0.56	0.85	0.76	0.11	0.20
720	8.37	8.49	9.16	0.78	0.78	0.76	0.77	0.01	0.01
1440	5.65	6.47	2.12	0.85	0.83	0.94	0.88	0.07	0.04
2160	3.74	5.43	4.46	0.90	0.86	0.88	0.88	0.02	0.02

Filler size: small (38 - 45 microns)									
Filler vol.% -->	**11.58%**								
Filler wt.% -->	**15%**								
	C=C peak (1634cm^-1) area			**DoC**					
Exposure dose (mJ/cm^2)	**Trial 1**	**2**	**3**	**1**	**2**	**3**	**Avg.**	**Upper error**	**Lower error**
0	38.39	38.39	38.39	0.00	0.00	0.00	0.00	0.00	0.00
60	11.98	10.10	10.36	0.69	0.74	0.73	0.72	0.02	0.03
120	7.30	4.87	6.77	0.81	0.87	0.82	0.84	0.04	0.03
180	7.50	6.98	5.24	0.80	0.82	0.86	0.83	0.03	0.02
240	6.03	5.69	5.59	0.84	0.85	0.85	0.85	0.00	0.01
360	1.31	5.52	3.33	0.97	0.86	0.91	0.91	0.05	0.06
720	2.18	6.49	2.89	0.94	0.83	0.92	0.90	0.04	0.07

1440	4.25	4.42	4.61	0.89	0.88	0.88	0.88	0.00	0.00
2160	2.04	1.87	3.25	0.95	0.95	0.92	0.94	0.01	0.02
Filler vol.% -->	**24.13%**								
Filler wt.% -->	**30%**								
	C=C peak (1634cm^-1) area			**DoC**					
Exposure dose (mJ/cm^2)	**Trial 1**	**2**	**3**	**1**	**2**	**3**	**Avg.**	**Upper error**	**Lower error**
0	38.39	38.39	38.39	0.00	0.00	0.00	0.00	0.00	0.00
60	11.07	7.50	8.12	0.71	0.80	0.79	0.77	0.04	0.06
120	3.79	6.14	12.16	0.90	0.84	0.68	0.81	0.09	0.12
180	3.02	5.92	8.76	0.92	0.85	0.77	0.85	0.08	0.07
240	4.42	5.51	5.29	0.88	0.86	0.86	0.87	0.02	0.01
360	4.34	4.76	5.92	0.89	0.88	0.85	0.87	0.02	0.02
720	4.50	5.57	4.28	0.88	0.85	0.89	0.88	0.01	0.02
1440	7.40	4.67	2.91	0.81	0.88	0.92	0.87	0.05	0.06
2160	5.06	5.25	6.08	0.87	0.86	0.84	0.86	0.01	0.02
Filler vol.% -->	**37.77%**								
Filler wt.% -->	**45%**								
	C=C peak (1634cm^-1) area			**DoC**					
Exposure dose (mJ/cm^2)	**Trial 1**	**2**	**3**	**1**	**2**	**3**	**Avg.**	**Upper error**	**Lower error**
0	38.39	38.39	38.39	0.00	0.00	0.00	0.00	0.00	0.00
60	7.24	5.56	20.22	0.81	0.86	0.47	0.71	0.14	0.24
120	4.89	5.2	10.23	0.87	0.86	0.73	0.82	0.05	0.09
180	3.11	4.05	2.88	0.92	0.89	0.92	0.91	0.01	0.02
240	2.99	6.01	3.12	0.92	0.84	0.92	0.89	0.03	0.05
360	3.18	7.03	3.37	0.92	0.82	0.91	0.88	0.04	0.07
720	2.55	5.34	3.05	0.93	0.86	0.92	0.91	0.03	0.04
1440	2.16	4.12	2.59	0.94	0.89	0.93	0.92	0.02	0.03
2160	2.51	2.93	3.50	0.93	0.92	0.91	0.92	0.01	0.01
Filler vol.% -->	**52.67%**								
Filler wt.% -->	**60%**								
	C=C peak (1634cm^-1) area			**DoC**					
Exposure dose (mJ/cm^2)	**Trial 1**	**2**	**3**	**1**	**2**	**3**	**Avg.**	**Upper error**	**Lower error**
0	38.39	38.39	38.39	0.00	0.00	0.00	0.00	0.00	0.00

60	12.25	9.27	8.68	0.68	0.76	0.77	0.74	0.04	0.06
120	3.99	4.33	2.39	0.90	0.89	0.94	0.91	0.03	0.02
180	5.33	3.85	4.12	0.86	0.90	0.89	0.88	0.02	0.02
240	4.01	6.39	4.14	0.90	0.83	0.89	0.87	0.02	0.04
360	10.39	5.81	5.39	0.73	0.85	0.86	0.81	0.05	0.08
720	4.06	0.49	3.45	0.89	0.99	0.91	0.93	0.06	0.04
1440	9.68	5.14	1.23	0.75	0.87	0.97	0.86	0.11	0.11
2160	6.00	2.45	0.56	0.84	0.94	0.99	0.92	0.06	0.08

Filler size: mixed (50/50 blend of small and large filler)									
Filler vol.%	**11.58%**								
Filler wt.%	**15%**								
	C=C peak (1634cm^-1) area			**DoC**					
Exposure dose (mJ/cm^2)	**Trial 1**	**2**	**3**	**1**	**2**	**3**	**Avg.**	**Upper error**	**Lower error**
0	38.39	38.39	38.39	0.00	0.00	0.00	0.00	0.00	0.00
60	11.98	10.10	10.36	0.69	0.74	0.73	0.72	0.02	0.03
120	7.30	4.87	6.77	0.81	0.87	0.82	0.84	0.04	0.03
180	7.50	6.98	5.24	0.80	0.82	0.86	0.83	0.03	0.02
240	6.03	5.69	5.59	0.84	0.85	0.85	0.85	0.00	0.01
360	1.31	5.52	3.33	0.97	0.86	0.91	0.91	0.05	0.06
720	2.18	6.49	2.89	0.94	0.83	0.92	0.90	0.04	0.07
1440	4.25	4.42	4.61	0.89	0.88	0.88	0.88	0.00	0.00
2160	2.04	1.87	3.25	0.95	0.95	0.92	0.94	0.01	0.02
Filler vol.%	**24.13%**								
Filler wt.%	**30%**								
	C=C peak (1634cm^-1) area			**DoC**					
Exposure dose (mJ/cm^2)	**Trial 1**	**2**	**3**	**1**	**2**	**3**	**Avg.**	**Upper error**	**Lower error**
0	38.39	38.39	38.39	0.00	0.00	0.00	0.00	0.00	0.00
60	11.07	7.50	8.12	0.71	0.80	0.79	0.77	0.04	0.06
120	3.79	6.14	12.16	0.90	0.84	0.68	0.81	0.09	0.12
180	3.02	5.92	8.76	0.92	0.85	0.77	0.85	0.08	0.07
240	4.42	5.51	5.29	0.88	0.86	0.86	0.87	0.02	0.01
360	4.34	4.76	5.92	0.89	0.88	0.85	0.87	0.02	0.02
720	4.50	5.57	4.28	0.88	0.85	0.89	0.88	0.01	0.02

1440	7.40	4.67	2.91	0.81	0.88	0.92	0.87	0.05	0.06
2160	5.06	5.25	6.08	0.87	0.86	0.84	0.86	0.01	0.02
Filler vol.%	**37.77%**								
Filler wt.%	**45%**								
	C=C peak (1634cm^-1) area			**DoC**					
Exposure dose (mJ/cm^2)	**Trial 1**	**2**	**3**	**1**	**2**	**3**	**Avg.**	**Upper error**	**Lower error**
0	38.39	38.39	38.39	0.00	0.00	0.00	0.00	0.00	0.00
60	7.24	5.56	20.22	0.81	0.86	0.47	0.71	0.14	0.24
120	4.89	5.2	10.23	0.87	0.86	0.73	0.82	0.05	0.09
180	3.11	4.05	2.88	0.92	0.89	0.92	0.91	0.01	0.02
240	2.99	6.01	3.12	0.92	0.84	0.92	0.89	0.03	0.05
360	3.18	7.03	3.37	0.92	0.82	0.91	0.88	0.04	0.07
720	2.55	5.34	3.05	0.93	0.86	0.92	0.91	0.03	0.04
1440	2.16	4.12	2.59	0.94	0.89	0.93	0.92	0.02	0.03
2160	2.51	2.93	3.50	0.93	0.92	0.91	0.92	0.01	0.01
Filler vol.%	**52.67%**								
Filler wt.%	**60%**								
	C=C peak (1634cm^-1) area			**DoC**					
Exposure dose (mJ/cm^2)	**Trial 1**	**2**	**3**	**1**	**2**	**3**	**Avg.**	**Upper error**	**Lower error**
0	38.39	38.39	38.39	0.00	0.00	0.00	0.00	0.00	0.00
60	12.25	9.27	8.68	0.68	0.76	0.77	0.74	0.04	0.06
120	3.99	4.33	2.39	0.90	0.89	0.94	0.91	0.03	0.02
180	5.33	3.85	4.12	0.86	0.90	0.89	0.88	0.02	0.02
240	4.01	6.39	4.14	0.90	0.83	0.89	0.87	0.02	0.04
360	10.39	5.81	5.39	0.73	0.85	0.86	0.81	0.05	0.08
720	4.06	0.49	3.45	0.89	0.99	0.91	0.93	0.06	0.04
1440	9.68	5.14	1.23	0.75	0.87	0.97	0.86	0.11	0.11
2160	6.00	2.45	0.56	0.84	0.94	0.99	0.92	0.06	0.08

Filler size: large (212 - 250 microns)									
Filler vol.%	**11.58%**								
Filler wt.%	**15%**								
	C=C peak (1634cm^-1) area			**DoC**					
Exposure dose (mJ/cm^2)	**Trial 1**	**2**	**3**	**1**	**2**	**3**	**Avg.**	**Upper error**	**Lower error**
0	38.39	38.39	38.39	0.00	0.00	0.00	0.00	0.00	0.00
60	20.25	10.43	7.25	0.47	0.73	0.81	0.67	0.14	0.20
120	6.92	13.58	6.97	0.82	0.65	0.82	0.76	0.06	0.12
180	4.33	5.39	3.48	0.89	0.86	0.91	0.89	0.02	0.03
240	3.57	4.14	2.51	0.91	0.89	0.93	0.91	0.02	0.02
360	3.95	4.57	3.09	0.90	0.88	0.92	0.90	0.02	0.02
720	2.25	4.73	3.11	0.94	0.88	0.92	0.91	0.03	0.04
1440	3.21	4.53	1.94	0.92	0.88	0.95	0.92	0.03	0.03
2160	5.60	3.11	3.03	0.85	0.92	0.92	0.90	0.02	0.04
Filler vol.%	**24.13%**								
Filler wt.%	**30%**								
	C=C peak (1634cm^-1) area			**DoC**					
Exposure dose (mJ/cm^2)	**Trial 1**	**2**	**3**	**1**	**2**	**3**	**Avg.**	**Upper error**	**Lower error**
0	38.39	38.39	38.39	0.00	0.00	0.00	0.00	0.00	0.00
60	10.06	21.32	12.25	0.74	0.44	0.68	0.62	0.12	0.18
120	7.77	7.6	3.2	0.80	0.80	0.92	0.84	0.08	0.04
180	4.29	7.8	9.7	0.89	0.80	0.75	0.81	0.08	0.06
240	3.82	2.09	2.84	0.90	0.95	0.93	0.92	0.02	0.02
360	2.52	3.65	3.67	0.93	0.90	0.90	0.91	0.02	0.01
720	3.26	2.08	3.6	0.92	0.95	0.91	0.92	0.02	0.02
1440	2.30	3.17	4.88	0.94	0.92	0.87	0.91	0.03	0.04
2160	1.63	2.53	4.21	0.96	0.93	0.89	0.93	0.03	0.04
Filler vol.%	**37.77%**								
Filler wt.%	**45%**								
	C=C peak (1634cm^-1) area			**DoC**					
Exposure dose (mJ/cm^2)	**Trial 1**	**2**	**3**	**1**	**2**	**3**	**Avg.**	**Upper error**	**Lower error**
0	38.39	38.39	38.39	0.00	0.00	0.00	0.00	0.00	0.00

60	8.46	5.72	20.66	0.78	0.85	0.46	0.70	0.15	0.24
120	4.69	7.43	4.86	0.88	0.81	0.87	0.85	0.03	0.05
180	7.16	3.52	6.46	0.81	0.91	0.83	0.85	0.06	0.04
240	4.11	2.76	2.73	0.89	0.93	0.93	0.92	0.01	0.02
360	4.61	3.2	3.69	0.88	0.92	0.90	0.90	0.02	0.02
720	3.65	3.73	4.14	0.90	0.90	0.89	0.90	0.00	0.01
1440	5.27	1.65	2.63	0.86	0.96	0.93	0.92	0.04	0.05
2160	3.78	3.48	1.55	0.90	0.91	0.96	0.92	0.04	0.02
Filler vol.%	**52.67%**								
Filler wt.%	**60%**								
	C=C peak (1634cm^-1) area			**DoC**					
Exposure dose (mJ/cm^2)	**Trial 1**	**2**	**3**	**1**	**2**	**3**	**Avg.**	**Upper error**	**Lower error**
0	38.39	38.39	38.39	0.00	0.00	0.00	0.00	0.00	0.00
60	13.03	19.70	16.07	0.66	0.49	0.58	0.58	0.08	0.09
120	5.62	6.35	3.45	0.85	0.83	0.91	0.87	0.04	0.03
180	5.29	6.67	4.66	0.86	0.83	0.88	0.86	0.02	0.03
240	2.35	2.2	1.51	0.94	0.94	0.96	0.95	0.01	0.01
360	3.97	1.95	4.86	0.90	0.95	0.87	0.91	0.04	0.03
720	1.40	1.65	3.5	0.96	0.96	0.91	0.94	0.02	0.03
1440	1.52	1.8	3.97	0.96	0.95	0.90	0.94	0.02	0.04
2160	3.11	4.19	2.53	0.92	0.89	0.93	0.91	0.02	0.02

Appendix C: Deconvoluted Raman spectra

NOTE: We show a selected number of spectra instead of all spectra due to the large number of specimens and most of the spectra have similar shape.

Acquisition parameters:

- Acq. time (s) = 5
- Accumulations = 3
- Range (cm^{-1}) = 1000...3000
- Windows = 1
- Spike filter = Multiple accum.
- Delay time (s) = 5
- Binning = 1
- Readout mode = Signal
- DeNoise = Lite
- ICS correction = Off
- Dark correction = Off
- Instrument = XploRA Plus
- Detector = Syncerity OE
- Objective = x5_VIS
- Grating = 1200 (750nm)
- Filter = 10%
- Laser = 532nm_Edge
- Slit = 200
- Hole = 500

Analysis software:

OriginPro (ver. 2023, learning edition)

Plot legend description:

- X-axis: Raman shift [cm^{-1}],
- Y-axis: intensity [counts],
- Black line: acquired Raman spectrum (baseline corrected and normalized),
- Red line: cumulative fit line,
- Green lines: deconvoluted peaks.

No filler (pure resin)

No filler, Φ = 0%, E_0 = 0 mJ/cm^2 (uncured, pure resin)

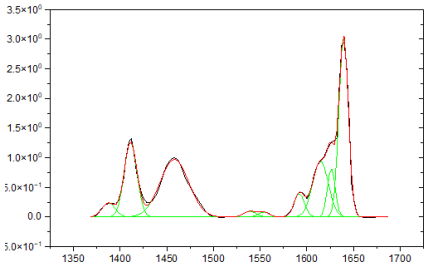

No filler, Φ = 0%, E_0 = 60 mJ/cm^2

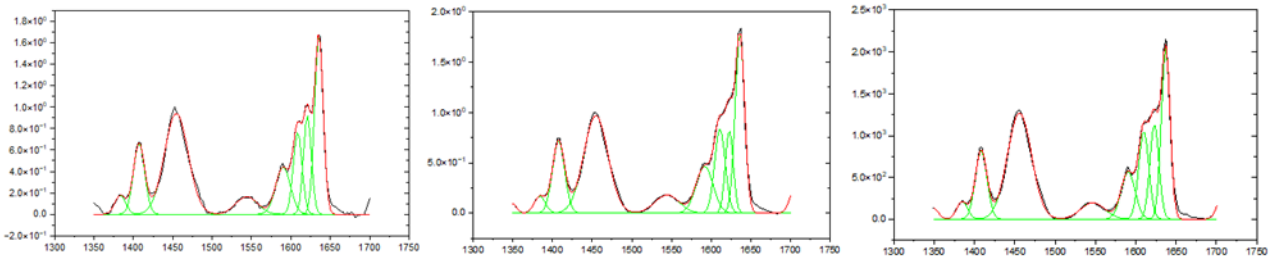

No filler, Φ = 0%, E_0 = 120 mJ/cm^2

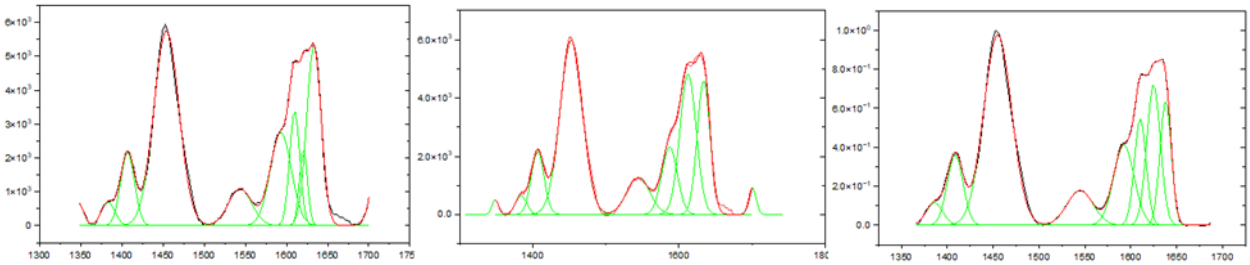

No filler, Φ = 0%, E_0 = 180 mJ/cm^2

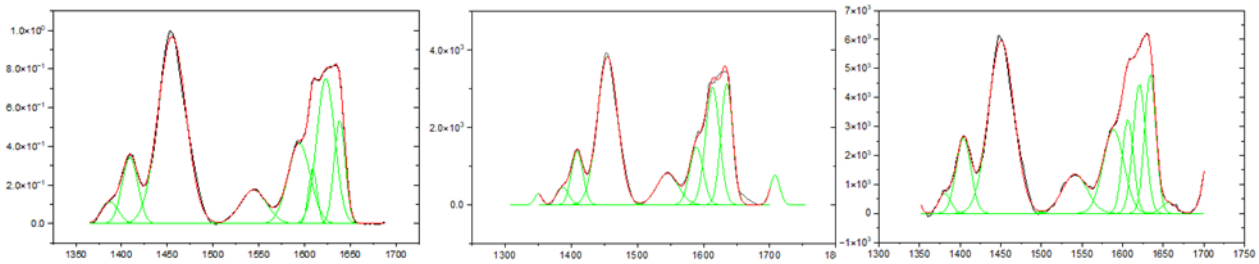

No filler, Φ = 0%, E_0 = 240 mJ/cm^2

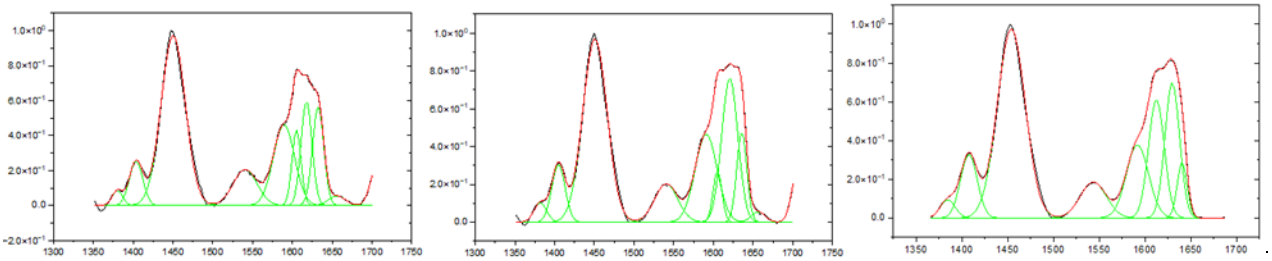

No filler, Φ = 0%, E_0 = 360 mJ/cm^2

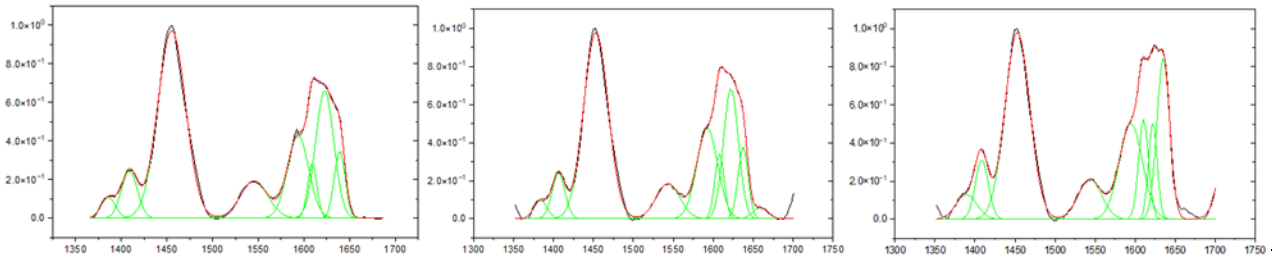

No filler, Φ = 0%, E_0 = 720 mJ/cm^2

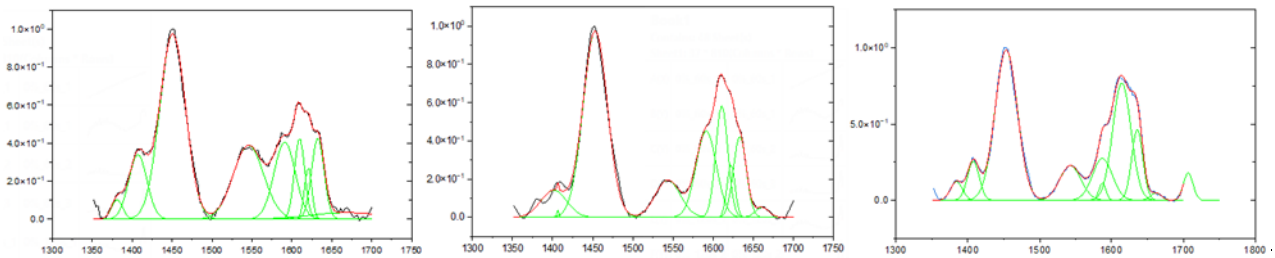

No filler, Φ = 0%, E_0 = 1440 mJ/cm^2

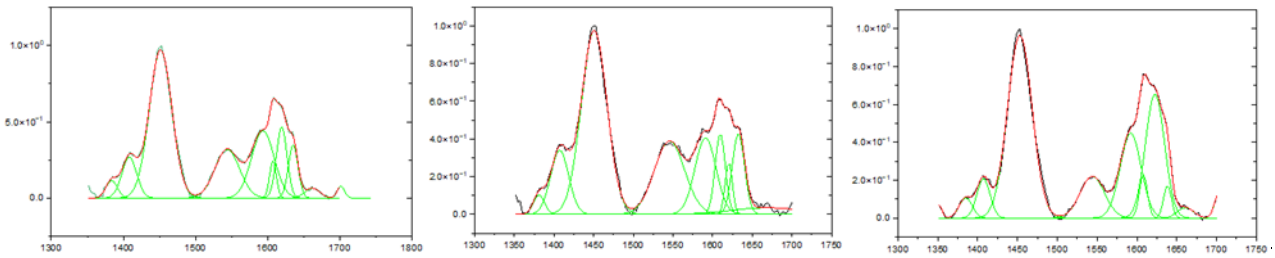

No filler, Φ = 0%, E_0 = 2160 mJ/cm^2

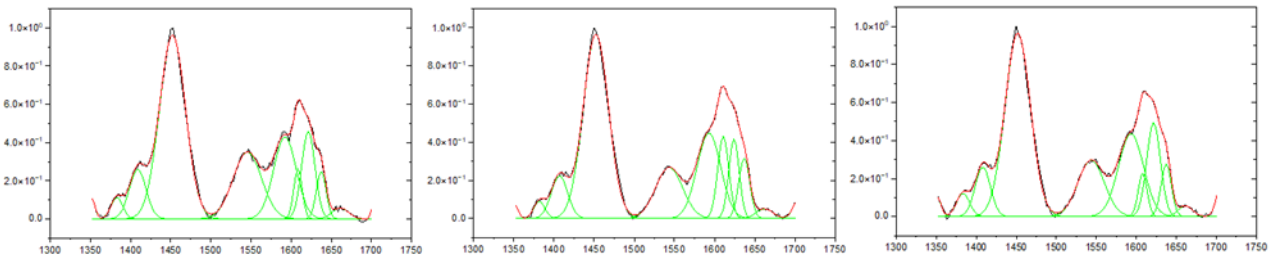

Filler size: small (38 – 45 microns)

Filler size: small, Φ = 11.58%, E_0 = 60 mJ/cm^2

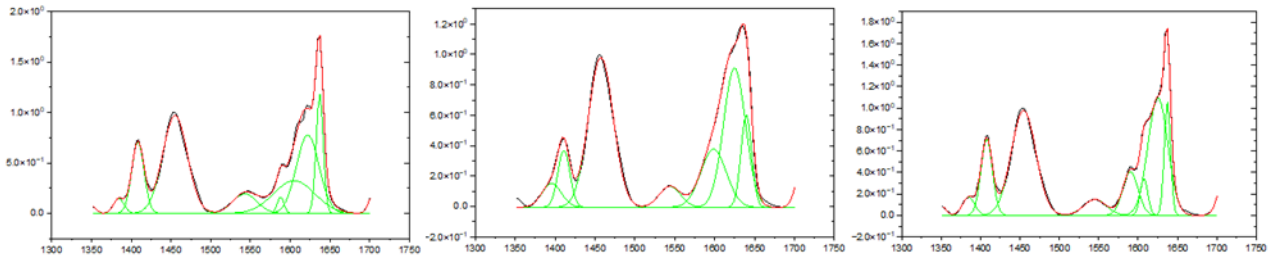

Filler size: small, Φ = 11.58%, E_0 = 120 mJ/cm^2

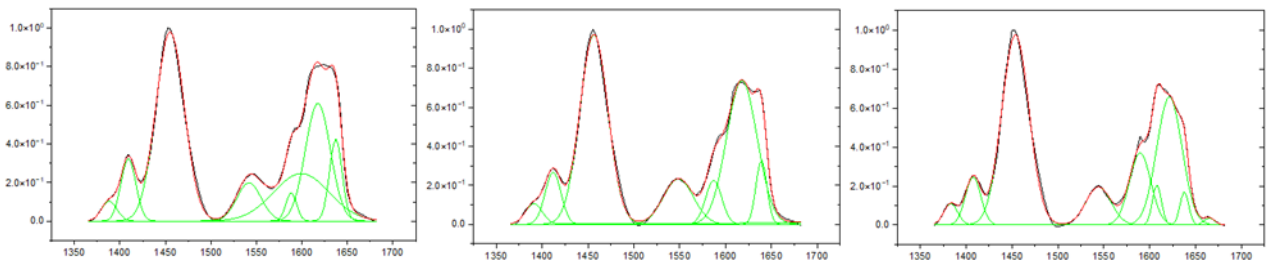

Filler size: small, Φ = 11.58%, E_0 = 180 mJ/cm^2

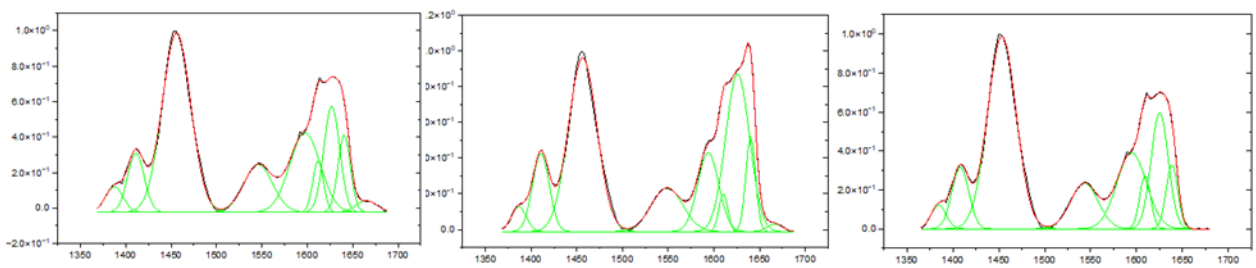

Filler size: small, Φ = 11.58%, E_0 = 240 mJ/cm^2

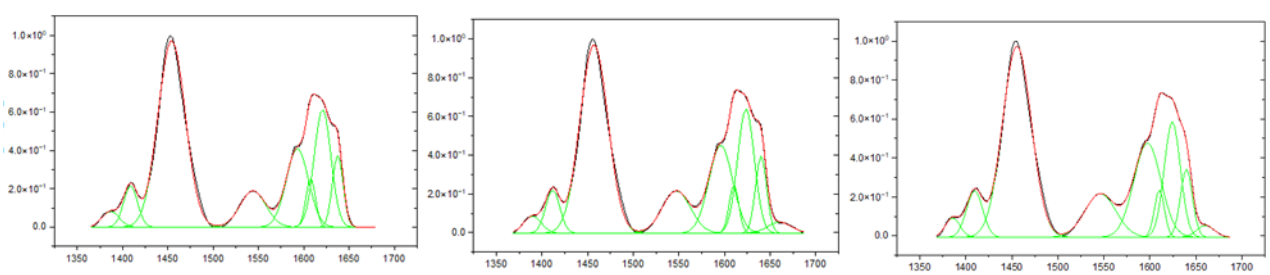

Filler size: small, Φ = 11.58%, E_0 = 720 mJ/cm^2

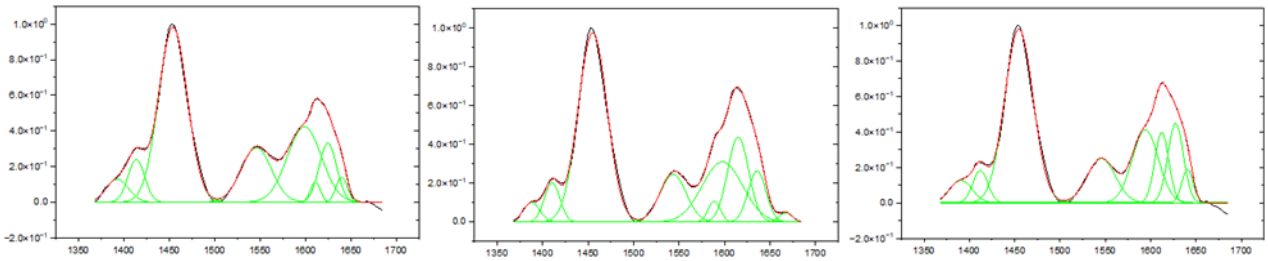

Filler size: small, Φ = 11.58%, E_0 = 2160 mJ/cm^2

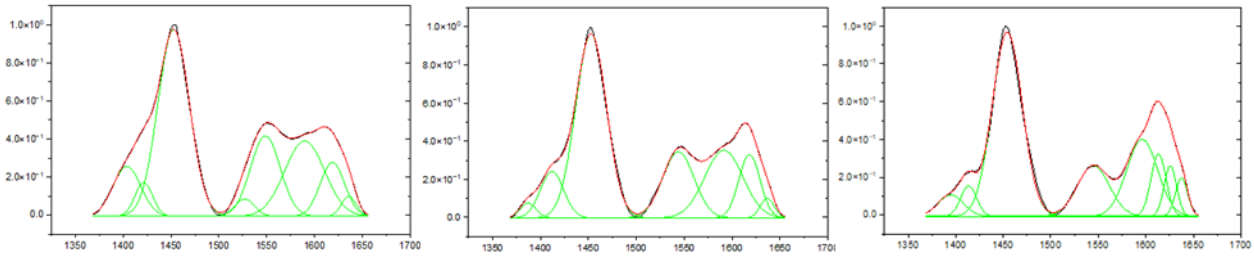

Filler size: small, Φ = 24.13%, E_0 = 60 mJ/cm^2

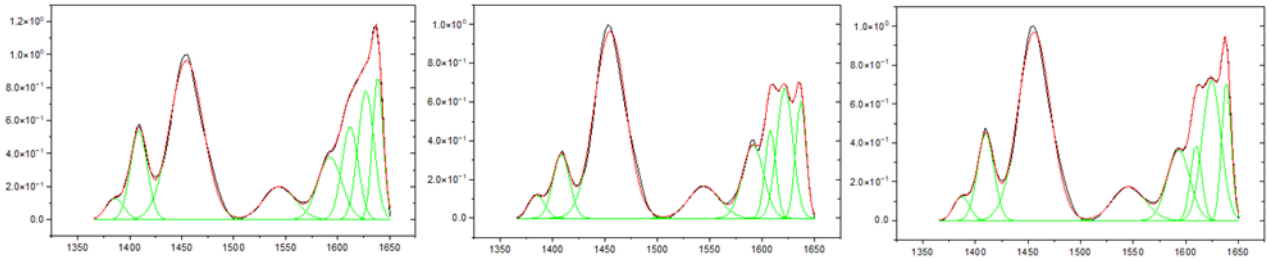

Filler size: small, Φ = 24.13%, E_0 = 2160 mJ/cm^2

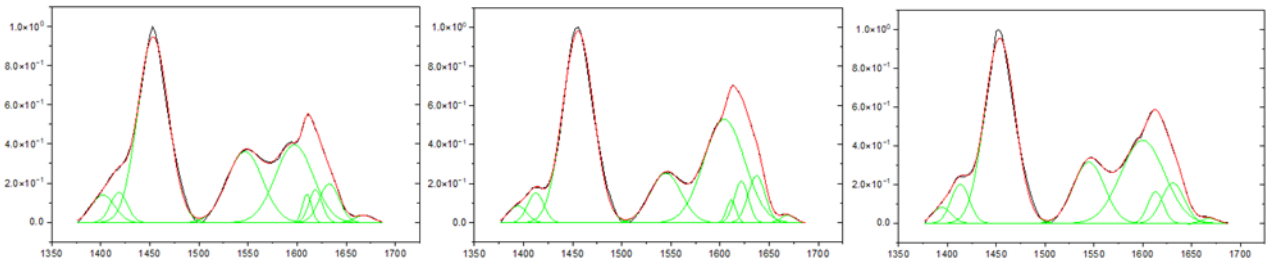

Filler size: small, Φ = 52.67%, E_0 = 60 mJ/cm^2

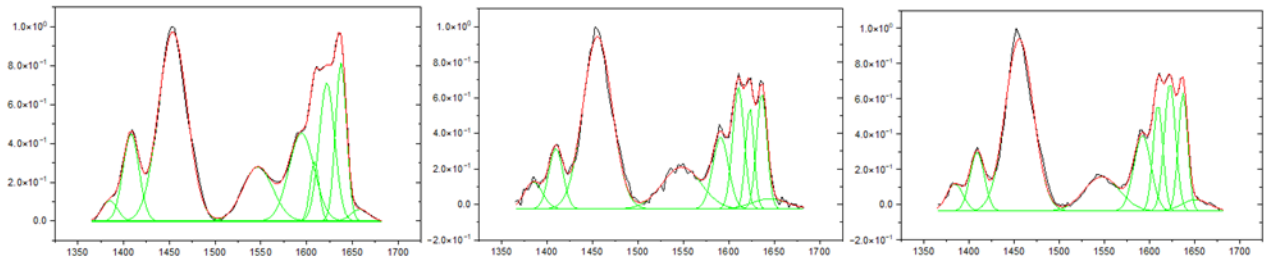

Filler size: small, Φ = 52.67%, E_0 = 2160 mJ/cm^2

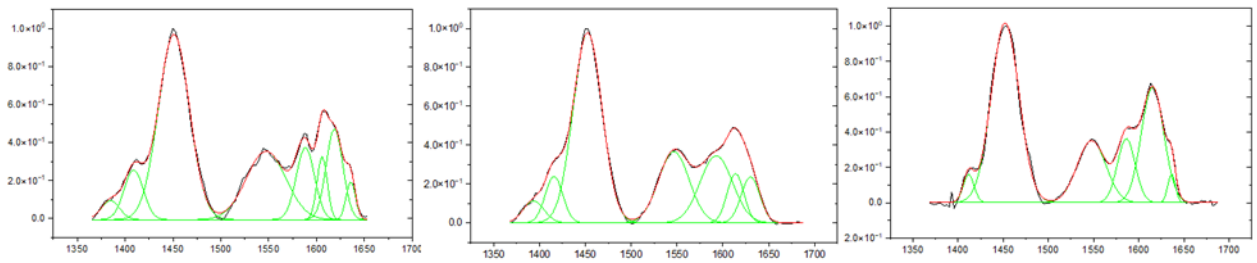

Filler size: mixed (50/50 blend of small and large filler)

Filler size: mixed, Φ = 11.58%, E_0 = 60 mJ/cm^2

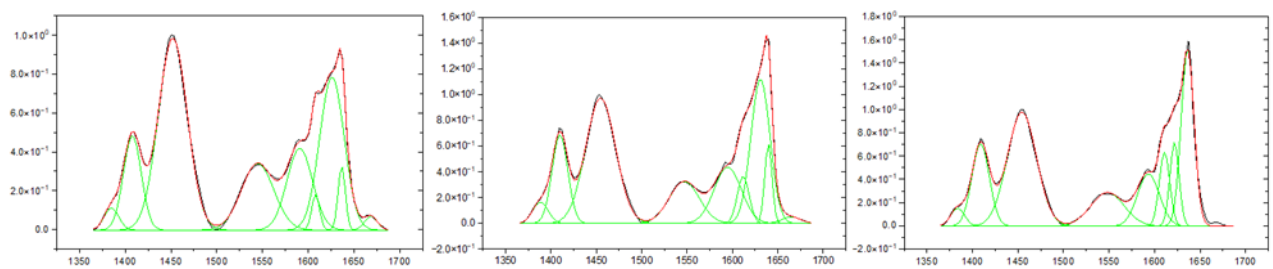

Filler size: mixed, Φ = 11.58%, E_0 = 2160 mJ/cm^2

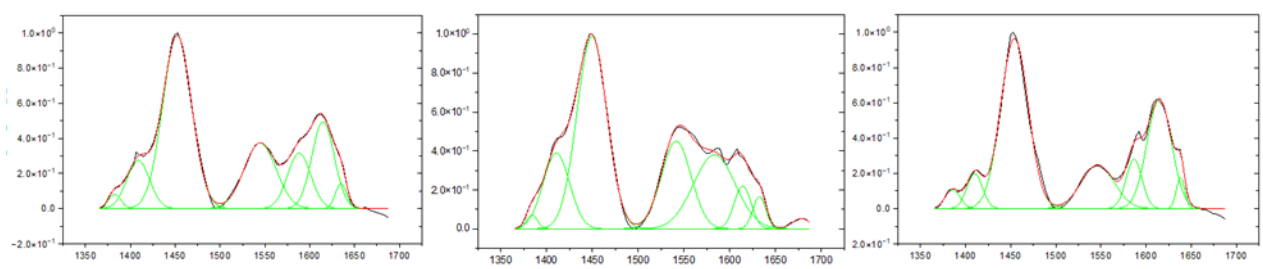

Filler size: mixed, Φ = 37.77%, E_0 = 60 mJ/cm^2

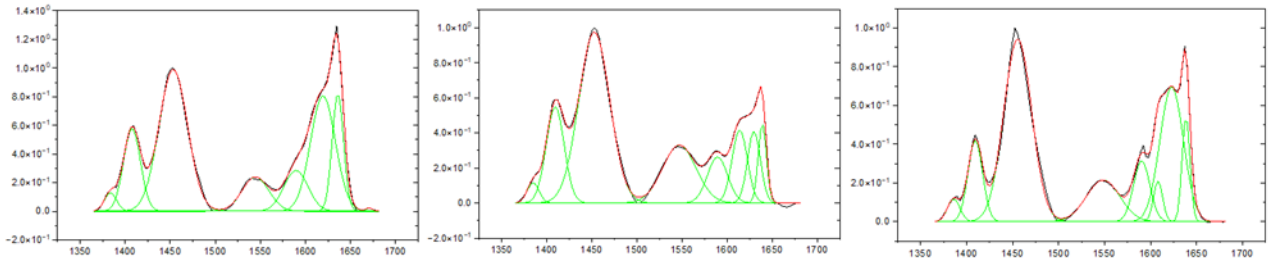

Filler size: mixed, Φ = 37.77%, E_0 = 2160 mJ/cm^2

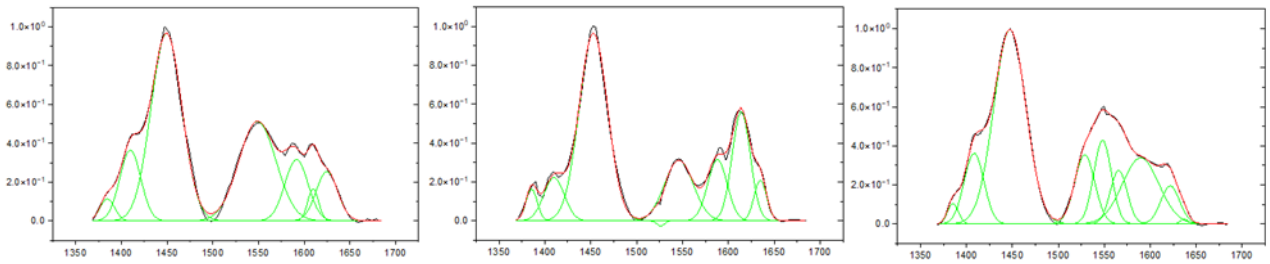

Filler size: mixed, Φ = 52.67%, E_0 = 60 mJ/cm^2

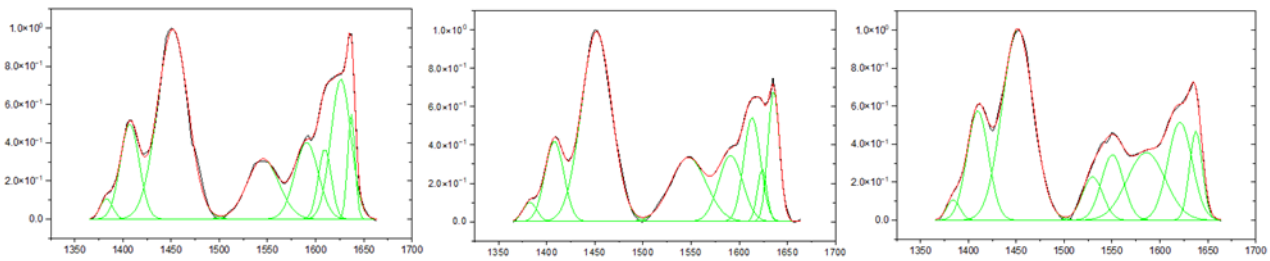

Filler size: mixed, Φ = 52.67%, E_0 = 2160 mJ/cm^2

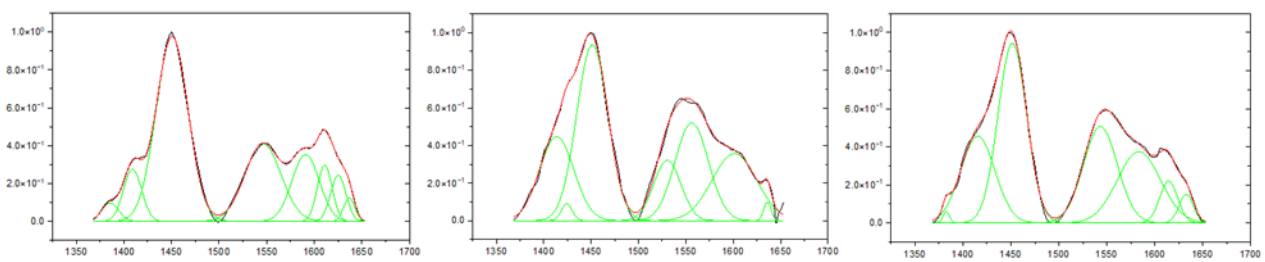

Filler size: large (212 – 250 microns)

Filler size: large, Φ = 11.58%, E_0 = 60 mJ/cm^2

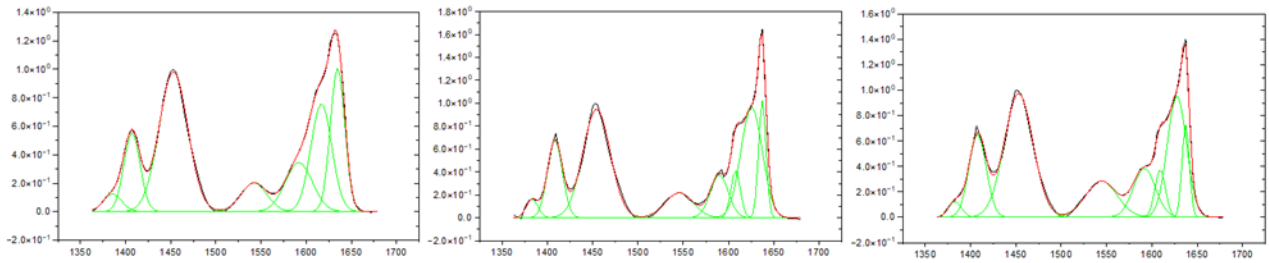

Filler size: large, Φ = 11.58%, E_0 = 2160 mJ/cm^2

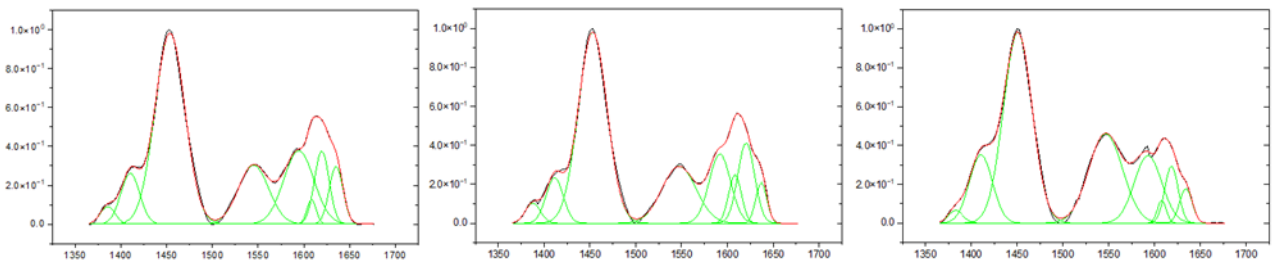

Filler size: large, Φ = 37.77%, E_0 = 60 mJ/cm^2

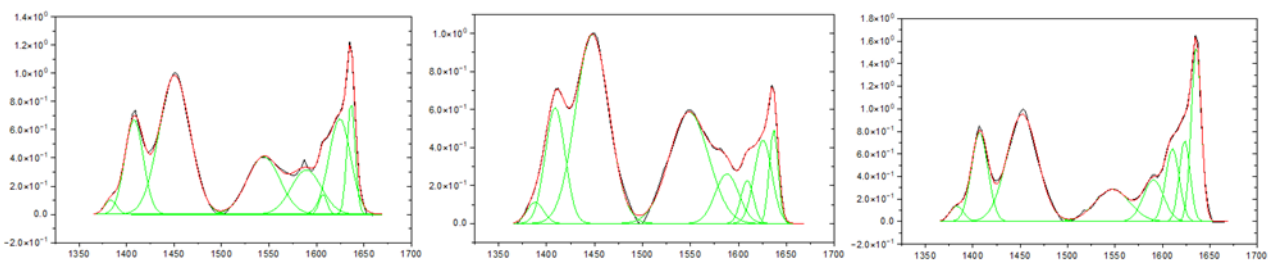

Filler size: large, Φ = 37.77%, E_0 = 2160 mJ/cm^2

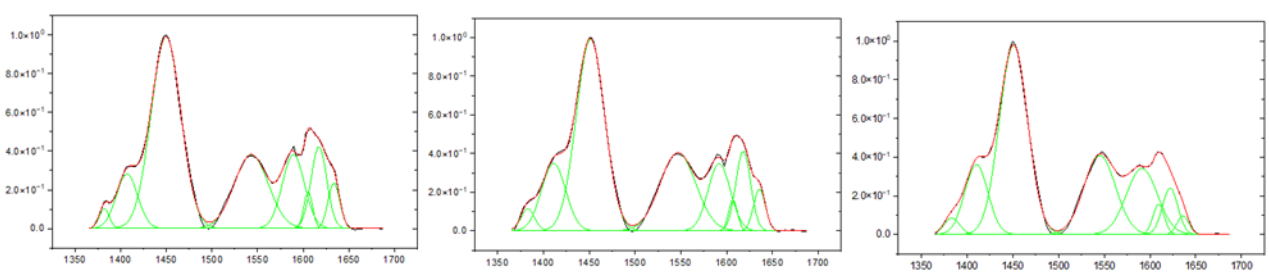

Filler size: large, Φ = 52.67%, E_0 = 60 mJ/cm^2

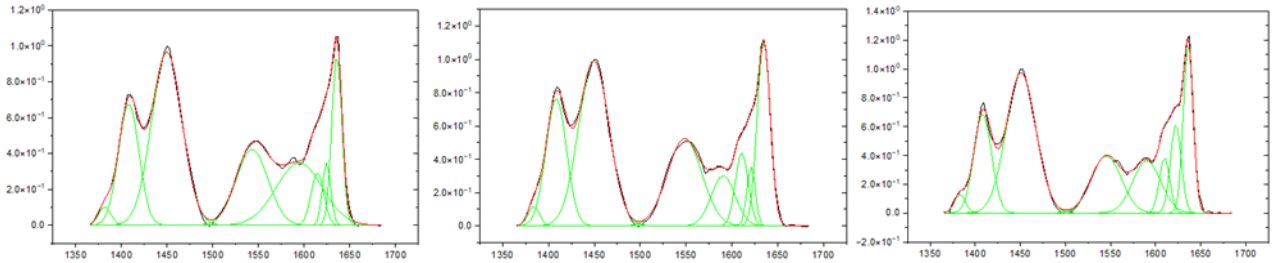

Filler size: large, Φ = 52.67%, E_0 = 2160 mJ/cm^2

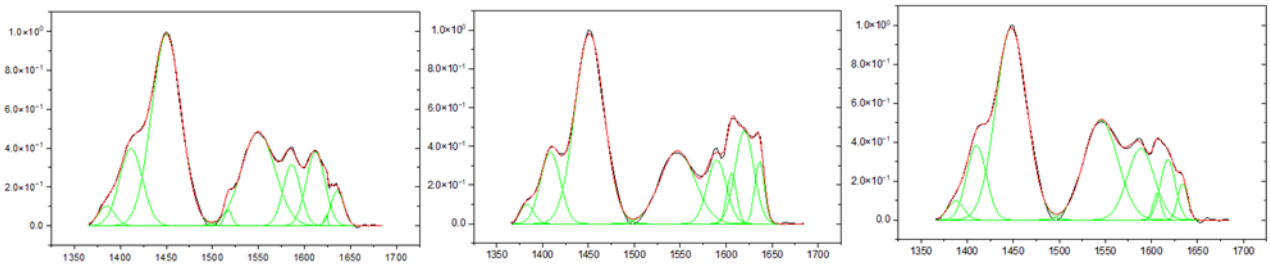

Appendix D: Surface roughness data

NOTE: We show a selected number of surface topography maps instead of all surface topography maps.

3D surface images scale bar:

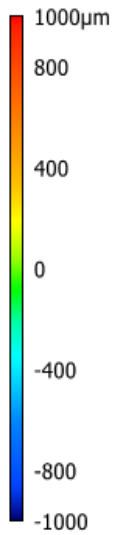

Filler size	Filler fraction Φ [vol.%]	Exposure dose E_0 [mJ/cm^2]	Optical surface images	3D surface images	Surface roughness data	
					Sa [µm]	Sz [µm]
-	0	120	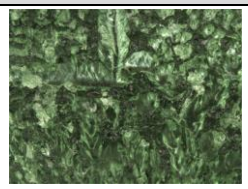	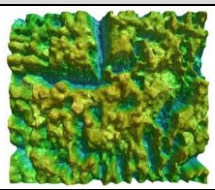	118.946	950.923
-	0	240	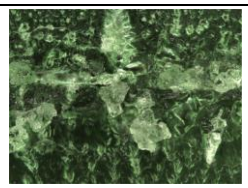	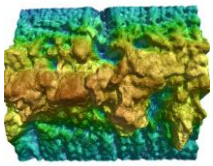	289.068	1516.479
-	0	720	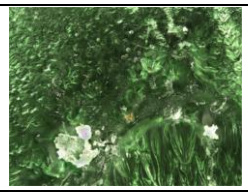	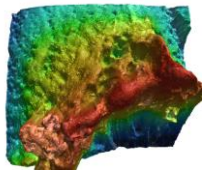	451.798	2649.228

-	0	2160		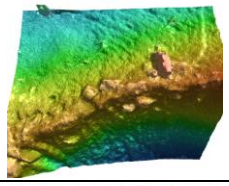	325.622	1985.538
Small	11.58	120	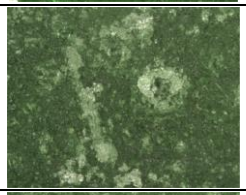	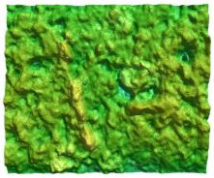	46.566	529.537
Small	11.58	240	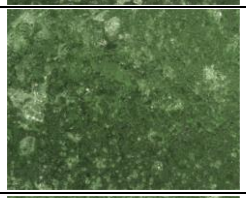	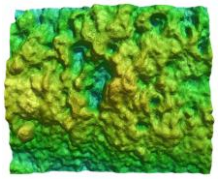	90.488	769.210
Small	11.58	720	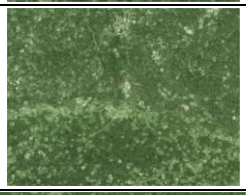	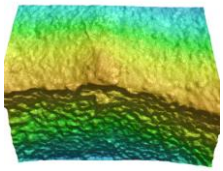	232.693	1123.485
Small	11.58	2160	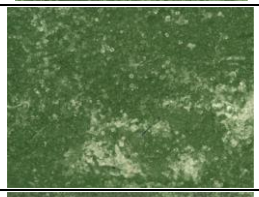	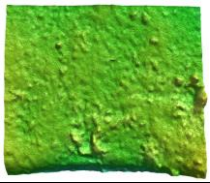	38.291	597.061
Small	24.13	120	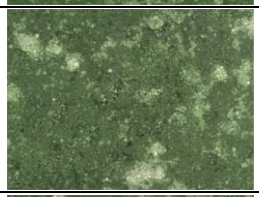	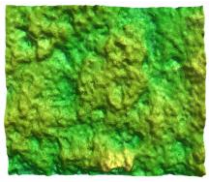	48.848	448.831
Small	24.13	240	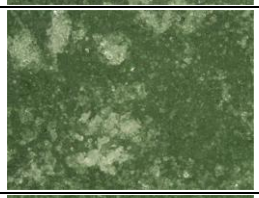	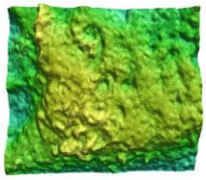	98.223	618.455
Small	24.13	720	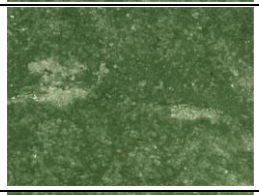	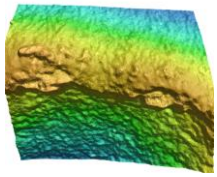	265.576	1412.167
Small	24.13	2160	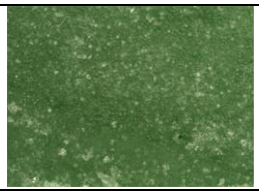	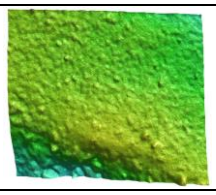	74.526	626.718

Small	37.77	120	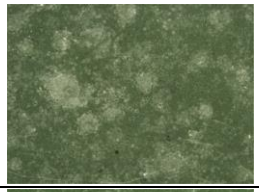	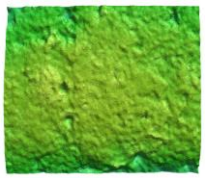	44.270	323.838
Small	37.77	240	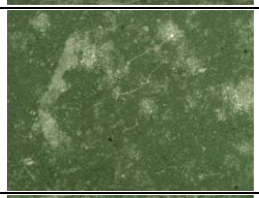	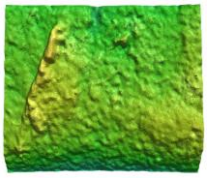	62.852	585.423
Small	37.77	720	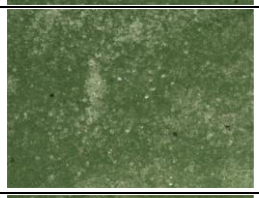	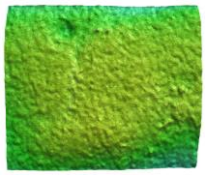	67.319	428.773
Small	37.77	2160	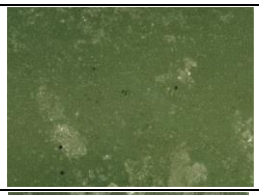	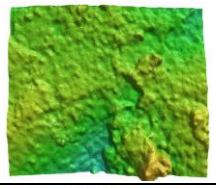	59.837	727.308
Small	52.67	120	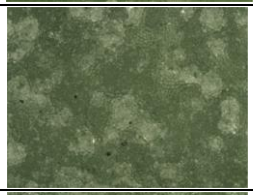	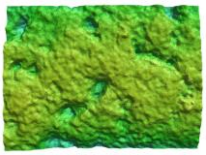	59.852	472.204
Small	52.67	240	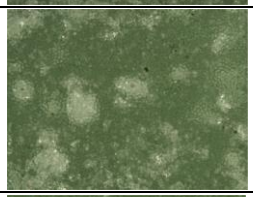	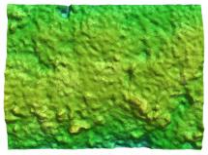	52.657	425.730
Small	52.67	720	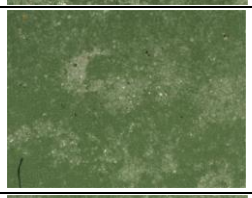	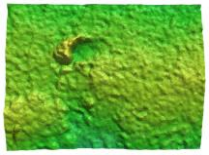	52.588	409.909
Small	52.67	2160	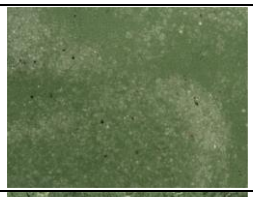	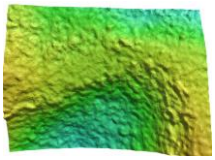	120.941	711.433
Large	11.58	120	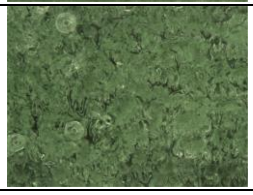	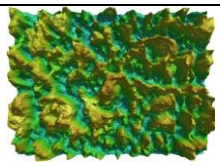	159.183	903.554

Large	11.58	240	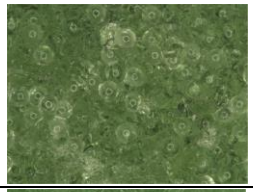	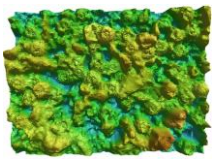	116.103	1216.002
Large	11.58	720		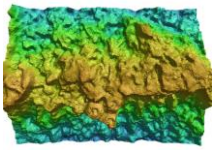	281.075	1315.050
Large	11.58	2160	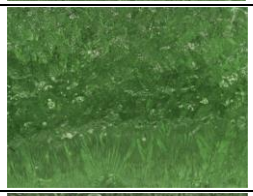	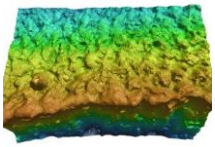	347.847	1933.114
Large	24.13	120	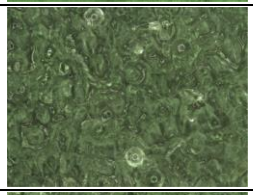	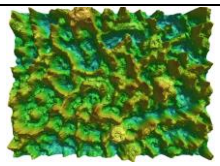	123.134	972.581
Large	24.13	240	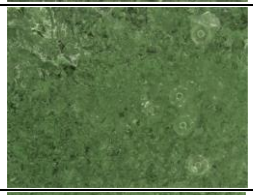	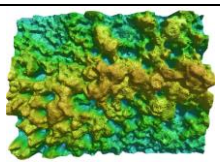	167.382	1042.951
Large	24.13	720	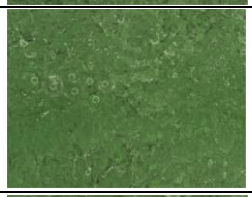	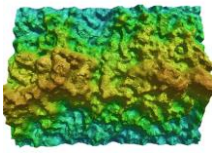	212.705	1243.372
Large	24.13	2160	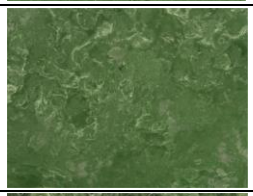	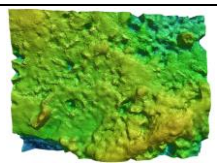	94.095	1116.874
Large	37.77	120	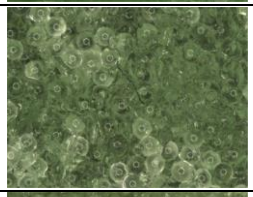	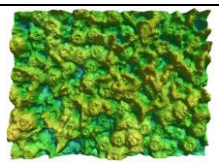	78.510	812.515
Large	37.77	240		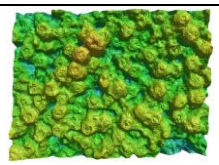	77.044	987.406

Large	37.77	720	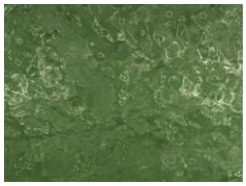	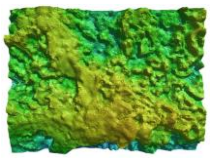	111.747	969.502
Large	37.77	2160	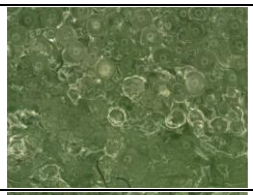	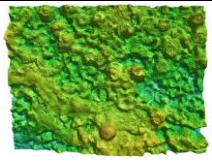	68.163	818.044
Large	52.67	120		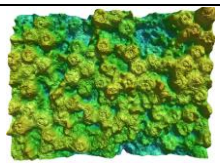	106.954	1185.737
Large	52.67	240	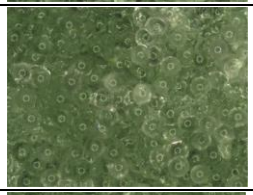	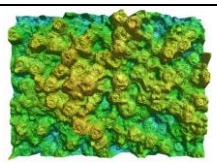	112.071	950.574
Large	52.67	720	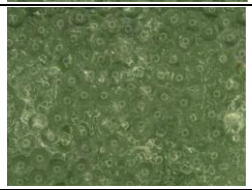	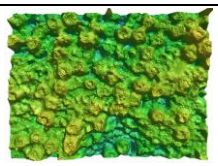	75.048	807.011
Large	52.67	2160	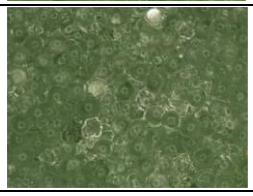	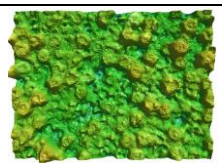	56.885	704.308